Thesis

NMR Study of Spin Fluctuation and Superconductivity in High-T_c Cuprates

($HgBa_2Ca_2Cu_3O_{8+\delta}$ & $TlSr_2CaCu_2O_{7-\delta}$)

by
Ko-ichi Magishi

OSAKA UNIVERSITY
Graduate School of Engineering Science
Department of Material Physics
Toyonaka Osaka

January 1996

Contents

Abstract

The electronic structure and the magnetic property in $HgBa_2Ca_2Cu_3O_{8+\delta}$ (Hg1223) compound, which currently has the highest value of the transition temperature (T_c = 133 K) in the exsiting superconductors, were investigated using the NMR technique. In the normal state, from the quantitative analyses of $^{63}(1/T_1)$ and $1/T_{2G}$, it is shown that the product of the staggered susceptibility and the characteristic energy of the spin fluctuations around the zone boundary, $\chi_Q\Gamma_Q$, for the square CuO_2 plane site is larger than that for $YBa_2Cu_3O_7$ ($YBCO_7$), although that for the pyramidal CuO_2 plane site is almost the same. Together with the result on $Tl_2Ba_2Ca_2Cu_3O_{10}$, this enhancement of $\chi_Q\Gamma_Q$ is a common property for the triple CuO_2 layer compounds, and is considered to be responsible for the higher T_c in Hg1223 than in $YBCO_7$. In the superconducting state, the behaviors of ^{63}K and $^{63}(1/T_1)$ can consistently be interpreted in terms of the d-wave pairing model with a smaller additional density of states (DOS), N_{res}, at the Fermi level than that for Bi- and Tl-based compounds. The small value of N_{res} indicates that the Hg1223 possesses good quality, as supported by the narrow NMR spectra. It is suggested that one of the origins for the high value of T_c in Hg1223 is due to the better quality than other high-T_c cuprates, such as Bi- and Tl-based compounds.

On the other hand, the magnetic and superconducting properties in heavily-doped region were investigated in $TlSr_2CaCu_2O_{7-\delta}$ (Tl1212) with two pyramidal CuO_2 planes such as $YBCO_7$. In the normal state, from the systematic measurements of $^{63}(1/T_1)$ and $1/T_{2G}$, the antiferromagnetic (**AF**) spin correlation is found to be weaker than that in $YBCO_7$, and to be suppressed with decreasing T_c, i.e. with increasing hole content. In the superconducting state, the T-dependences of ^{63}K and $^{63}(1/T_1)$ have shown that the superconductivity is in a gapless regime with a finite DOS at the Fermi surface as in the cases for Hg1223 and other high-T_c compounds. It is established that the NMR results below T_c are almost consistent with a d-wave pairing model.

These properties can be explained in terms of the spin-fluctuation-induced superconductivity model as well, and thus it is concluded that the high-T_c superconductivity is due to the spin fluctuations.

Part I
General Introduction

1 Background of High-T_c Cuprates

In order to explore the mechanism of the high-T_c superconductivity, numerous works have been carried out in various high-T_c materials, e.g. lightly-doped $La_{2-x}Sr_xCuO_4$ (LSCO) with a single CuO_2 layer, $YBa_2Cu_3O_{6+x}$ ($YBCO_{6+x}$), $YBa_2Cu_4O_8$ (Y124) and $Bi_2Sr_2CaCu_2O_8$ (Bi2212) with double CuO_2 layers and heavily-doped $Tl_2Ba_2CuO_{6+x}$ (Tl2201) with a single CuO_2 layer.[1] Among the extensive experimental efforts, NMR study is playing important role in clarifying the electronic state in the CuO_2 plane, which is crucial for the occurrence of the high-T_c superconductivity. Thus far, there are numerous NMR and neutron scattering studies with respect to the magnetic nature in high-T_c cuprates. Apparently, the **AF** spin correlation remains in the normal state of the superconducting compounds, and it is a controversial issue whether the spin fluctuations mediate effectively the formation of the Cooper-pair.

On the other hand, as for the superconducting properties, there have been several experiments which are consistent with a d-wave model. From the earlier stage of the NMR study, Kitaoka *et al.*[2] have claimed that the result of the nuclear spin-lattice relaxation rate, $1/T_1$, which is close to the T^3-behavior without a coherence peak just below T_c, should be interpreted in terms of an anisotropic energy gap model (say d-wave model) with gap zeros on lines at Fermi surface. Monien and Pines[3] pointed out that the measured values of the spin Knight shift, K_s, and $1/T_1$ in the superconducting state would seem to require d-wave pairing. In addition to these results, Ishida *et al.*[4] have found that the impurity effect on the superconductivity is consistently understood in the framework of a d-wave model as well. However, it seems that a general consensus has not been reached yet.

The recent discovery of superconductivity at 94 K in the $HgBa_2CuO_{4+\delta}$ system, a single CuO_2 layer compound, by Putilin *et al.*[5] was enough to attract many investigators' attention as a new family of the high-T_c compounds, because it was expected that the highest T_c would occur in a mercury-based compound with more CuO_2 layers, as in bismuth- and

thalium-based compounds. A successive increase of T_c is achieved in the mercury-based homologous family ($HgBa_2Ca_{n-1}Cu_nO_{2n+2+\delta}$, $n = 1, 2, 3, 4$).[6] The $n = 1$, 2 and 3 mercury-based compounds possess the highest T_c's for any known single, double and triple CuO_2 layer compounds – 98, 128 and 135 K, respectively, as seen in Fig.I-1(a). It suggests that the increase of the number of CuO_2 sheets is a key factor to increase T_c value. Furthermore, under high pressure, T_c's are found to increase surprisingly by more than 20 K in these compounds, to temperature exceeding $\sim$ 150 K for $HgBa_2Ca_2Cu_3O_{8+\delta}$ (Hg1223).[7] However, the detailed information on the electronic structure and magnetic properties in the CuO_2 planes in the mercury-based compound, which is essential to the understanding of superconductivity mechanism in these multiple Cu-O layered systems, is not available yet. Therefore, in order to elucidate why T_c in the mercury-based compound is quite high from the microscopic point of view, ^{63}Cu NMR measurements for the Hg1223 compound have been carried out.

On the other hand, from a viewpoint of hole carrier concentration, it is widely accepted that the high-T_c superconductivity occurs in an intermediate region between an antiferromagnetic insulator and a metal in the phase diagram of high-T_c superconductors, as seen in Fig.I-1(b). This feature suggests that the high-T_c superconductivity is connected with a state described as either a spin-liquid or Fermi-liquid. Therefore, in order to formulate a mechanism of high-T_c superconductivity, the studies of both extremes of the behaviors are important.

It is well known that the normal-state properties of high-T_c cuprates show unusual behaviors, such as T-linear resistivity and anomalous T-dependence of Hall coefficient, etc.[1] In particular, the magnetic properties in lightly-doped compounds are quite unusual. Namely, the uniform spin susceptibility, $\chi_s(T)$, decreases with decreasing temperature. Also, $^{63}(1/T_1)$ does not obey a T_1T = const. law, but $^{63}(1/T_1T)$ follows a Curie-Weiss law above T_c in LSCO,[8] whereas it exhibits a peak well above T_c in $YBCO_{6+x}$[9, 10] and Y124.[11] The latter unique behavior is so-called a spin gap behavior, that is, a low energy part of spin fluctuation is suppressed before the onset of the superconductivity as evidenced clearly by the neutron inelastic scattering experiments.[12] Such a spin-gap behavior has drawn much attention with an expectation that the superconductivity may occur in a new framework

of spin-charge separation based on an RVB model.[13)]

In contrast, in an optimum doped system represented by $YBa_2Cu_3O_7$ and heavily-doped system like $Tl_2Ba_2CuO_{6+y}$ where T_c decreases with increasing holes,[14)] the $\chi_s(T)$ deduced from the Knight shift of ^{63}Cu is T-independent, whereas $^{63}(1/T_1T)$ for high-T_c samples increases upon lowering temperature down to T_c as well as in LSCO,[8)] although its magnitude is considerably reduced by an increase of holes.[15)] The latter anomalous T-dependence of $^{63}(1/T_1T)$, which is rather commonly seen in most of high-T_c materials than a spin gap behavior, has been described first in terms of the phenomenological antiferromagnetic (**AF**) spin fluctuation model[16)] and the self-consistent renormalization (SCR) theory,[17)] and later in terms of more microscopic models.[18, 19, 20)] A remarkable finding was that the **AF** spin fluctuation disappeared for the heavily-doped $Tl_2Ba_2CuO_{6+y}$ compound exhibiting no longer superconductivity, instead obeying the T_1T=const. law in a wide T-range.[15)] These results have suggested that the **AF** spin correlation plays a role for the occurrence of the superconductivity.

However, in order to reach to a final answer of the mechanism of the high-T_c superconductivity, more extensive informations covering not only the lightly-doped region near an insulator to superconducting boundary, but also the heavily-doped region involving a superconducting to metal boundary must be driven by necessary. So far, there are few systematic experiment on the heavily-doped system except for the Tl2201 compounds with a single CuO_2 layer. In order to establish further the magnetic and superconducting properties in heavily-doped superconductors, the extensive ^{63}Cu NMR studies of $TlSr_2CaCu_2O_{7-\delta}$ (Tl1212) compounds with **two pyramidal CuO_2 layers** in the unit cell as in $YBCO_{6+x}$ have been carried out.

In this thesis, the ^{63}Cu NMR experiments for the mercury-based triple Cu-O layered superconductor, $HgBa_2Ca_2Cu_3O_{8+\delta}$ (Hg1223, T_c = 133 K) are presented in **part II**, and the thalium-based double layered superconductor, $TlSr_2CaCu_2O_{7-\delta}$ (Tl1212, $T_c = 70 \sim 0$ K) in **part III**.

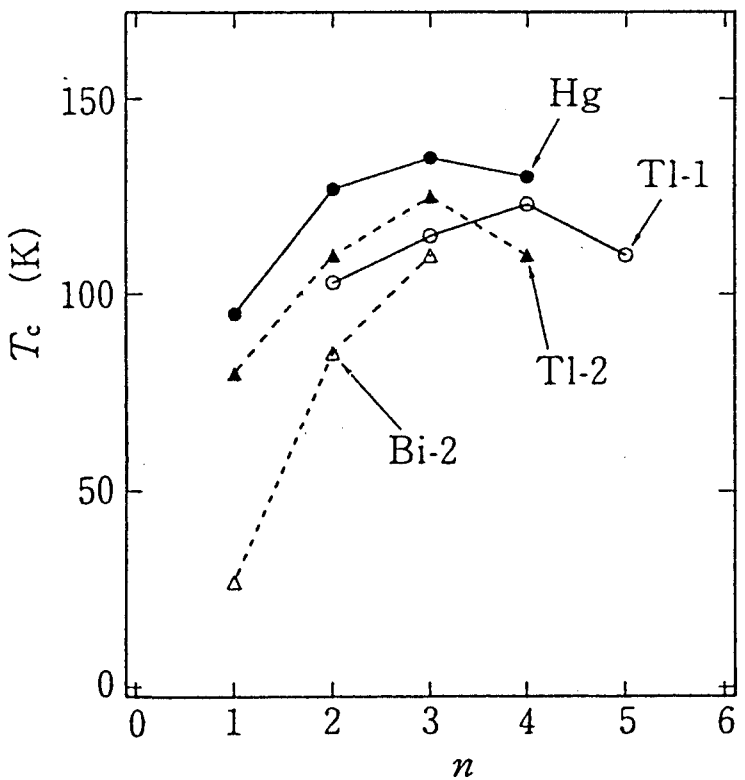

Fig.I-1(a). Relation between the number of CuO_2 sheets and T_c for Hg-, Tl- and Bi-based compounds.

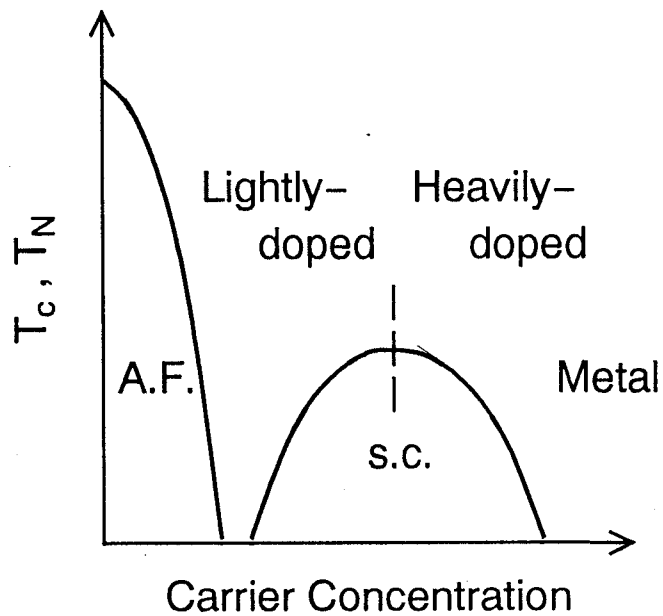

Fig.I-1(b). Schematic phase diagram for the high-T_c cuprates.

2 NMR Theory

A nuclear spin interacts with its electronic environment through electric and magnetic hyperfine couplings.[21] In the presence of an applied magnetic field, $\mathbf{H_0}$, the Hamiltonian of a nuclear spin, $\mathbf{I}$, having a quadrupole moment, eQ, can be written as

$$H = H_Z + H_Q + H_{hf} \tag{1}$$

with

$$H_Z = -\gamma_N \hbar H_0 [I_z \cos\theta + I_y \sin\theta \sin\phi + I_x \sin\theta \cos\phi] \tag{2}$$

$$H_Q = \frac{eQV_{zz}}{4I(2I-1)}[3I_z^2 - I(I+1) + \frac{\eta}{2}(I_+^2 + I_-^2)] \tag{3}$$

and

$$H_{hf} = \gamma_N \hbar (\sum_j \mathbf{I} \cdot \mathbf{A}_j \cdot \mathbf{S}_j + \mathbf{I} \cdot \mathbf{O} \cdot \mathbf{L}) \tag{4}$$

Here, $V_{\alpha\alpha}$ ($\alpha = x, y, z$) denote the principal components of the electric field gradient (EFG) tensor, $\mathbf{V}$, with the axes labeled according to the convention $|V_{xx}| \leq |V_{yy}| \leq |V_{zz}|$. The asymmetry parameter of $\mathbf{V}$, η, is defined as $\eta = (V_{xx} - V_{yy})/V_{zz}$. For a particular site, x, y, z are chosen as the frame of reference in eqs.(1)–(4). For example, in all Y-Ba-Cu-O compounds due to symmetry, one permutation of the x, y, z set coincides with the orthorhombic a, b and c crystal axes. θ and ϕ are the polar and azimuth angles, respectively, of $\mathbf{H_0}$, in this crystal frame. $\mathbf{S}_j$ is the electron spin operator at the copper site, j, and $\mathbf{A}_j$ is its spin hyperfine tensor. In high-T_c cuprates, the sum over j includes only on-site copper and its first neighbors. $\mathbf{L}$ is the electron orbital angular momentum and $\mathbf{O}$ is its on-site orbital hyperfine tensor. γ_N is the nuclear gyromagnetic ratio.

Nuclear magnetic resonance (NMR) spectroscopy has proved to be a powerful tool in the study of high-T_c superconductors as being an element- and site-specific local probe. It has therefore been playing an important role in helping to understand the physical mechanism of superconductivity. Among the nuclei used for NMR studies of high-T_c superconductors, copper attracts most attention, since the CuO_2 planes are known to be responsible for superconductivity in these materials.

The analysis of NMR in the high-T_c family begins with the **Mila-Rice model**,[22] in which one assumes that there is only one spin degree of freedom which resides on the

planar Cu^{2+} sites (one-component model). $^{63}Cu^{2+}$ spins interact with this single copper spin degree of freedom via the following hyperfine Hamiltonian:

$$H_{MR} = {}^{63}\gamma_N \hbar \, {}^{63}\mathbf{I}(\mathbf{r}_i)[\mathbf{A}(\mathbf{r}_i)\mathbf{S}(\mathbf{r}_i) + \mathbf{B}\sum_{j}^{nn}\mathbf{S}(\mathbf{r}_j)] \tag{5}$$

where $\mathbf{A}$ is a tensor which represents the direct, on-site coupling of a nuclear ^{63}Cu spin to the Cu^{2+} spins, and $\mathbf{B}$ is the strength of super-transferred hyperfine coupling of the ^{63}Cu nuclei to the four nearest neighbor Cu^{2+} spins in the CuO_2 planes. $\mathbf{A}$ contains anisotropic dipole-dipole, spin-orbit and isotropic core polarization contributions for Cu-3d orbit, and $\mathbf{B}$ originates from isotropic 4s-Fermi contact interaction through the $Cu(3d_{x^2-y^2})$-$O(2p\sigma)$-Cu(4s) hybridization.

The single-component description of the NMR experiments in $YBCO_7$ has its basic justification in the observation by Alloul *et al.*[23] and Takigawa *et al.*[24] that the ^{63}Cu, ^{17}O and ^{89}Y Knight shifts see the same spin susceptibility.

2.1 Nuclear Quadrupole Frequency, ν_Q

In the absence of an applied or an internal magnetic field, the remaining H_Q gives rise to doubly degenerate energy levels between which NQR transitions can be induced. For copper, there exist two isotopes ^{63}Cu and ^{65}Cu both having spin 3/2 and thus two doubly degenerate $\pm 1/2$ and $\pm 3/2$ energy levels. For each isotope, a transition between these levels yields a single NQR signal at frequency

$$^{63,65}\nu_Q = \frac{e^{63,65}QV_{zz}}{2h}\sqrt{(1+\frac{1}{3}\eta^2)}. \tag{6}$$

The EFG tensor is a ground-state property of a crystal depending sensitively on the charge distribution in the material. In a semiempirical approach, one assumes that the tensor can be written as the sum of two terms, a **lattice** and a **valence** contribution:

$$V_{\alpha\alpha} = (1-\gamma_\infty)V_{\alpha\alpha}^{lattice} + V_{\alpha\alpha}^{valence} \tag{7}$$

where γ_∞ is the so-called Sternheimer antishielding factor.

The first contribution arises from all charges outside the ion under consideration. Using the point-charge model, this term is given by

$$V_{ij}^{lattice} = \sum_k q^k \left(\frac{3x_i^k x_j^k - \delta_{ij}\left|\vec{x}^k\right|^2}{\left|\vec{x}^k\right|^5}\right) \tag{8}$$

where q^k and x^k are the charge and the position of the k-th ion, respectively.

The second term in eq.(7) arises from nonfilled shells of the subject ion. For instantnce, in case of Cu^{+2} ions and taking into account only holes in the Cu $3d_{x^2-y^2}$ orbital, it can be written as follows:

$$V_{zz}^{valence} = \frac{4}{7}e\langle r^{-3}\rangle_{3d} \cdot n_{x^2-y^2} \tag{9}$$

where $n_{x^2-y^2}$ is the number of holes in the $3d_{x^2-y^2}$ orbital.

Because, in high-T_c cuprates, the positively charged on-site holes predominantly reside on the d-orbitals extending towards the negatively charged neighbor oxygen ions, the lattice and the valence contributions in eq.(7) have opposite sign.

2.2 Knight Shift, K

The magnetic coupling between the nuclear spin and its electronic environment as expressed by the hyperfine Hamiltonian, H_{hf} [eq.(4)], can be viewed as a coupling of the nuclear spin with a time dependent local magnetic hyperfine field, $H_L(t)$, generated by the electron spin and the electron orbital motion. The static part of $H_L(t)$, $\langle H_L(t) \rangle$, gives rise to a NMR line shift expressed by the magnetic shift, K_α, (which is usually called the Knight shift), whose components, in the x, y, z reference frame, can be decomposed in a T-dependent **spin** and an T-independent **orbital** part:

$$K_\alpha = K_{s,\alpha}(T) + K_{orb,\alpha} \tag{10}$$

In the high-T_c compounds, K_{orb} is predominantly temperature independent, whereas the temperature dependent K_s is expected to vanish in the superconducting state due to singlet spin pairing.

Each part of the K can be expressed by the respective hyperfine interaction and the static electron susceptibility as

$$K_{s,\alpha} = \frac{1}{g\mu_B} \sum_j A_{j,\alpha} \chi_{s,\alpha} \tag{11}$$

$$K_{orb,\alpha} = \frac{1}{\mu_B} O_\alpha \chi_{orb,\alpha} \tag{12}$$

where χ_s and χ_{orb} are the local spin and orbital (Van Vleck) susceptibility at an atomic site, respectively.

According to the Mila-Rice Hamiltonian,[22] the ^{63}Cu spin Knight shift component, $^{63}K_s$, in high-T_c cuprates is expressed as follows:

$$^{63}K_{s,\alpha} = \frac{(A_\alpha + 4B)}{N\mu_B} \cdot \chi_s(T) \qquad (\alpha = ab, c) \tag{13}$$

where $\chi_s(T)$ is assumed to be isotropic. On the other hand, χ_{orb} is expressed as follows:

$$\chi_{orb,\alpha} = 2\mu_B^2 w \sum \frac{\langle e | L_\alpha | g \rangle^2}{E_e - E_g} \tag{14}$$

where e, g and w denote the excited state, the ground ($= d_{x^2-y^2}$) state and the weight of the ground state in the Cu-O covalent bond, respectively.

2.3 Nuclear Spin-Lattice Relaxation Rate, $1/T_1$

The fluctuating part of $H_L(t)$, $\delta H_L(t)$, is the source of the nuclear spin-lattice relaxation. In the case of high-T_c compounds, the main contribution to the copper spin-lattice relaxation stems from the electron spin fluctuations. This contribution is related to the imaginary part of the dynamical spin susceptibility, $\chi''(q,\omega_0)$,[25] and the relaxation rate per temperature unit, $(T_1T)^{-1}$, is given by

$$(\frac{1}{T_1T})_\alpha = \frac{\gamma_N k_B}{2\mu_B^2} \sum_{q,\alpha' \neq \alpha} |A_{\alpha'}(q)|^2 \frac{\chi''_\alpha(q,\omega_0)}{\omega_0} \tag{15}$$

$$A_\alpha(q) = \sum_j A_{j,\alpha} \exp(i\mathbf{q} \cdot \mathbf{r_j}) \tag{16}$$

Here, ω_0 is the nuclear resonance frequency. α denotes the direction of quantization, i.e. the direction of $\mathbf{H_0}$ in NMR experiment, and α' is the direction perpendicular to α. A_j is the on-site ($r_j = 0$) and the transferred ($r_j \neq 0$) hyperfine coupling tensor for the nuclei under consideration. Thus, relaxation rate per temperature unit provides information about the q averaged imaginary part of $\chi(q,\omega)$.

According to the Mila-Rice Hamiltonian,[22] $(1/T_1T)$'s of ^{63}Cu are given as follows:

$$\begin{aligned} {}^{63}(1/T_1T)_c &= \frac{{}^{63}\gamma_N^2 k_B}{2\mu_B^2} \sum_q F_{ab}(q)^2 \frac{\chi''(q,\omega_0)}{\omega_0} \\ {}^{63}(1/T_1T)_{ab} &= \frac{{}^{63}\gamma_N^2 k_B}{4\mu_B^2} \sum_q [F_{ab}(q)^2 + F_c(q)^2] \frac{\chi''(q,\omega_0)}{\omega_0} \end{aligned} \tag{17}$$

The hyperfine form factors are given as follows:

$$\begin{aligned} F_{ab}(q) &= A_{ab} + 2B[\cos(q_x a) + \cos(q_y a)] \\ F_c(q) &= A_c + 2B[\cos(q_x a) + \cos(q_y a)] \end{aligned} \tag{18}$$

where a is the distance between Cu atoms.

It has been established that the **AF** spin fluctuations play the crucial role in $1/T_1$ of ^{63}Cu nuclei in high-T_c cuprates showing the superconductivity, whereas for other nuclei the contribution of the **AF** spin fluctuations is filtered away through the Mila-Rice hyperfine form factor.[26]

2.4 Nuclear Spin-Spin Relaxation Rate, $1/T_{2G}$

While the nuclear spin-lattice relaxation is caused by a low frequency spin excitations $[\chi''(q,\omega_n \rightarrow 0)]$, the static susceptibility $[\chi'(q,\omega = 0) \equiv \chi'(q)]$ gives rise to the indirect nuclear spin-spin coupling which causes the transverse nuclear spin relaxation.[27] Such Ruderman-Kittel-Kasuya-Yosida (RKKY) like indirect nuclear spin-spin coupling is written as $[a^{\alpha\alpha}(\mathbf{r}_{ij})]_{ind} I_i^\alpha I_j^\alpha$, where

$$[a^{\alpha\alpha}(\mathbf{r}_{ij})]_{ind} = -\frac{(^{63}\gamma_N\hbar)^2}{\mu_B^2}\sum_q [A_{\alpha\alpha}(q)]^2\chi'(q)\exp(i\mathbf{q}\cdot\mathbf{r_{ij}}) \tag{19}$$

$\mathbf{r}_{ij}$ is the vector connecting the two nuclear spins $\mathbf{I}_i$ and $\mathbf{I}_j$, $\chi'(q)$ is the static q-dependent susceptibility, and α is the direction of the magnetic field. Such coupling causes the transverse nuclear spin relaxation. The transverse nuclear relaxation rate, $1/T_{2G}$, is related to the nuclear spin-spin coupling constant and can be approximated by a Gaussian, $\exp[-(1/2)(t/T_{2G})^2]$, where

$$(\frac{1}{T_{2G}})^2_{ind} = \frac{c}{8\hbar^2}\sum_{\mathbf{r}_{ij}}[a^{\alpha\alpha}(\mathbf{r}_{ij})]^2_{ind} \sim \sum_q [A_{\alpha\alpha}(q)]^4\chi'(q)^2. \tag{20}$$

and c is the natural abundance of the active NMR nuclei isotope. One can see that $(1/T_{2G})_{ind}$ is determined by $\chi'(q)$.

The measured relaxation rate contains the additional contribution from the direct dipolar coupling, $a_{ij}^{\alpha\alpha} = (a_{ij}^{\alpha\alpha})_{ind} + (a_{ij}^{\alpha\alpha})_{dip}$, neglecting the interference term, as follows:

$$(\frac{1}{T_{2G}})^2 = (\frac{1}{T_{2G}})^2_{ind} + (\frac{1}{T_{2G}})^2_{dip} \tag{21}$$

where the suffices *ind* and *dip* stand for the contributions of the indirect and dipole coupling, respectively, and the summation over j is taken for the lattice. If only the nuclear dipole-dipole interaction contributes to $1/T_{2G}$, the results should be temperature independent with a much slower rate due to the smaller dipolar coupling constants.

In high-T_c cuprates, the c-axis component of the indirect nuclear spin-spin coupling dominates $1/T_{2G}$, because ab-components of indirect coupling are much smaller than the c-component due to the anisotropy of hyperfine coupling. Thus, it is clear that one obtains information about the q-dependence of $\chi'(q)$ from the measurement of $1/T_{2G}$.

2.5 Quasi-particle Density of States in the Superconducting State

2.5.1 s-wave

In BCS superconductor mediated by electron-phonon interaction, the energy gap opens over an entire region on the Fermi surface. Since the energy of the quasiparticle is $E^2 = \epsilon^2 + \Delta^2$ with ϵ and Δ being one electron energy measured from the Fermi energy and superconducting energy gap, respectively, the density of states in the superconducting states, $N_{BCS}(E)$, is known to be given by

$$\begin{aligned} N_{BCS}(E) &= N_0 \frac{E}{\sqrt{(E^2 - \Delta^2)}} \qquad \text{for} E \geq \Delta \\ N_{BCS}(E) &= 0 \qquad \text{for} E \leq \Delta \end{aligned} \tag{22}$$

where N_0 is the density of states in the normal state, shown in Fig.I-2(a). Therefore, various physical quantities obey an **exponential-law** well below T_c. A coherence effect of quasiparticle scattering inherent to the singlet paired state plays an important role near T_c.

2.5.2 d-wave

The gap function of d-wave pairing $\Delta(\theta, \phi)$ is complicated, with zero on points and/or lines on the Fermi surface and then the sign of the order parameter changes in the q-space, reflecting the q-dependence of the effective pairing interaction. For example, the order parameter of 2D d-wave pairing with $d_{x^2-y^2}$ symmetry is given by

$$\Delta_{\vec{q}} \propto \cos(q_x) - \cos(q_y) \tag{23}$$

The density of states, $N(E)$, is shown in Fig.I-2(b). It is noteworthy that $N(E)$ exhibits a logarithmic divergence at the gap edge, whereas it is proportional to $\sim E$ at low energy.

It is a common property of superconductivity due to anisotropic pairing that $N(E)$ in the quasiparticle excitation spectrum gives rise to a **power-law** in the low-temperature behavior of various physical quantities instead of the exponential one for the conventional s-wave superconductor. In high-T_c cuprates, there are a number of evidences that the energy gap vanishes on lines at the Fermi surface.

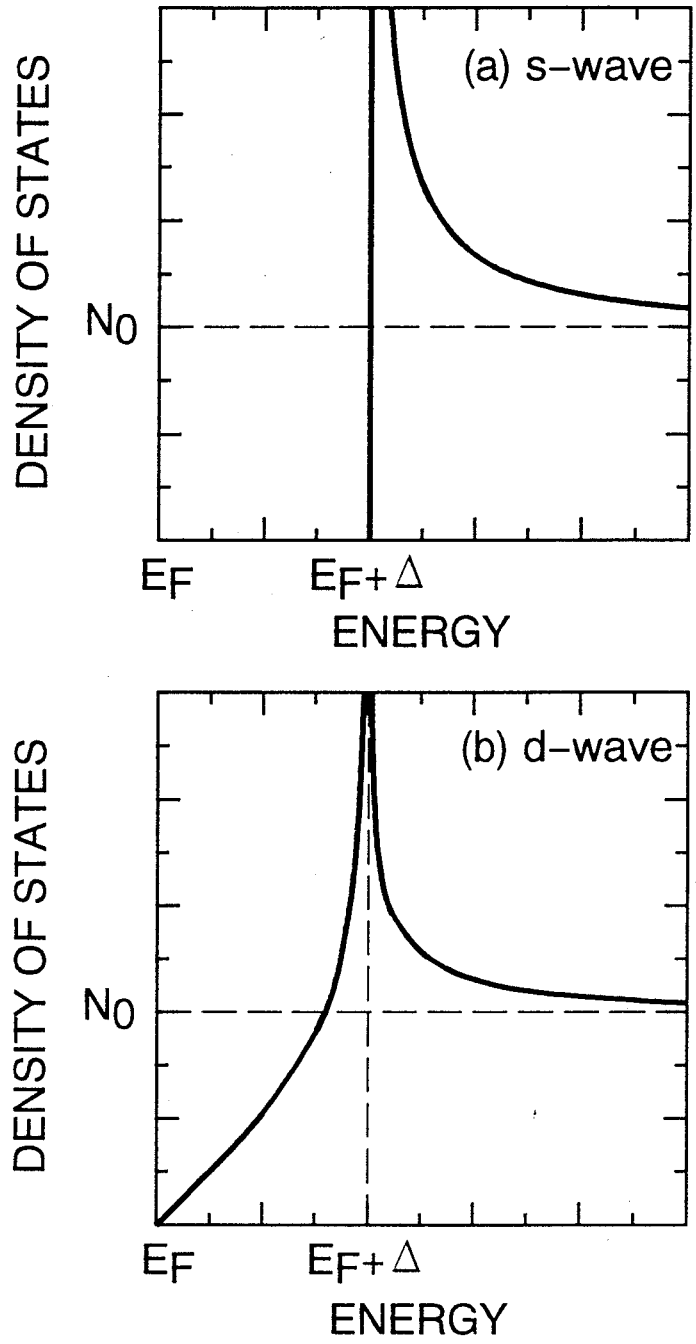

Fig.I-2. Densitiy of states for (a)s- and (b)d-wave model.

2.6 T-dependences of K and $1/T_1$ in the Superconducting State

The Knight shift is the only convenient measure of the local spin susceptibility reflecting the symmetry of the order parameter, since diamagnetic shielding by supercurrents overwhelms all other contribution to the bulk susceptibility. In the presence of applied field, $\mathbf{H_0}$, the spin magnetization, M_s, i.e. the difference in the number of spin-up and -down quasiparticles, is

$$M_s = \mu_B(n_\uparrow - n_\downarrow) = \mu_B \sum_k [f(\epsilon_k - \mu_B H_0) - f(\epsilon_k + \mu_B H_0)] = -2\mu_B^2 H_0 \sum_k \frac{df(\epsilon_k)}{d\epsilon_k}, \quad (24)$$

where $f(\epsilon_k)$ is the Fermi distribution function for an electron of energy ϵ_k measured from the Fermi level. Then

$$\chi_n = \frac{M_s}{H_0} = -2\mu_B^2 \int_{-\infty}^{\infty} N(E)[\frac{df}{d\epsilon}]dE = 2\mu_B^2 N_0 \quad (25)$$

In a singlet s- or d-wave superconducting state, since all ground state pairs contribute nothing to the spin susceptibility, the populations are given by a $f(E_k)$ with the excited-state energy, E_k.

It is usually assumed[28] that the susceptibility of the superconducting state, χ_s, is related to the normal-state susceptibility, χ_n, which is taken as temperature independent, via

$$\chi_s(T) = Y_l(T)\chi_n, \quad (26)$$

where

$$Y_l(T) = \int_{-\infty}^{\infty} N_l(E)[-\frac{df}{dE}]dE \quad (27)$$

is a function which depends on the angular momentum, l, involved in the pairing. $N_l(E)$ is the superconducting density of states. The Yosida function, $Y_l(T)$, determines the variation of the Knight shift with temperature. For $l = 0$, $Y_0(T)$ describes the conventional BCS weak-coupling spin-singlet s-wave mechanism.[29]

For the conventional BCS superconductor, $Y(T)$ dies off exponentially like $Y(T) \sim \exp(-\Delta/k_B T)$ at low temperature; on the other hand, for a gapless superconductor with a line of nodes on the Fermi surface, the density of states is proportional to the energy ($\propto E$) at small energies and the Yosida function becomes zero in proportion to $\sim T$ at low temperature.

On the other hand, $1/T_1$ in the superconducting state is given as follows:

$$\begin{aligned}(1/T_1T) &\sim \sum_q \chi''(q,\omega)/\omega \\ &= \int_{-\infty}^{\infty} dE[-\frac{\partial f}{\partial E}][N^2(E)+M^2(E)],\end{aligned} \tag{28}$$

where $N(E)$ is the density of states

$$N(E) = \langle Re[E/(E^2-\Delta_k^2)^{1/2}]\rangle_{FS} \tag{29}$$

and $M(E)$ is called the anormalous density of states, defined by

$$M(E) = \langle Re[\Delta_k/(E^2-\Delta_k^2)^{1/2}]\rangle_{FS}, \tag{30}$$

by taking into account the **coherence factor** present for the s-wave state. For d-wave state, e.g. 2D $d_{x^2-y^2}$ symmetry, owing to the weak divergence of $N(E)$ at the gap edge together with the absence of $M(E)$ because $\langle\Delta_k\rangle_{FS}=0$ due to $\Delta(\vec{q}+\vec{Q}) = -\Delta(\vec{q})$ where $\vec{Q}=(\pi,\pi)$, the coherence peak becomes small, being zero when Δ/k_BT_c is large.

Also, for the d-wave states, the density of states is proportional to the energy at low energies so that we expect a spin-relaxation rate $1/T_1 \sim T^3$ at low temperature; for the s-wave states, it vanishes exponentially.

3 Experimental Procedures

3.1 NMR Apparatus and Measurements

^{63}Cu NMR measurements were performed in a T-range of 1.4−300 K and in the high magnetic field by use of the superconducting magnet (12 T at 4.2 K) to improve the signal to noise ratio.

High field NMR measurements of ^{63}Cu was performed in a cryostat shown in Fig.I-3. The cryostat enables us to control temperature between $T = 1.4 \sim 300$ K and apply field up to 12 T. The sample was set at the center of the superconducting magnet. The temperature was monitored by Pt thin film ($T \geq 30$ K) and carbon glass thermometer ($T \leq 30$ K). Inhomogeneity of the magnetic field at the center of the superconducting magnet is less than 10^{-5} Tesla. Thus, the precise measurement of the Knight shift is possible.

Spin-echo measurement was carried out by a conventional phase-coherent home-made pulsed spectrometer. The block diagram of the typical apparatus is shown in Fig.I-4. ^{63}Cu NMR spectrum arising from the $(1/2 \leftrightarrow -1/2)$ central transition was obtained using a boxcar integrator averaging spin-echo intensity by sweeping magnetic field. $1/T_1$ and $1/T_{2G}$ were measured by observing the spin-echo intensity after saturation pulse (saturation-recovery method).

In NMR experiment, the nuclear relaxation function, $m(t)$, for the $(1/2 \leftrightarrow -1/2)$ central transition of I = 3/2 among the quadrupolar spilit lines is expressed as follows:[30]

$$m(t) = [M(\infty) - M(t)]/M(\infty) = 0.9\exp(-6t/T_1) + 0.1\exp(-t/T_1) \tag{31}$$

where $M(t)$ is the nuclear magnetization at time t after saturation pulse. T_1 is obtained by a least square fitting to eq.(31). $1/T_1$ measurements for ^{63}Cu were made at $f = 125.1$ MHz in a wide T-range of $1.4 \sim 300$ K at a magnetic field of ~ 11 T parallel and perpendicular to the c-axis.

The spin-echo amplitude, E, recorded as a function of time, τ, between the first and second pulses, could be fitted to the expression[27]

$$E(2\tau) = E_0\exp[-\frac{2\tau}{T_{2R}} - \frac{1}{2}(\frac{2\tau}{T_{2G}})^2] \tag{32}$$

where T_{2G}, a fitting parameter, is the Gaussian component of the spin-echo decay rate due

to the spin-spin relaxation process (T_2 process), and T_{2R} is the Lorentzian-Redfield term, which stands for the decay rate due to the spin-lattice relaxation process (T_1 process). T_{2R}^{-1} was determined from the expression $T_{2R}^{-1} = (3 + R)T_1^{-1}$,[27, 31] where R is the anisotropy of the spin-lattice relaxation rate. T_{2G} measurements for ^{63}Cu were made at $f = 125.1$ MHz in a T-range of $130 \sim 300$ K at ~ 11 T parallel to the c-axis.

3.2 Sample Alignment

Cuprate oxides which show high-T_c superconductivity have layer structures, in which several kinds of oxide layers are periodically stacked along the c-axis. Physical properties in the layerd crystals are highly anisotropic. In this respect, single crystals are preferable in studies of the intrinsic properties. However, there are reports of growing single crystals of neither Hg1223 nor Tl1212 compound. Instead of using single crystals in this work, we have prepared c-axis-aligned powder sample of Hg1223 and/or Tl1212 to investigate the CuO_2 plane characteristics.

To obtain the c-axis-aligned powder sample, the method of Farrell *et al.*[32] was employed. The sintered single-phase superconducting pellets were ground to a powder with an average microcrystalline grain size of 20 μm for NMR measurements, mixed with the stycast 1266 epoxy in a sample case of diameter 6 mm with a typical powder to epoxy ratio of 1 : 2 and then aligned for 8 hours with an external magnetic field of $\sim$11 T at room temperature using anisotropic normal-state magnetic susceptibility.

In this work, powder samples and their characterizations of Hg1223 and Tl1212 are supplied by Ihara group in Electrotechnical Laboratory and Kubo group in Fundamental Research Laboratories, NEC Corporation, respectively.

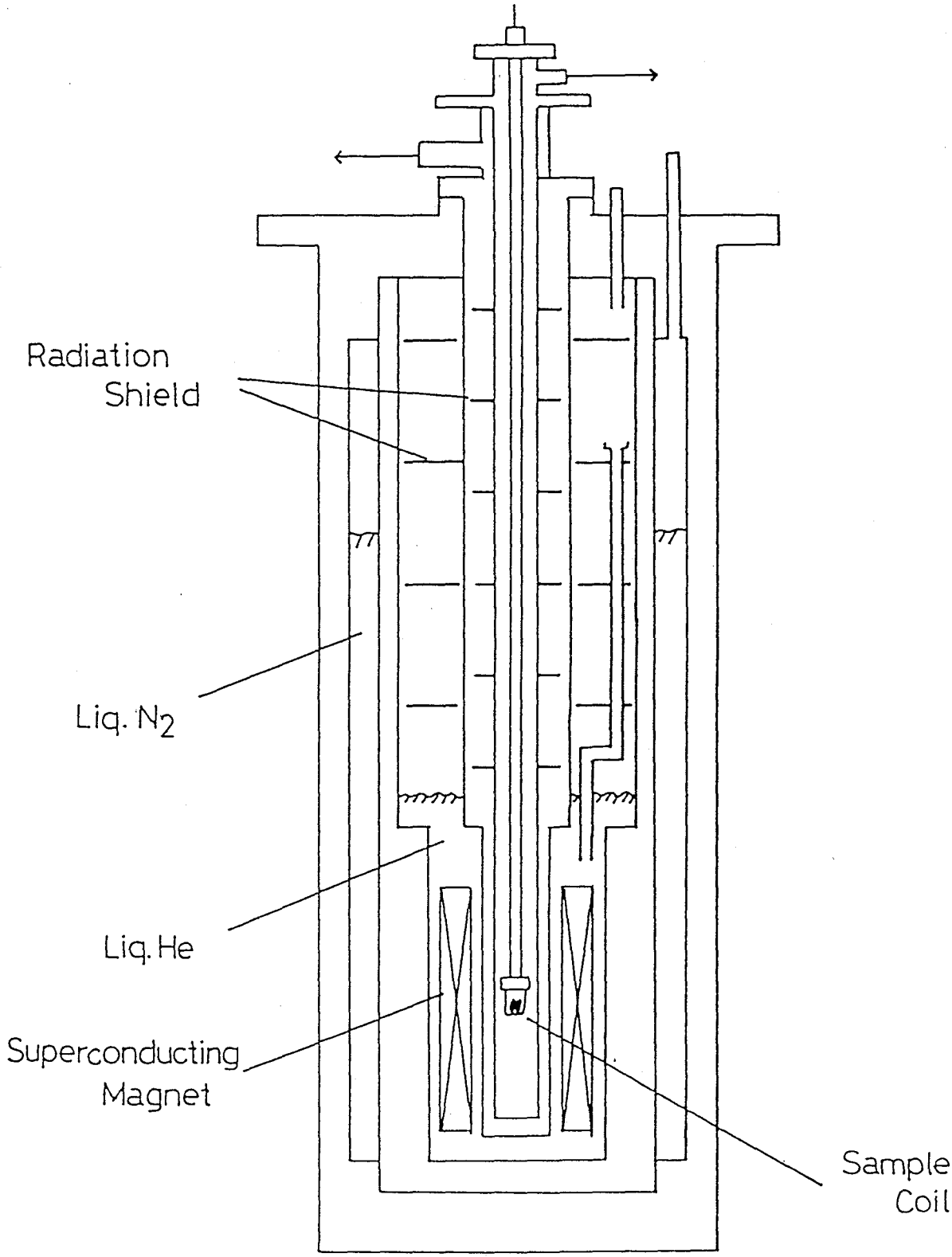

Fig.I-3. Cryostat for the high-field NMR.

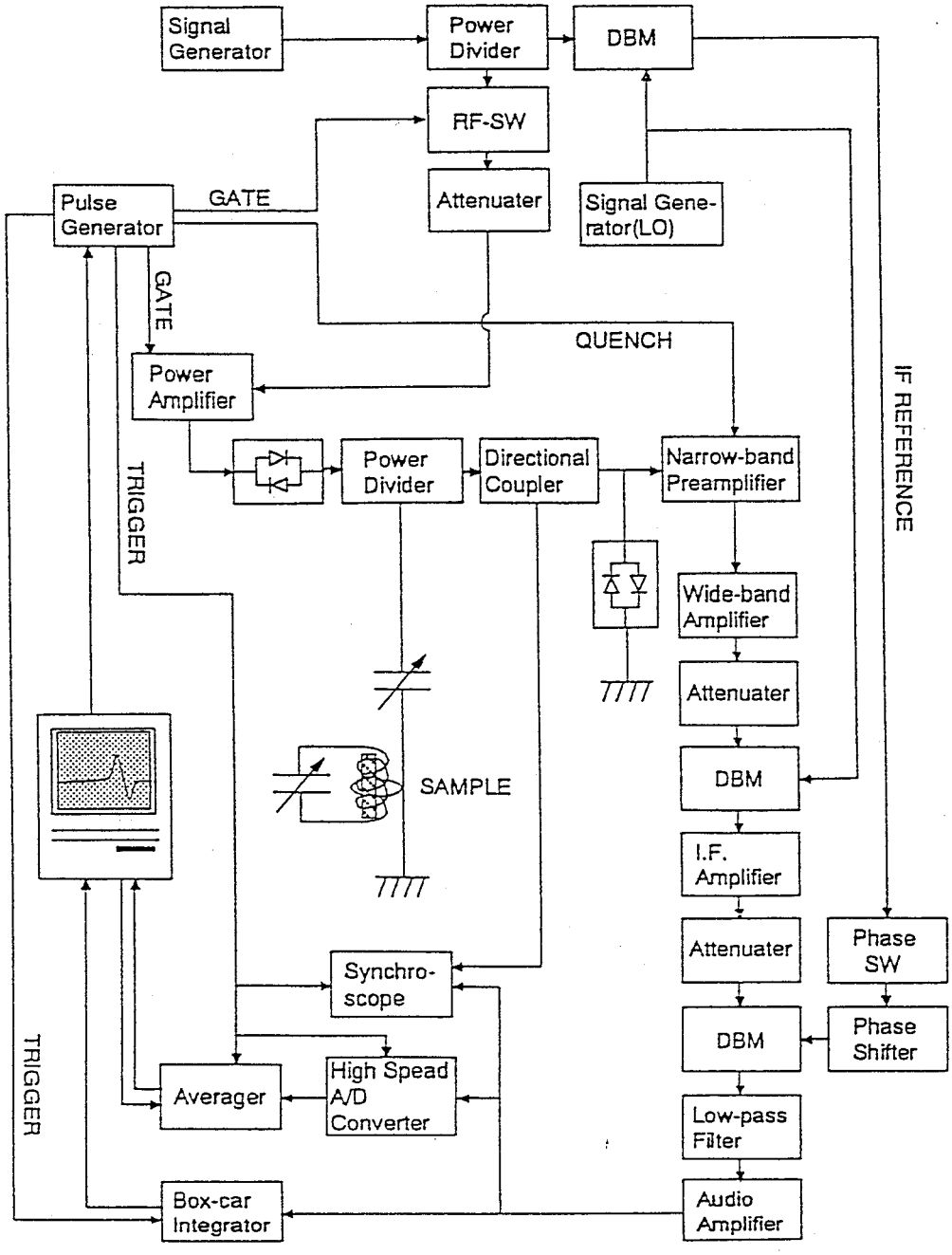

Fig.I-4. Block diagram of phase-coherent pulsed spectrometer.

Part II
^{63}Cu NMR Study of $HgBa_2Ca_2Cu_3O_{8+\delta}$ (Hg1223)

4 Introduction

Among the mercury-based homologous series of $HgBa_2Ca_{n-1}Cu_nO_{2n+2+\delta}$ (n=1,2,3,4) compounds, the n=3 member $HgBa_2Ca_2Cu_3O_{8+\delta}$ (Hg1223) has especially drawn much interest due to its highest superconducting transition temperature of T_c=133 K, the highest one known to date.[6] Furthermore, it was remarkable that T_c was largely enhanced to $\sim$ 150 K by applying pressure.[7] The Hg1223 system consists of three CuO_2 sheets, and there are two crystallographic copper sites, one of which has pyramidal ($5-fold$) layers, while another has a square ($4-fold$) layer sandwiched by two Ca layers.[33] Therefore, the Hg1223 system provides a good opportunity to investigate the relationship between T_c and the number and/or the type of CuO_2 sheets, i.e. the role played by each CuO_2 sheet in the mechanism of high-T_c superconductivity. It is well known that a key factor to increase T_c value is to increase the number of CuO_2 layers from one to three. It is, however, not fully understood why T_c in Hg1223 is so high as compared with the Bi- and Tl-based compounds comprising of three CuO_2 layers as well. To elucidate why T_c in this system is so high, i.e. what is the primary factor for T_c from a microscopic point of view, ^{63}Cu-NMR measurements of the Hg1223 system have been carried out.

In this part (**II**), in order to unravel the nature of spin correlation and superconductivity in Hg1223 with the highest T_c to date, it is focused on the nuclear quadrupole frequency, ν_Q, the Knight shift, K, the nuclear spin-lattice relaxation rate, $1/T_1$, and the transverse relaxation rate, $1/T_{2G}$, of ^{63}Cu for both the square and the pyramidal CuO_2 planes in a T-range of 1.4$\sim$300 K under a magnetic field of $\sim$ 11 T.

The rest of this part (**II**) is organized as follows. The next **section 5** contains the sample synthsis and characterization of Hg1223 compound. The experimental results in the normal and superconducting states, followed by discussions are presented and analyzed in the **section 6**, and a summary in the **section 7**.

5 Sample Synthesis and Characterization

5.1 Preparation and Crystal Structure

The Hg1223 single-phase sample was prepared with **the high-pressure synthesis technique.**[34] The source material for the high-pressure synthesis was a mixture of precursor materials of $Ba_2Ca_2Cu_3O_7$ and yellow HgO. The precursor materials were prepared by calcining a well-ground mixture of $BaCO_3$, $CaCO_3$ and CuO powders with a nominal composition at 930°C for 20 hours in O_2. After regrinding and mixing with yellow powdered HgO, the pressed pellets were sealed in a gold capsule of 4 mm diameter and 6 mm length. The sample capsule was heated in an internal graphite tube at 850°C for 1 hour under a pressure of 5 GPa. The sample was subsequently quenched to room temperature before the pressure was released. Finally, the sample was annealed at 300°C for 5 hours in flowing oxygen gas.

Judging from the powder X-ray diffraction pattern (XRD), the sample was close to the single phase of Hg1223 to a high degree having the **tetragonal** structure of the space group of $P4/mmm$, presented in Fig.II-1, with lattice constants of $a = 3.852$ $\AA$ and $c = 15.822$ $\AA$.[34] The crystal structure of this compound is very similar to that of the single-layer thalium compound, $TlSr_2Ca_2Cu_3O_{9-\delta}$. The only difference in the crystal structures between these two compounds is the amount of oxygen deficiency in the Hg-O plane as compared to that in the Tl-O plane. In the Hg1223 structure, the oxygen atom is nearly absent in the Hg-O plane in a stoichiometric composition. Defects within the Hg-O layers are found to determine the T_c of this compound.

The superconducting transion temperature, T_c, was determined as 133 K at the onset temperature of the diamagnetic signal appearing in ac-susceptibility.

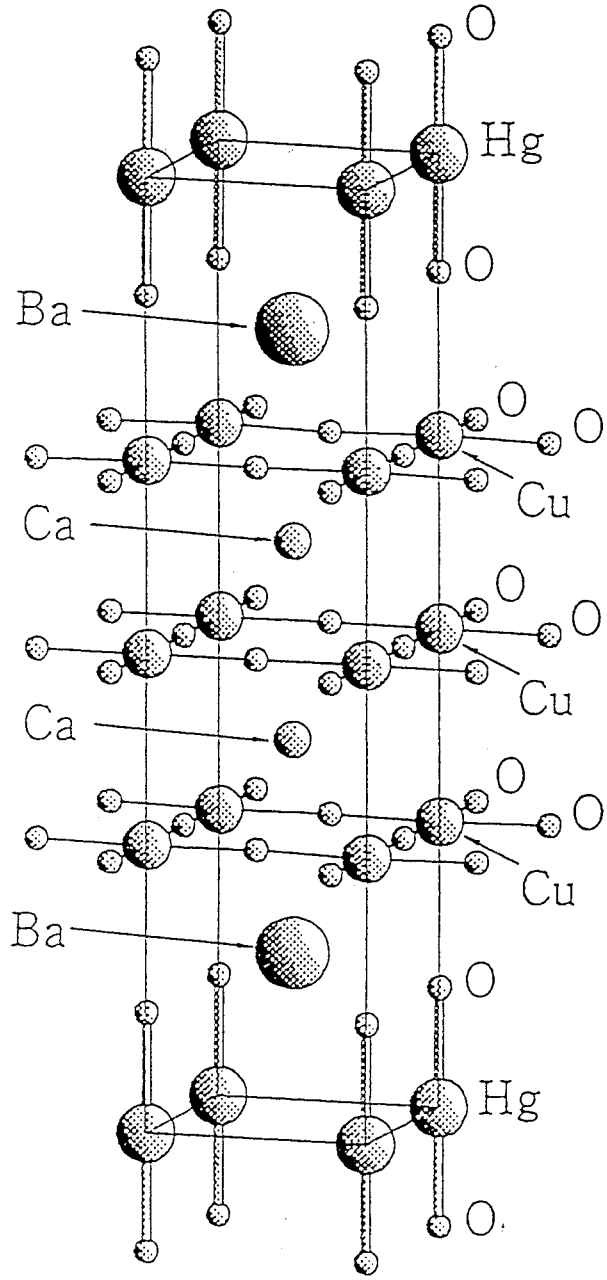

Hg-1223

Fig.II-1. Crystal-structure model of $HgBa_2Ca_2Cu_3O_{8+\delta}$ (Hg1223).

5.2 Characterization

Figure II-2(a) shows the temperature dependence of the resistivity for the sample annealed for 5 hours (open circles) in comparison with the preannealed sample (triangles).[34] The onset of T_c value of the annealed sample is 131.6 K, which is higher than that of 115.2 K for the preannealed sample. It is noted that the transition is sharp, and that the resistivity in the normal state has a linear relationship with the temperature for both samples. The resistivity of the annealed sample increased in comparison with the preannealed sample by a factor of three, which is caused partly by the decrease of carrier concentration. Annealing for 10 hours caused a resistivity higher by a factor of seven and a slight increase of T_c by 1.0 K in comparison with annealing for 5 hours.[34]

Figure II-2(b) shows the zero-field cooling (ZFC) magnetic susceptibility for the 5-hour-annealed sample, which shows an onset temperature of the superconducting transition of 131.7 K.[34] The onset temperature is in agreement with the onset value measured resistivity. In the external field of $H = 10$ Oe, the zero-field cooling susceptibility (ZFC) amounts to $\sim 30\%$ of $1/4\pi$ at $T = 10$ K. The value is smaller than the result of Schilling *et al.*[6] (100 %) by a factor of three. The field cooling susceptibility (FC), however, amounts to $\sim 25\%$ of $1/4\pi$ at $T = 10$ K, which is larger than that of Schilling *et al.*[6] (10 %) by a factor of two. Susceptibility decreases steeply and monotonically with the decrease of temperature. This indicates that the sample consists of a single superconducting phase of Hg1223.

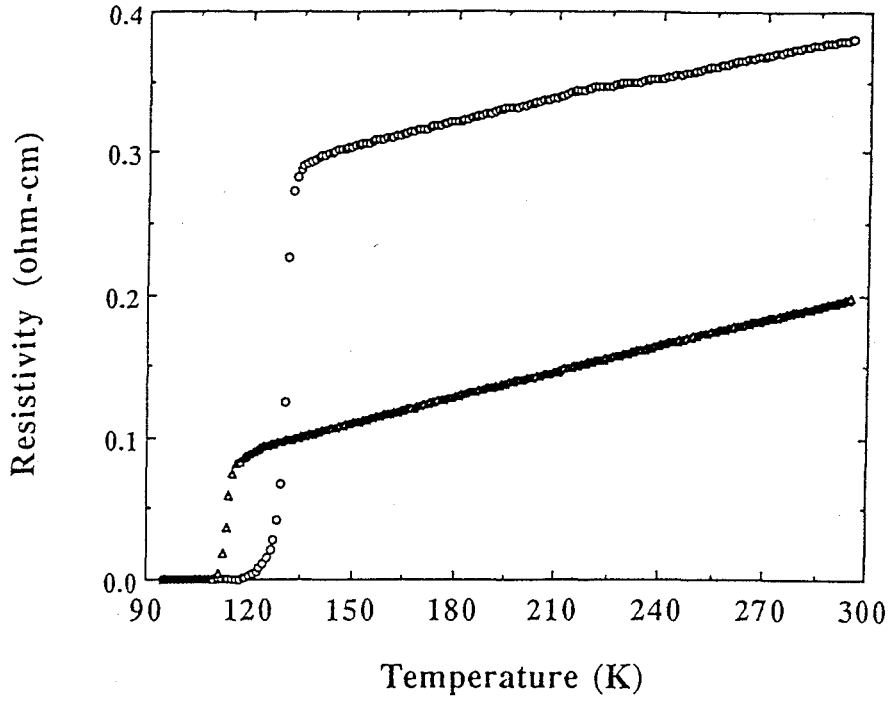

Fig.II-2(a). T-dependence of the resistivity for 5-hour-annealed Hg1223 sample (open circles) and the preannealed sample (triangles).[34)]

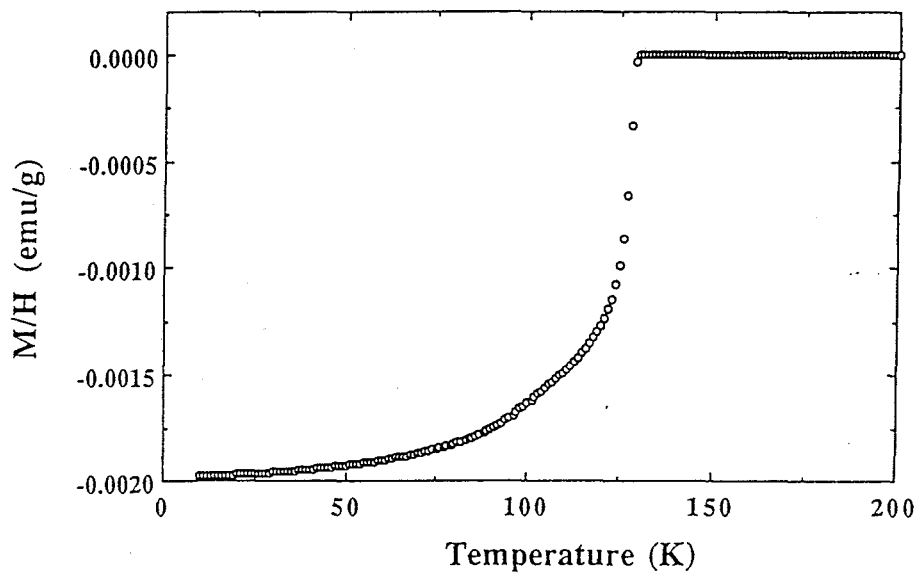

Fig.II-2(b). Zero-field cooling (ZFC) magnetic susceptibility for 5-hour-annealed Hg1223 sample, measured in $H = 10$ Oe.[34)]

5.3 Pressure Effect on T_c

Figure II-3 shows the pressure effect on the onset T_c, (T_{c0}), for the Hg1223 phase sample and the Hg1223 and 1234 mixed-phase samples A and B.[35] Mixed-phase sample B was measured after it was left for 1 week in a desiccator after being cut from the same lot sample as sample A. For mixed-phase sample A, T_{c0} has the highest value of 156 K at 25 GPa. The T_{c0} value of the present Hg1223 and Hg1234 mixed-phase sample A is higher than the value of the Hg1223 phase sample of Chu *et al.*[7] (153 K) by 3 K. The maximum T_{c0} of the Hg1223 single phase sample is 140 K at 13 GPa. The T_{c0} value of the present Hg1223 phase sample is, however, lower than the value of the Hg1223 phase sample of Chu *et al.*[7] by 13 K. The maximum T_{c0} of the mixed-phase sample B is 149 K at 25 GPa. The difference in the T_{c0}-P curve and rate of dT_{c0}/dP between mixed-phase sample A and B are caused by the deterioration due to the absorption of CO_2 and H_2O in air, because sample B was left in a desiccator for 1 week. The lower T_{c0} of the present Hg1223 phase compared with that of the Hg1234 mixed-phase is not caused by the deterioration. These results suggest that the sample of Chu *et al.*[7] probably contains some of the Hg1234 phase in addition to the Hg1223 phase.

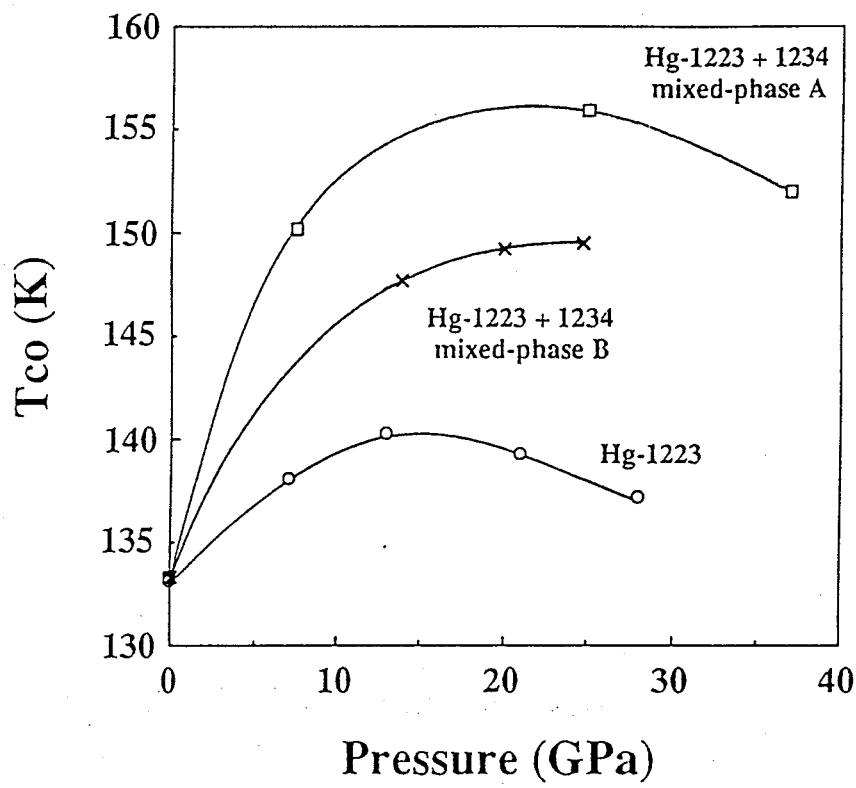

Fig.II-3. Pressure dependence of the onset T_c (T_{c0}) for the Hg1223 phase sample and Hg1223 and Hg1234 mixed-phase samples A and B.[35)]

6 Experimental Results and Discussions

6.1 Static Properties in the Normal State

6.1.1 ^{63}Cu NMR Spectra

Figures II-4(a) and (b) show the ^{63}Cu NMR spectra at $T = 140$ K and $f = 125.1$ MHz for the central transition $(1/2 \leftrightarrow -1/2)$ in partially-aligned powder with the c-axis parallel and perpendicular to the external magnetic field, H, respectively. In Fig.II-4(b), where $c \perp H$, there are two well-resolved peaks corresponding to two different Cu sites in the pyramidal and the square CuO_2 planes. On the other hand, in Fig.II-4(a), where $c \| H$, two peaks in lower field region arise from the oriented powder with the c-axis parallel to the field, while the broad spectrum with a single peak in higher field region is associated with the unoriented powder. This is because the spectrum for the unoriented powder is distributed with two peaks for each Cu site as denoted by arrows in Fig.II-4(a), where solid and dash arrows correspond to the peaks arising from grains with $\theta = 90°$ and 41.8° to the c-axis, respectively. As expected, the position of the single peak in high field region in Fig.II-4(a) coincides with that for the spectrum with the narrower linewidth in Fig.II-4(b) for $c \perp H$. From the integrated intensity ratio of the spectra with the two peaks in low field region to the broad spectrum with the single peak, a fraction of the oriented powder with the c-axis parallel to the field is anticipated to be $\sim 60\%$ of the whole powder. Furthermore, from the ratio of the relative integrated intensity of the well-resolved two spectra for the oriented powder, i.e. of the sharp to broad NMR line being about one-second, it is deduced that the higher- and the lower-field peaks are assigned to $4-$ and $5-fold$ Cu sites, respectively, because the number of Cu site for the former is one-second of that for the latter.

The full-width at the half-maximum (FWHM) of the NMR spectra for $c \| H$ are relatively narrow with about ~ 80 and ~ 130 Oe for $4-$ and $5-fold$ sites, respectively, assuring that the sample possesses better quality than Bi-[36] and Tl-based compounds.[15, 37, 38]

For $c \perp H$, it is likely that the spectrum for each Cu site may overlap with the peaks for $\theta = 41.8°$ (dash arrows in Fig.II-4(a)) arising from the unoriented powder. However, since T_1 for $c \perp H$ has been determined with a single component as described later, some contribution to the spectrum from the unoriented powder is considered to be negligible if

any.

On the other hand, for $c||H$, it was not possible to measure T_1 for both Cu sites separately at low temperature because the spectrum for one Cu site overlaps with another upon lowering temperature below 60 K due to nearly the same value of the Knight shift, as seen in Fig.II-5(a), in contrast to the case of $c \perp H$, shown in Fig.II-5(b). Accordingly, the T-dependence of $^{63}(1/T_1)$ below T_c is presented only in case of $c \perp H$, as will be described in Sec.6.3.1.

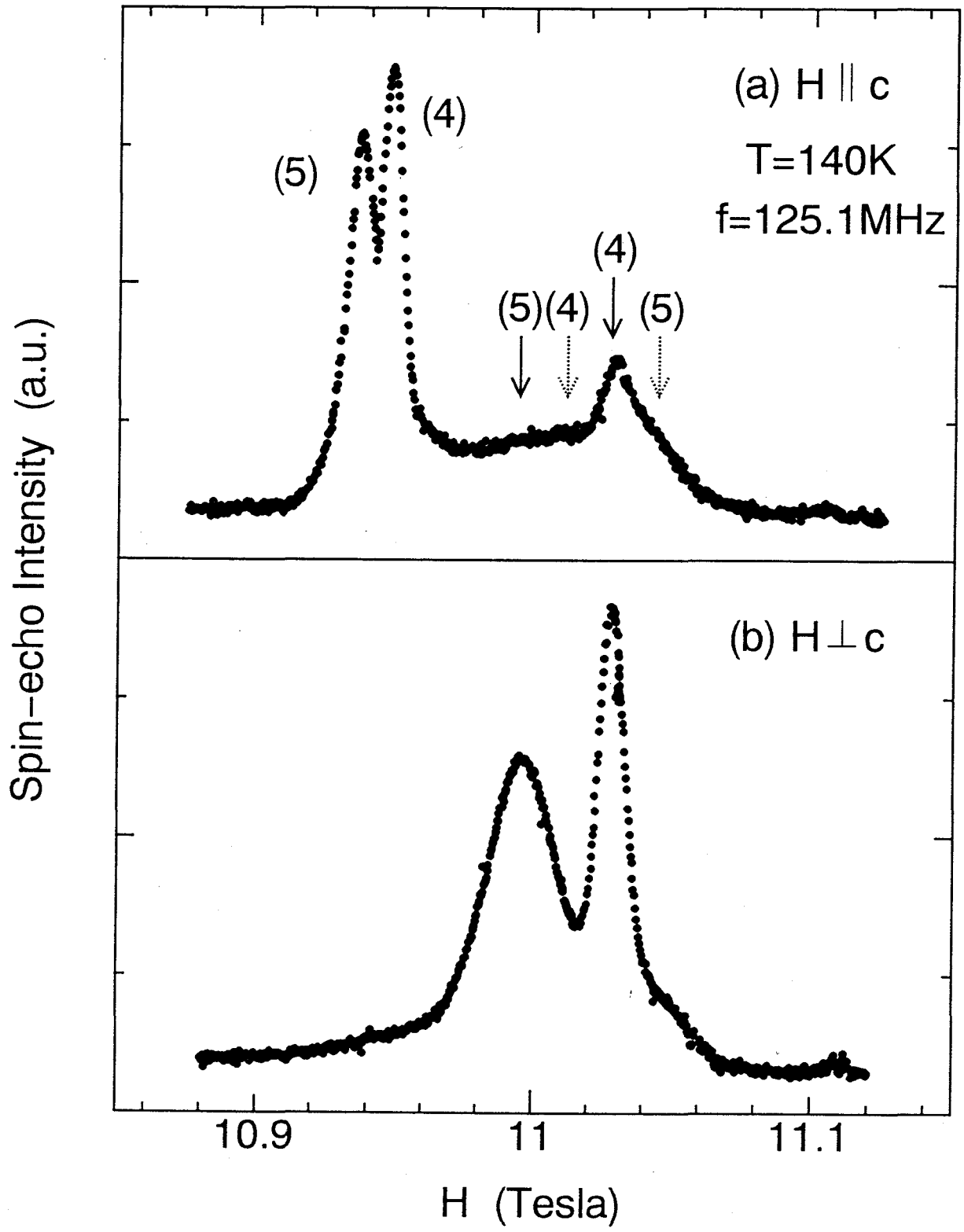

Fig.II-4. ^{63}Cu NMR spectra of Hg1223 at $T = 140$ K and $f = 125.1$ MHz for (a) $H \| c$ and (b)$H \perp c$, respectively. Solid and dash arrows correspond to the peaks arising from grains associated with the unoriented powder with $\theta = 90°$ and 41.8° to the c-axis, respectively.

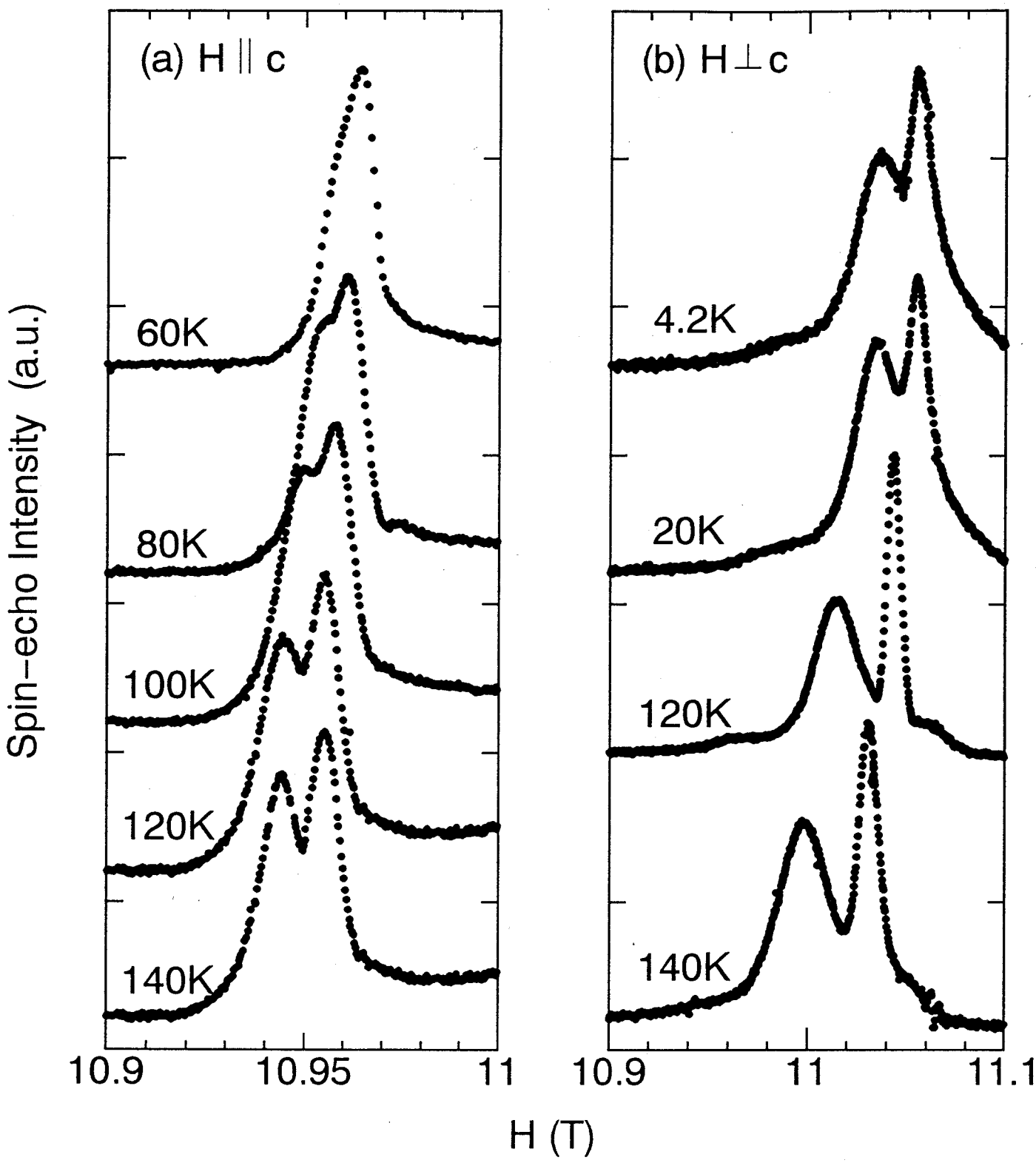

Fig.II-5. ^{63}Cu NMR spectra of Hg1223 at several temperatures below T_c for (a)$H \| c$ and (b)$H \perp c$, respectively.

6.1.2 $^{63}\nu_Q$ and Local Hole Density

The nuclear quadrupole frequency, ν_Q, for each Cu site was estimated from the analysis of the series of NMR spectra.

In the presence of a large external magnetic field, $\mathbf{H_0}$, i.e. $H_Q \ll H_Z$, the NMR signal is split into a central line arising from the central transition, $(1/2 \leftrightarrow -1/2)$, and into satellite lines for each isotope and each site. When H is perpendicular to the c-axis, the obtained shift consists of the Knight shift and the second-order quadrupolar shift. The Knight shift component, K_{ab} and ν_Q of ^{63}Cu can be expressed for the central transition $(1/2 \leftrightarrow -1/2)$ according to the second-order perturbation theory as follows:[21, 39]

$$\frac{\omega - \gamma_N H_{res}}{\gamma_N H_{res}} = K_{ab} + \frac{3\nu_Q^2}{16(1+K_{ab})(\gamma_N H_{res})^2} \tag{33}$$

where H_{res} is the field where the resonance is observed, γ_N is the nuclear gyromagnetic ratio and ω is the NMR frequency, respectively. K_{ab} and ν_Q were determined from the extrapolation to zero of $(\gamma_N H_{res})^{-2}$ and the slope of line, respectively. In order to determine the Knight and the quadrupolar shift separately, the measurements of the spectra have been performed at several different frequencies in a range of 80.1 $\sim$ 125.1 MHz, as seen in Fig.II-6. The shift was determined from the gravity of the spectra. The result of the Knight shift will be described in Sec.6.1.3. $^{63}\nu_Q$ are estimated to be $\sim$ 10.2 and $\sim$ 16.1 MHz for 4$-$ and $5-fold$ site, respectively. These $^{63}\nu_Q$'s are similar to those in Tl2223,[37] whose crystal structure is similar to that of Hg1223 system, and are the smallest values reported so far.

As mentioned in Sec.2.1, ν_Q probes the local hole density at each site. For high-T_c cuprates, the observed ν_Q is dominated by the contribution from the asymmetry of the on-site electron distribution, i.e. the Sternheimer antishielding factor, γ_∞, is negligible.[40] Schwarz *et al.*[40] indicated that the on-site contribution was from not only $3d_{x^2-y^2}$ holes but also 4p electrons. Thus, the observed $^{63}\nu_Q$ is related to the hole density, $n_{x^2-y^2}$, as follows;

$$^{63}\nu_Q = n_{x^2-y^2} \cdot {}^{63}\nu_{Q,0} + {}^{63}\nu_{4p} \tag{34}$$

$$^{63}\nu_{Q,0} = \frac{1}{2}\frac{e^{63}Q}{h}\frac{e}{4\pi\varepsilon_0}\frac{4}{7}\langle r^{-3}\rangle_d \tag{35}$$

where $^{63}\nu_{Q,0}$ (= 117 MHz) is the quadrupolar frequency due to one-hole state of $3d^9$ by using the Hartree-Fock value $\langle r^{-3}\rangle_d$ = 8.269 a.u..[41] ν_{4p} was estimated as -69 MHz by

Ohta *et al.*.[42] By using these values, $n_{x^2-y^2}$ was estimated as ~ 0.68 and ~ 0.73 for $4-$ and $5-fold$ sites, respectively, smaller than those in cuprates reported so far, in the range of $0.7 \sim 0.9$ such as La- and Y-systems.[43]

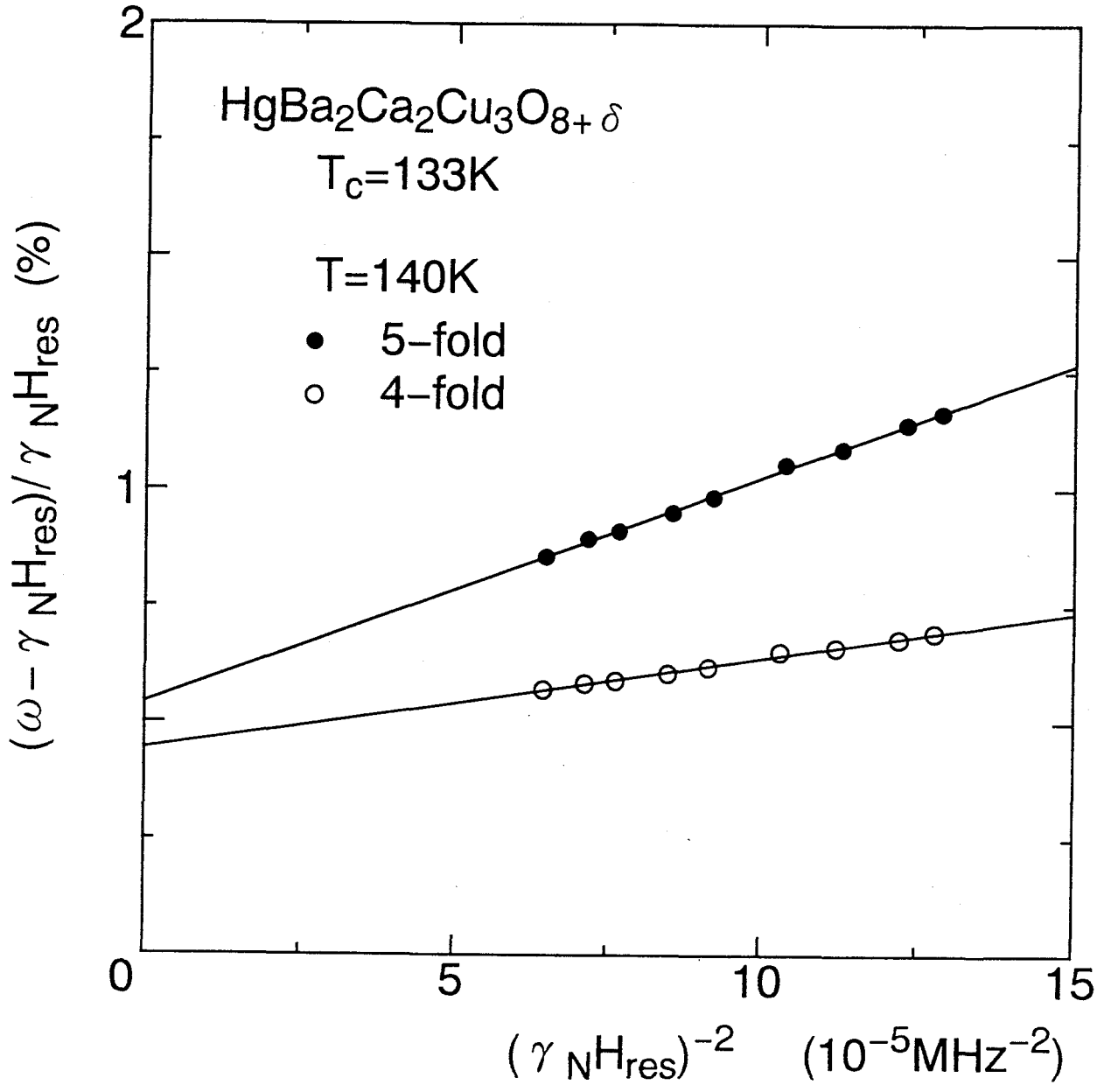

Fig.II-6. The value of $(\omega - \gamma_N H_{res})/(\gamma_N H_{res})$ is plotted against $(\gamma_N H_{res})^{-2}$ in the field perpendicular to the c-axis for different NMR frequencies. H_{res} is the field for resonance corresponding to $4-$ (o) and $5-fold$ (•) sites, respectively.

6.1.3 ^{63}K and Hyperfine Coupling Constants

Figure II-7 shows the T-dependence of the Knight shifts perpendicular, $^{63}K_{ab}$, and parallel, $^{63}K_c$, to the c-axis for 4− and $5-fold$ sites. In the normal state, $^{63}K_{ab}$ and $^{63}K_c$ decrease with decreasing temperature below around 250 K for both sites, which is similar to the behavior observed in Bi2212,[36] Tl2223[37] and ortho-Tl2201[38] as well, although the origin and the relationship to the superconducting are still unclear.

The T-decreasing behavior of $^{63}K_c$ is in contrast to the T-independence of $^{63}K_c$ in lightly-doped LSCO,[44] Y124[45] and $YBCO_{6+x}$.[24] For the latter, the T-independent orbital contribution dominates the K_c as a result of cancellation of the hyperfine field along the c-axis.

As seen in Fig.II-8, a linear relationship between $^{63}K_c(T)$ and $^{63}K_{ab}(T)$ is obtained as follows:

$$\begin{aligned} {}^{63}K_c(T) &= {}^{63}K_{ab}(T) \times 0.43 + 1.06 \qquad (4-fold) \\ {}^{63}K_c(T) &= {}^{63}K_{ab}(T) \times 0.48 + 1.09 \qquad (5-fold) \end{aligned} \tag{36}$$

From eq.(13), the observed linear relationship expressed by eqs.(36) leads to the following relationship:

$$\frac{\partial^{63}K_c}{\partial^{63}K_{ab}} = \frac{{}^{63}K_{s,c}}{{}^{63}K_{s,ab}} = \frac{A_c + 4B}{A_{ab} + 4B}. \tag{37}$$

$\partial^{63}K_c/\partial^{63}K_{ab}$ is obtained as ∼0.43 and ∼0.48 and then from these values, B is estimated to be $\sim$ 80 and $\sim$ 90 kOe/μ_B for 4− and $5-fold$ sites, respectively. Here the on-site hyperfine field is assumed to be the same as $A_{ab} \sim 37$ kOe/μ_B and $A_c \sim -170$ kOe/μ_B for lightly-doped compounds[24, 44, 45] and $YBCO_7$.[46, 47, 48] Remarkably, the supertransferred hyperfine fields, B's, for both sites in Hg1223 are larger than $B \sim 40$ kOe/μ_B in lightly-doped compounds[24, 44, 45] and $YBCO_7$,[46, 47, 48] similar to that for Bi-[36] and Tl-based compounds.[37, 38] This suggests that Cu($3d_{x^2-y^2}$)-O($2p\sigma$)-Cu(4s) hybridization is stronger than that in lightly-doped compounds and $YBCO_7$, since the B-term originated from the interaction from the neighbor Cu spins via the covalency effect between Cu and O.

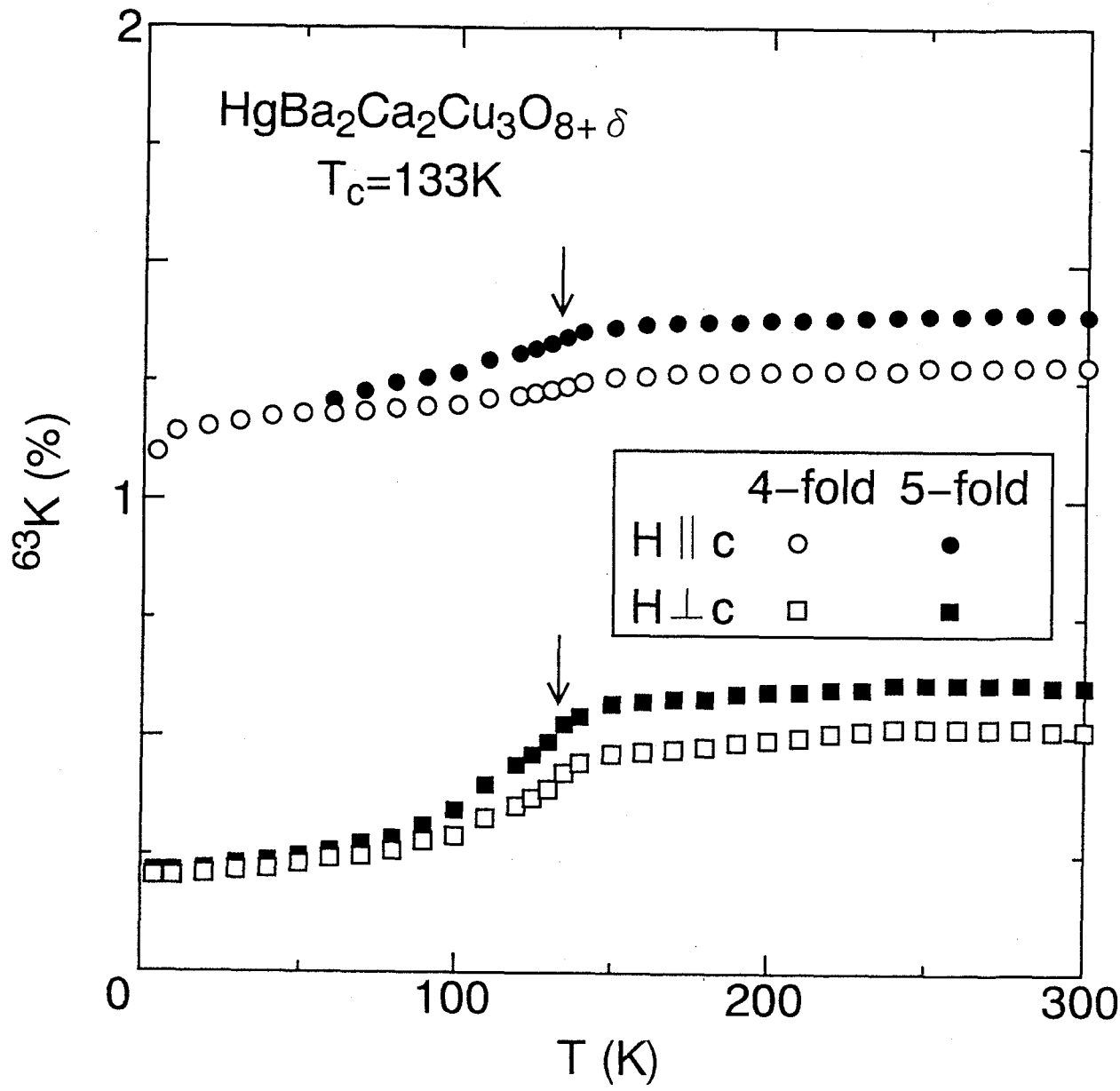

Fig.II-7. T-dependence of the Knight shift components parallel, ${}^{63}K_c(\circ, \bullet)$ and perpendicular, $(\square, \blacksquare)$ to the c-axis for $4-$ and $5-$ *fold* sites, respectively.

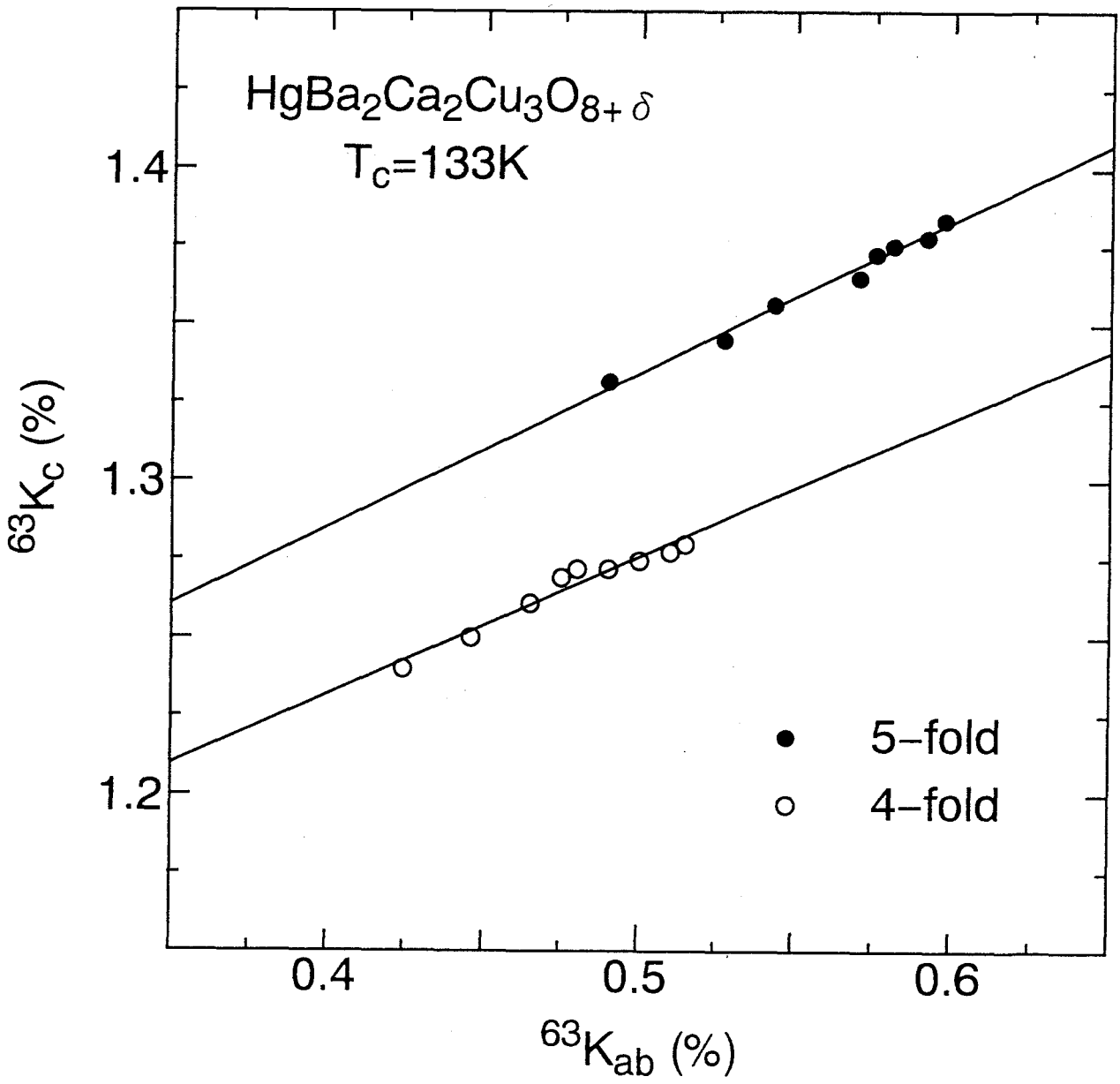

Fig.II-8. $^{63}K_c$ is plotted against $^{63}K_{ab}$ with T as an implicit parameter. The solid lines are obtained from the least squares fitting.

6.2 Character of Spin Fluctuation in the Normal State

6.2.1 $^{63}(1/T_1)$

Figures II-9(a) and (b) show the relaxation curve of $m(t)$ plotted against the time, t, after saturation pulse in Hg1223 at $T = 140$ K for $4-$ and $5-fold$ sites, respectively, under the magnetic field of ~ 11 T perpendicular to the c-axis. Solid lines in the figures are the best fit to eq.(31). As shown in figures, the data above T_c was well fitted by eq.(31) with a single T_1 component, suggesting that some contribution from the unoriented powder is considered to be negligible if any. Similarly, for $c\|H$, the data was also well fitted with single T_1 component above T_c, as seen in Figs.II-10(a) and (b) for $4-$ and $5-fold$ sites, respectively. It is suggested that the effect of overlapping with the spectrum for one Cu site with another one is also considered to be negligible. Thus, T_1 is estimated accurately for both cases of $c \perp H$ and $c\|H$ in the normal state.

Figure II-11 shows the T-dependences of $^{63}(1/T_1T)$ for $c \parallel H$ and $c \perp H$. As seen in the figure, $^{63}(1/T_1T)_c$ and $^{63}(1/T_1T)_{ab}$ have a broad peak around $T^* \sim$160 K (just above T_c), followed by a Curie-Weiss like behavior above T^* for both $4-$ and $5-fold$ sites. This Curie-Weiss like behavior of $^{63}(1/T_1T)$ is observed in most of high-T_c cuprates.

In genaral, for the nearly antiferromagnetic metal, $1/T_1T$ is dominated by the spin fluctuation around the staggered component, $\vec{Q} = (\pi, \pi)$, and as a result is proportional to the staggerd spin susceptibility, χ_Q, in two dimensional case. The Curie-Weiss like behavior for χ_Q is compatible with the prediction by the phenomenological treatments in the antiferromagnetic Fermi liquid model,[16] the self-consistent renormalization (SCR) theory[17] and the random phase approximation (RPA) with nesting Fermi surface for the Hubbard model[18] or the t-J model.[13] Recently, it is shown that the experimental Curie-Weiss-type T-dependence of the staggered spin susceptibility, χ_Q, at high temperatures is well reproduced by the SCR calculation but not by the RPA, from the quantitative analysis of the staggered spin susceptibility in $YBCO_7$ and Y124.[49] This result means that the experimental Curie-Weiss-type T-dependence of χ_Q for the high-T_c cuprates results from the SCR antiferromagnetic spin fluctuations through a mode-mode coupling. Therefore, the Curie-Weiss like behavior of $^{63}(1/T_1T)$ in Hg1223 probes the presence of the **AF** spin

correlations.

A strong signature of AF spin correlation with $Q = (\pi, \pi)$ is also supported by the anisotropy of the nuclear spin-lattice relaxation rate of ^{63}Cu shown in the inset of Fig.II-11, i.e. $^{63}R = {}^{63}(1/T_1T)_{ab}/{}^{63}(1/T_1T)_c$ being nearly T-independent with $^{63}R \sim 2.0$ and $\sim$1.9 for $4-$ and $5-fold$ sites, respectively.

In general, $1/T_1T$ is expressed by eq.(17). The q-dependence of the hyperfine form factors, see eq.(18), is shown in Fig.II-12. Therefore, ^{63}R reflects indirectly the q-dependence of spin fluctuations.[15, 48] Actually, ^{63}R is evaluated using A_α and B in two specialized cases. In case in which the spin fluctuations are largely dominated by the AF spin correlations around $Q = (\pi, \pi)$, from such an expression as

$$^{63}R_{AF} = \frac{(A_{ab} - 4B)^2 + (A_c - 4B)^2}{2(A_{ab} - 4B)^2} \tag{38}$$

$^{63}R_{AF}$ is calculated as 2 and 1.85 with B=80 and 90 kOe/μ_B for $4-$ and $5-fold$ sites, respectively. Provided that the spin fluctuations are q-independent, from such an expression as

$$^{63}R_r = \frac{(A_{ab}^2 + 4B^2) + (A_c^2 + 4B^2)}{2(A_{ab}^2 + 4B^2)} \tag{39}$$

$^{63}R_r$ is calculated as 1.5 and 1.4 as well. Apparently, the experimental values, $^{63}R = 2.0$ and 1.9 are close to the former case, as seen in Fig.II-13 together with the results for $YBCO_7$.[50] It is signaling that the $\chi''(q, \omega)$ at low energy prevails around $Q = (\pi, \pi)$.

When the dominant part of the spin fluctuations is the mode around the staggered component, $Q = (\pi, \pi)$, an expansion form may be used for the dynamical susceptibility[16, 17]

$$\chi(Q + q, \omega) = \frac{\chi_{Q+q}}{1 - i\omega/\Gamma_{Q+q}} \tag{40}$$

with

$$\begin{aligned} \chi_{Q+q} &= \chi_Q/(1 + q^2\xi^2) \\ \Gamma_{Q+q} &= \Gamma_Q(1 + q^2\xi^2) \\ \chi_Q &= \alpha\xi^2 \end{aligned} \tag{41}$$

where the parameters, χ_Q, Γ_Q, ξ and α are the staggered susceptibility, the characteristic energy of the spin fluctuations around $q = Q$, the magnetic coherence length and a scale

factor to relate χ_Q to ξ^2, respectively. This form is generic if the ground state is a Fermi-liquid state. Millis, Monien and Pines[16] and Monien, Pines and Takigawa[47] used this form to analyze the experimental data of $1/T_1$ in $YBCO_7$ and explained its behavior as well.

Assuming a Lorentzian form for the energy distribution as

$$\frac{\chi''(Q+q,\omega)}{\omega} = \frac{\chi_Q}{1+q^2\xi^2}\frac{\Gamma_q}{\omega^2+\Gamma_q^2} \tag{42}$$

for the system with strong AF spin correlations,

$$^{63}(1/T_1T)_c \simeq \frac{\gamma_N^2 k_B}{2\mu_B^2}(A_{ab}-4B)^2\frac{\chi_Q}{\Gamma_Q\xi^2}(\propto \alpha/\Gamma_Q) \tag{43}$$

is derived since $\omega \to 0$. In order to obtain information on the energy distributions of **AF** spin correlations in Hg1223, the T-dependence of $^{63}(1/T_1T)_c$ divided by the square of the form factor at $q = Q$, i.e. $(A_{ab}-4B)^2$ $(\propto \chi_Q/\Gamma_Q\xi^2)$, is shown in Fig.II-14, together with the results for $YBCO_7$.[4] It is found that $\chi_Q/\Gamma_Q\xi^2$'s in Hg1223 are more significantly suppressed than that in $YBCO_7$.

From the anisotropy and the Curie-Weiss law of $^{63}(1/T_1T)$, it is shown that the q-dependence of the spin fluctuations, i.e. χ_q **peaks around** $q = Q$ for both $YBCO_7$ and Hg1223, whereas from a considerable reduction of $^{63}(1/T_1T)_c/(A_{ab}-4B)^2$ in going from $YBCO_7$ to Hg1223, $\Gamma_Q\xi^2$ **is suggested to be significantly enhanced**. Namely, an enhancement of $\Gamma_Q\xi^2$ is anticipated to increase T_c from 93 K for $YBCO_7$ to 133 K for Hg1223.

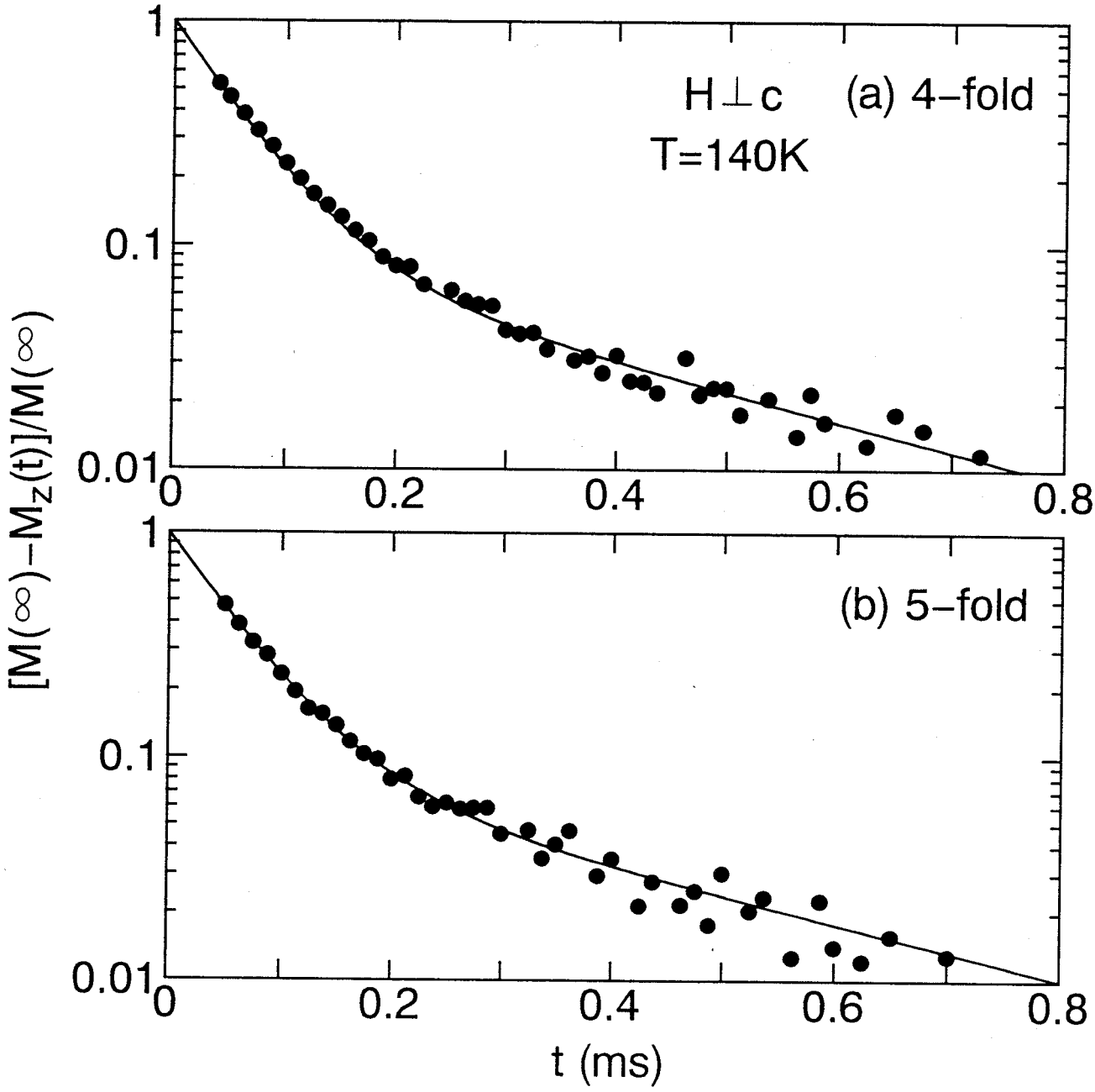

Fig.II-9. Relaxation curves plotted against t after saturation pulse for $H \perp c$ at $T = 140$ K for (a)4− and (b)5 − *fold* sites, respectively. Solid lines are the results fitted by the relaxation function of eq.(31).

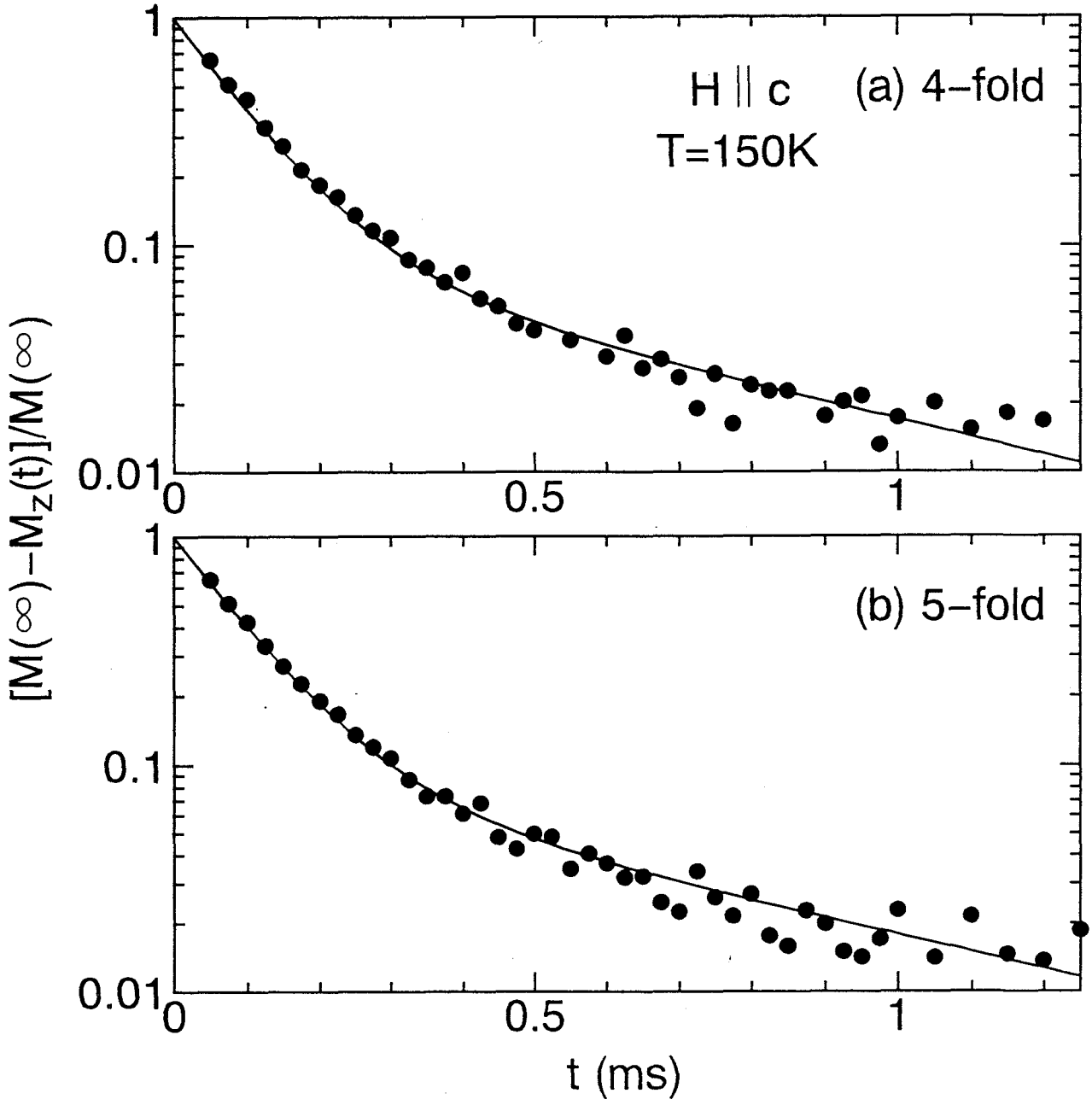

Fig.II-10. Relaxation curves plotted against t after saturation pulse for $H \| c$ at $T = 150$ K for (a)4− and (b)5 − *fold* sites, respectively. Solid lines are the results fitted by the relaxation function of eq.(31).

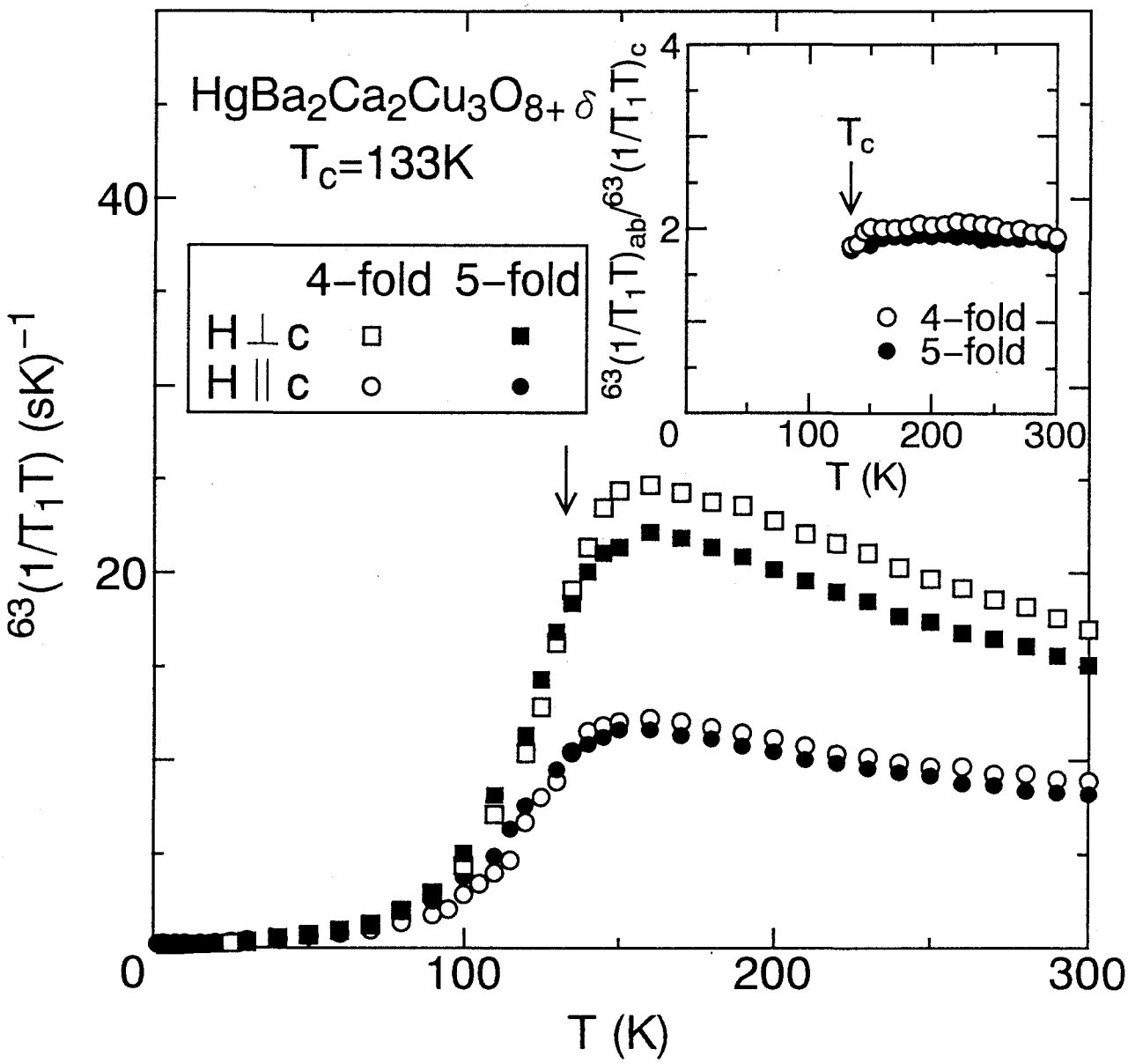

Fig.II-11. T-dependence of $^{63}(1/T_1T)$ for $c \| H(\circ, \bullet)$ and $c \perp H(\square, \blacksquare)$ for $4-$ and $5-fold$ sites, respectively. Inset indicates T-dependences of the anisotropy of $^{63}(1/T_1T)$, which is nearly T-independent for both $4-$ and $5-fold$ sites.

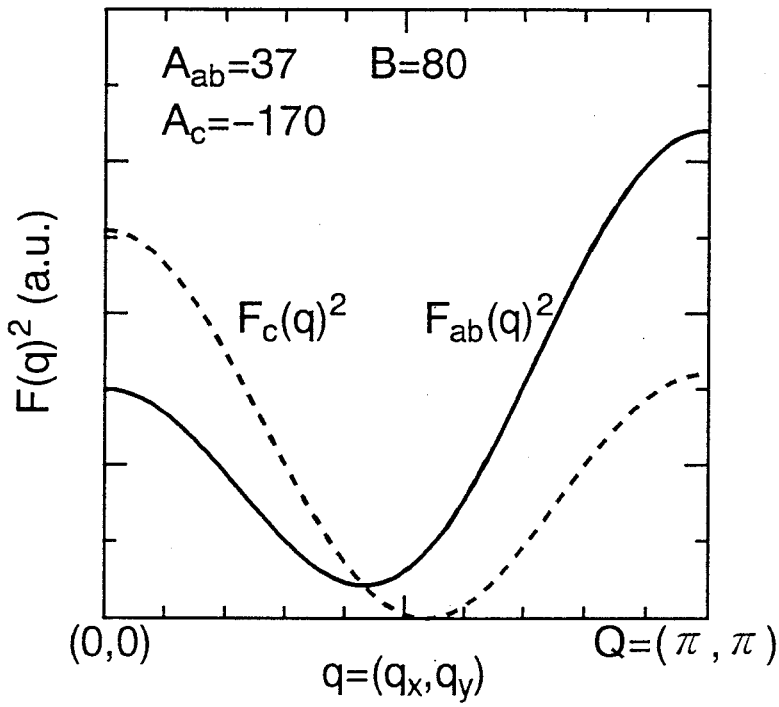

$$F_c(q)^2 = [A_{ab}+2B\{\cos(q_x)+\cos(q_y)\}]^2$$

$$F_{ab}(q)^2=[[A_c+2B\{\cos(q_x)+\cos(q_y)\}]^2+F_c(q)^2]/2$$

Fig.II-12. q-dependence of the hyperfine form factors, $F_{ab}(\mathbf{q})^2$ and $F_c(\mathbf{q})^2$.

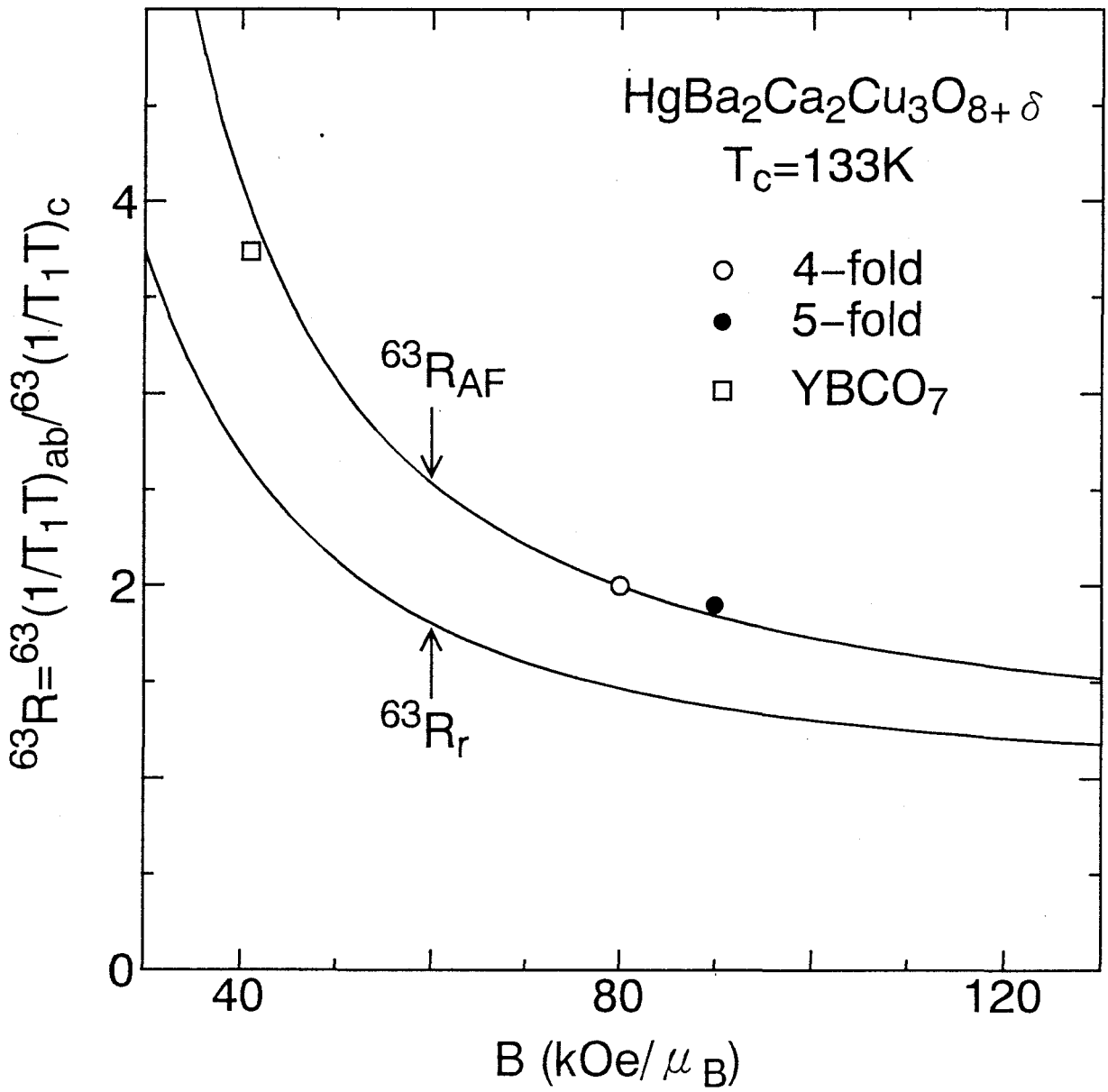

Fig.II-13. Anisotropy of $^{63}(1/T_1T)$, ^{63}R, for $4-(\circ)$ and $5-fold(\bullet)$ sites, respectively, plotted against the super-transferred hyperfine coupling constant, B, together with the result for $YBCO_7$ ($\square$).[50]

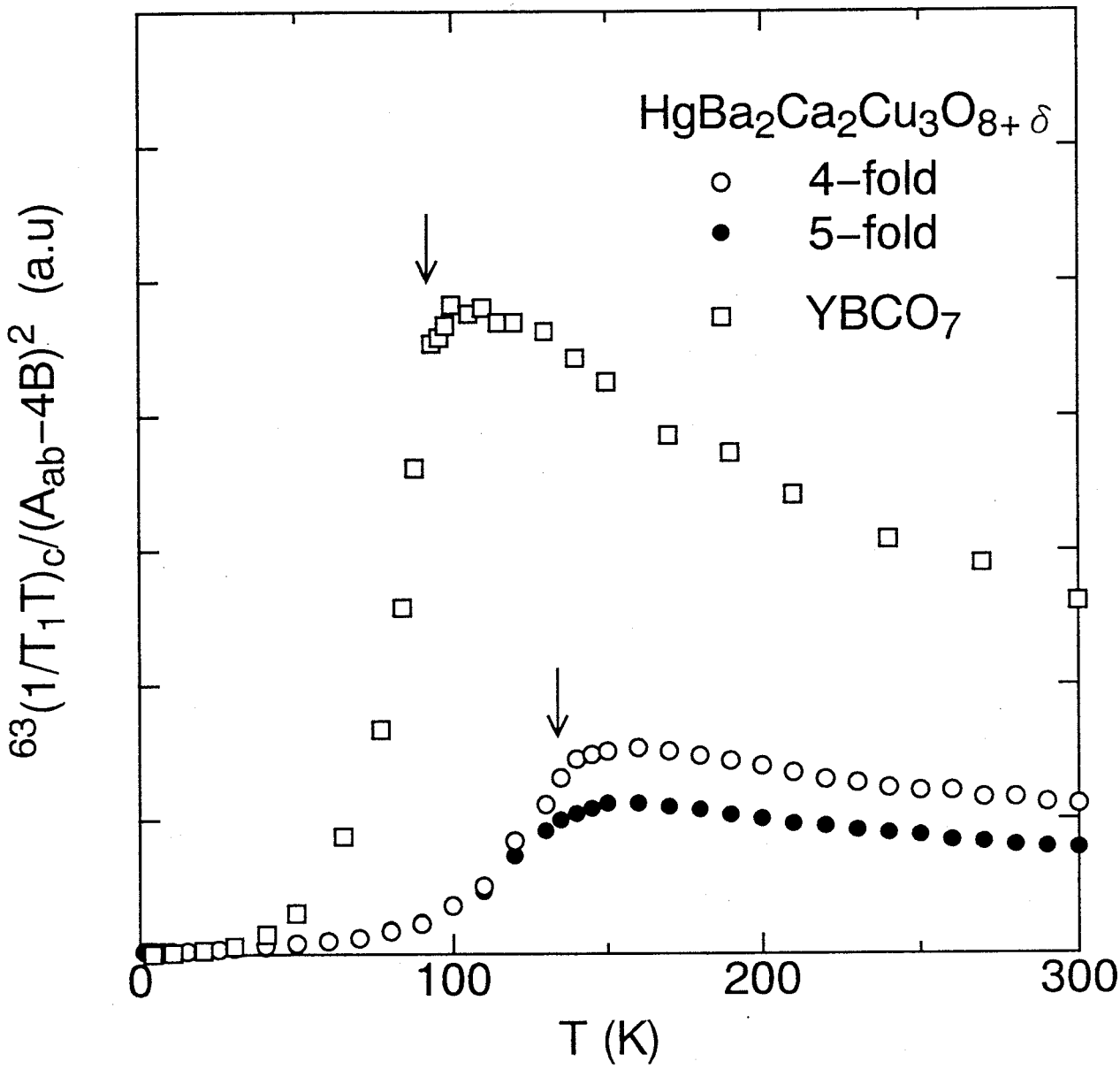

Fig.II-14. Comparison of the value of $^{63}(1/T_1T)_c/(A_{ab}-4B)^2$ in Hg1223, scaled approximately to $\sim \chi_Q/\Gamma_Q\xi^2$, with the result for $YBCO_7$.[4)]

6.2.2 $1/T_{2G}$

As demonstrated by Pennington *et al.*,[27] the measurement of the nuclear transverse relaxation rate, $1/T_{2G}$, provides an important information with respect to the static q-dependent spin susceptibility, χ_q, which is complementary to the information from the $^{63}(1/T_1T)$. A general expression for $1/T_{2G}$ is derived with the use of χ_q as[51, 52]

$$(\frac{1}{T_{2G}})^2 = \frac{0.69(\gamma_N\hbar)^4}{8\mu_B^4\hbar^2}[\sum_q F_c(q)^4\chi_q^2 - [\sum_q F_c(q)^2\chi_q]^2]. \quad (44)$$

By applying eq.(42) in the limit of large ξ to the above expression, the following expression is obtained as follows:

$$\frac{1}{T_{2G}} \simeq (\frac{0.69}{32\pi})^{1/2}\frac{\gamma_N^2\hbar}{\mu_B^2}\cdot(A_c - 4B)^2\frac{\chi_Q}{\xi}(\propto \alpha\xi) \quad (45)$$

Thus, $1/T_{2G}$ is related to $\propto \xi(T) \propto \sqrt{\chi_Q(T)}$.

Figure II-15 shows the ^{63}Cu nuclear spin-echo decay at $T = 140$ K for $4-$ (o) and $5-fold$ (•) sites, respectively, plotted against t, where t is the time interval between the $\pi/2$ pulse and the spin-echo. The spin-echo decay curves (the solid lines) was well fitted to eq.(32).

In order to determine $1/T_{2G}$ accurately, the line width of the NMR spectrum must be small compared with the rf-exciting field, because the nuclear spins are uniformly flipped by the exciting pulse. If the spin-excitation is incomplete, the spin-echo decay times comes to be longer. The strength of the rf-exciting field, H_1, used in the measurements are about $\sim$ 80 and $\sim$ 130 Oe for $4-$ and $5-fold$ site, respectively, estimated from the width of rf-pulse, which are the same value as each FWHM of ^{63}Cu NMR spectrum, and the fitting to the experimental points appears satisfactory, as seen in Fig.II-15. So, most of spins may be flipped. In practice, the H_1-dependece of $1/T_{2G}$ in the normal state is measured, and confirmed a saturated behavior for both sites.

Figure II-16 shows the T-dependence of $1/T_{2G}$ in Hg1223 for $4-$ (o) and $5-fold$(•) sites, respectively, together with the result for $YBCO_7$.[53] A remarkable feature is that $1/T_{2G}$ for both sites increase with decreasing temperature followed by a peak around $T^* \sim$ 150 K, which is almost the same temperature at which $^{63}(1/T_1T)$ shows a broad peak. This behavior is similar to that observed in Tl2223,[37] with similar crystal structure to Hg1223, but different from that in lightly-doped $YBCO_{6.63}$[51] and Y124,[54] showing a spin-gap like

behavior, where $1/T_{2G}$ continuously increases until just above T_c, while $^{63}(1/T_1T)$ shows a broad peak near $\sim$ 150 K.

As seen in eq.(45), ξ's for both sites increase with decreasing temperature down to T^*. It is suggested that the spin correlation grows stronger with decreasing temperature. Also, it is found that the magnutude of ξ for $4-fold$ site is larger than that for $5-fold$ one, if the scale factor, α, is invariable for both sites, as shown in the inset of Fig.II-16. It suggests that the spin correlation in the $4-fold$ CuO_2 plane is stronger than that in the $5-fold$ one, So, it is expected that the magnetic property in the $4-fold$ CuO_2 plane may be very important for the primary factor for higher T_c in Hg1223. This is in contrast with the electron-doped high-T_c compounds, such as Nd-system having only a square CuO_2 plane and a low value of T_c.

It was also confirmed that $(1/T_{2G})^2$ resembles the T-dependence of $^{63}(1/T_1T)$ with $^{63}(T_1T)_c/(T_{2G})^2$ being nearly constant as seen in Fig.II-17. Such a formula as

$$\frac{^{63}(T_1T)_c}{(T_{2G})^2} \simeq \frac{0.69(^{63}\gamma\hbar)^2F_c(Q)^2}{16\pi\mu_B^2\hbar k_B}(2\times^{63}R-1)(\chi_Q\hbar\Gamma_Q) \qquad (46)$$

derived for large ξ allows us to estimate the product of the characteristic energy and the staggered susceptibility of spin fluctuations at $Q=(\pi,\pi)$, $\chi_Q\hbar\Gamma_Q$ ($\sim \Gamma_Q\xi^2$). It should be noted that the $\chi_Q\hbar\Gamma_Q$ is estimated to be $\sim$ 5.4 and $\sim$ 3.1 for the square and the pyramidal CuO_2 planes in Hg1223, respectively (*e.g.* $\chi_Q\hbar\Gamma_Q$ = 3.5 for $YBCO_7$),[52, 53] as seen in the inset of Fig.II-17. It is remarkable that the value of $\chi_Q\Gamma_Q$ for the square site is larger than that for $YBCO_7$, although that for the pyramidal site is almost the same.

Zheng *et al.*[37] revealed, by analysing the T_1 and T_{2G} data in Tl2223 compound with triple CuO_2 sheets on the Millis, Monien and Pines (MMP) model, $\chi_Q=\chi_s\sqrt{\beta\xi^2}$,[16] where β is a scale factor, that $\chi_Q\hbar\Gamma_Q$ ($\sim$ 5.1) was larger than that in $YBCO_7$ and that, especially, Γ_Q was larger than that in $YBCO_7$, while ξ did not differ much from each other.

Moriya *et al.*[16] and Monthoux and Pines (MP)[55] showed that the cutoff energy for the effectiveness of the spin-fluctuation-induced attractive interaction for superconductivity scales with the value of the characteristic energy, Γ_Q, and the magnetic coherence length of the **AF** spin fluctuation, ξ. In MP's expression, $T_c=\Gamma_Q(\xi/a)^2((1-\delta)/0.79)\exp(-1/\lambda)$ ($\propto \chi_Q\Gamma_Q$), where $0.42\leq\lambda\leq0.48$. In this context, the higher T_c in Hg1223 may qualitatively be ascribed to the larger $\chi_Q\Gamma_Q$ for the square CuO_2 plane site than that for $YBCO_7$.

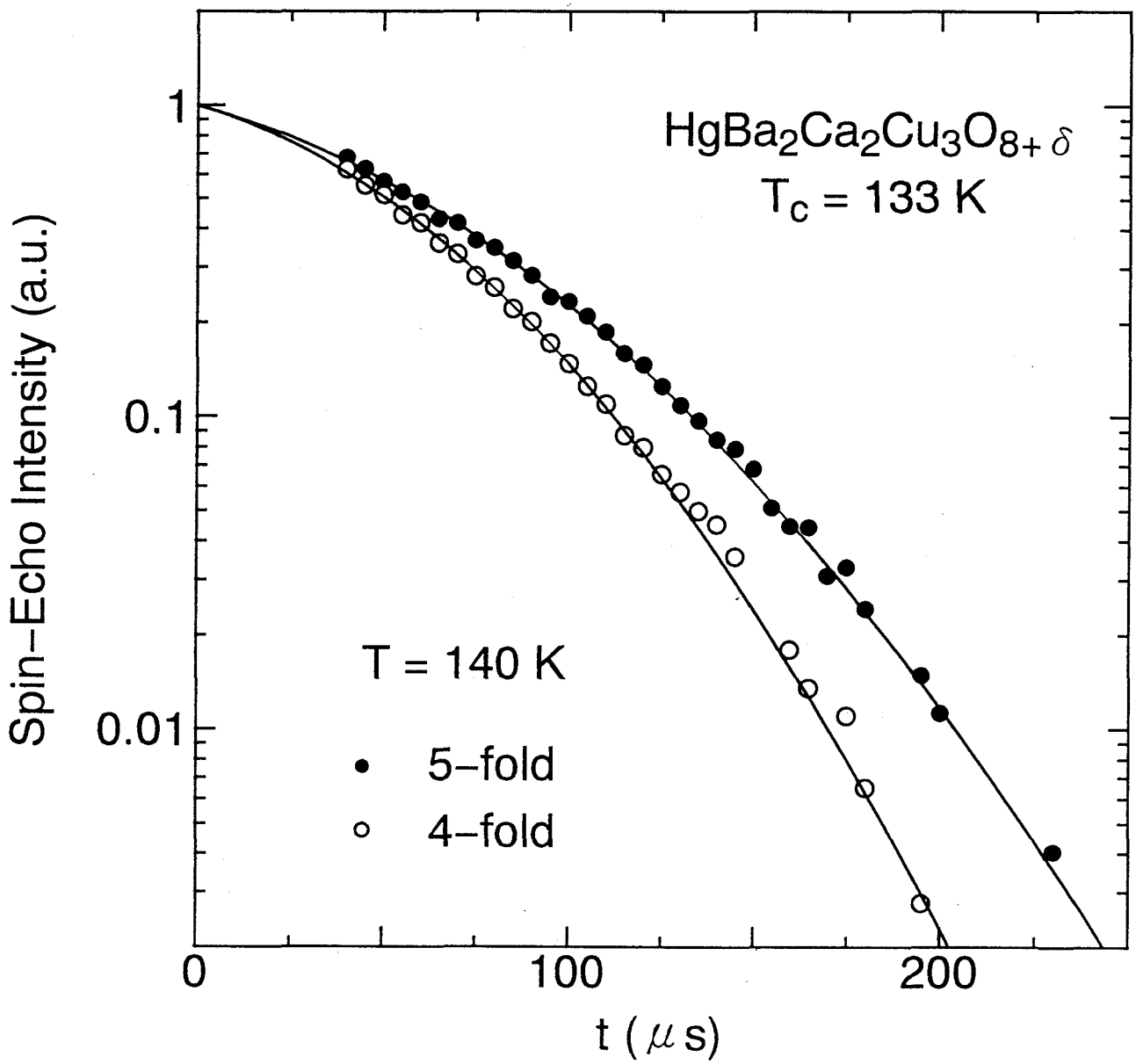

Fig.II-15. Spin-echo decay curves at $T = 140$ K for $4-$ (○) and $5-fold$(●) sites plotted against t, where t is the time interval between the 1st pulse and the spin-echo. Solid lines are the results fitted by eq.(32).

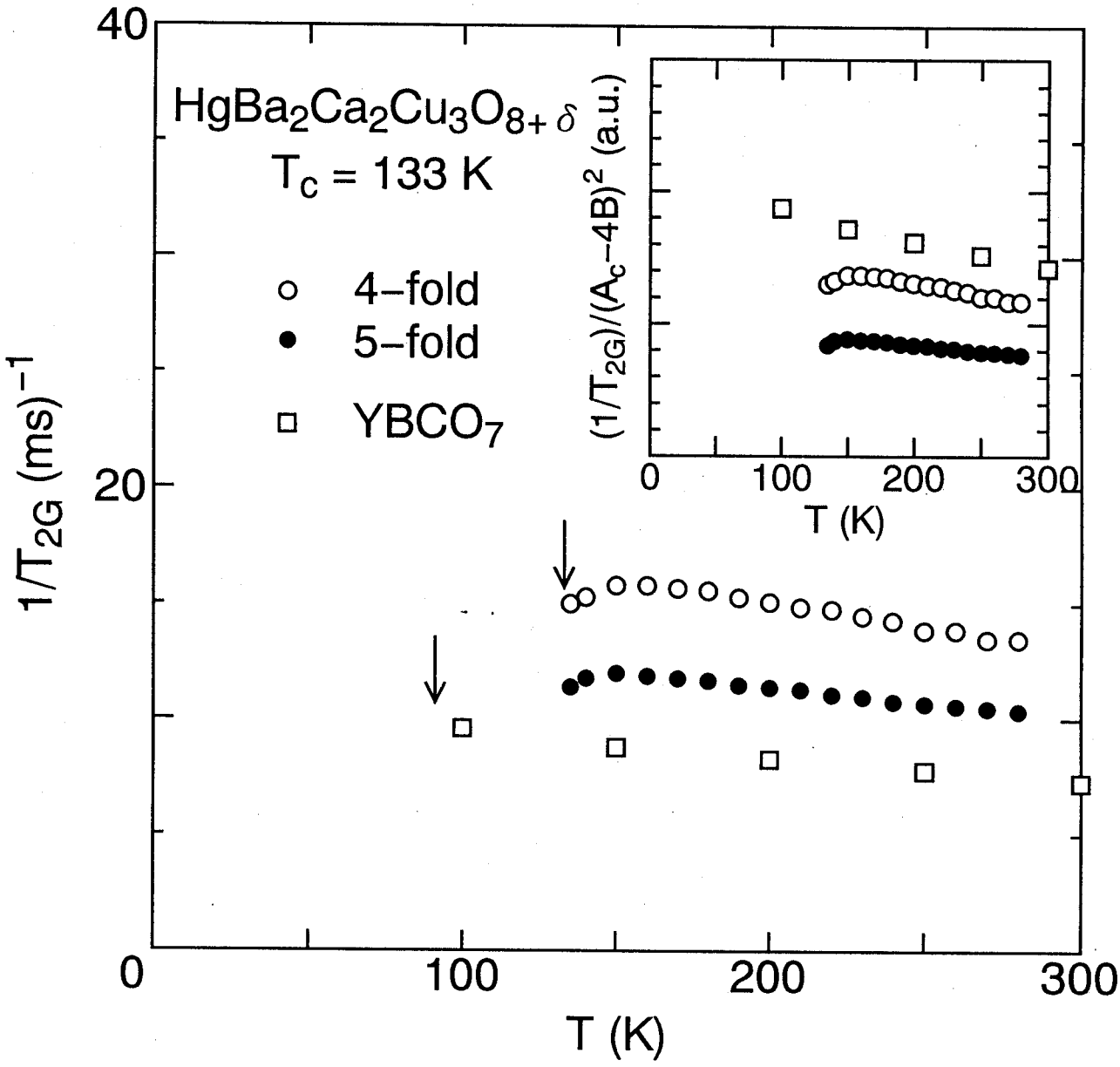

Fig.II-16. T-dependence of the Gaussian component of the nuclear spin-spin relaxation rate, $1/T_{2G}$, for $4-$(o) and $5-fold$(•) sites, respectively, together with the result for $YBCO_7$(□).[53] Inset indicates the comparison of the value of $(1/T_{2G})/(A_c-4B)^2$, scaled approximately to $\sim \chi_Q/\xi(=\alpha\xi)$.

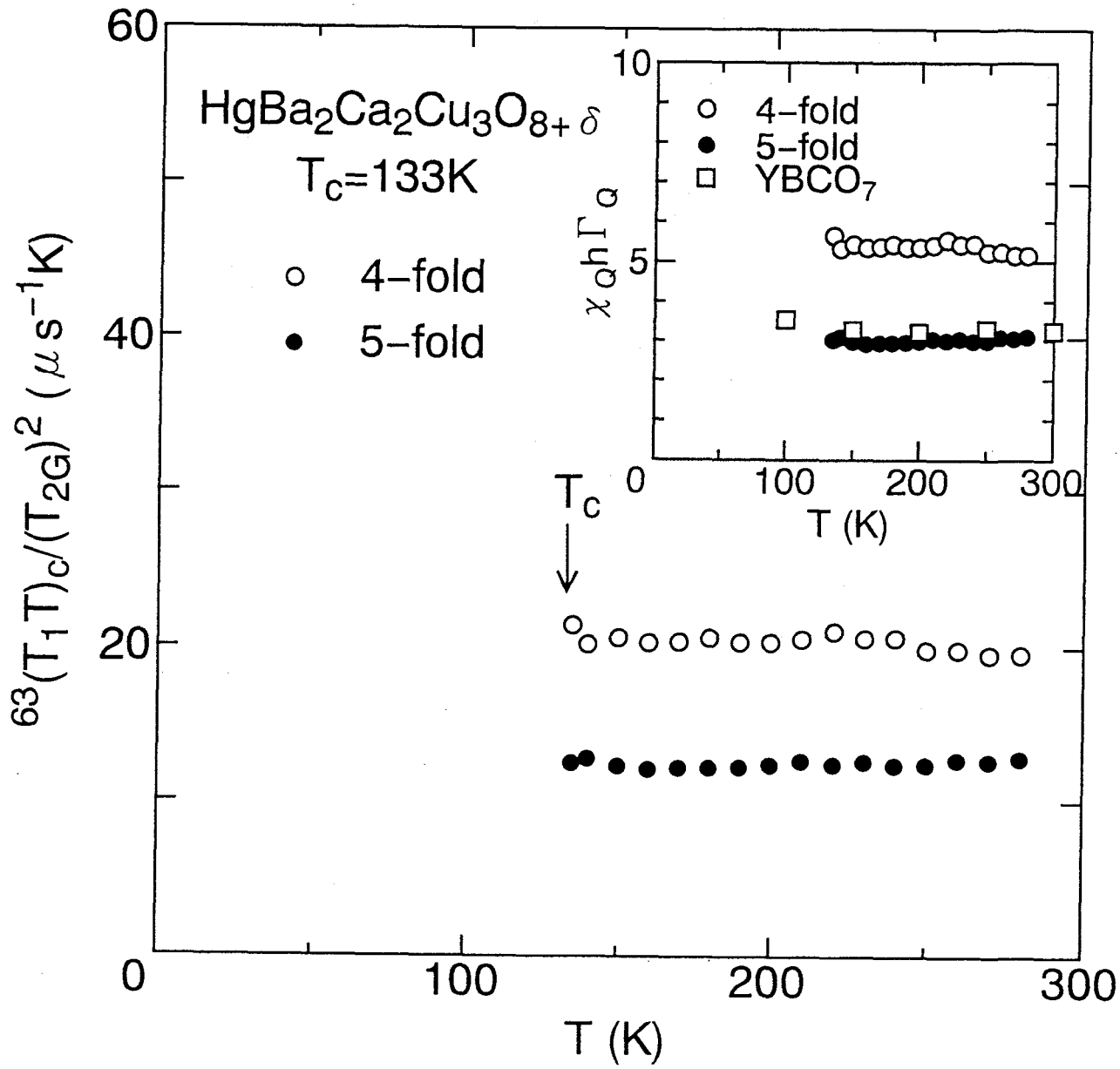

Fig.II-17. T-dependence of the ratio, $^{63}(1/T_1T)_c/(T_{2G})^2$, for $4-$ (o) and $5-fold(\bullet)$ sites, respectively. Inset indicates the comparison of the value of $\chi_Q\hbar\Gamma_Q$ with the result for $YBCO_7(\square)$.[53]

6.3 Symmetry of Pairing State

The symmetry of the pairing state of high-T_c cuprates is a matter of much controversy. The nature of the pairing state is important because different pairing mechanisms can yield different pairing state. Standard phonon-mediated superconductivity gives rise to a spin-singlet, orbital s-wave pairing state, but some spin-fluctuation models have spin-siglet, orbital d-wave pairing.[18, 56, 57, 58] Thus, the knowledge of the pairing state can aid in distinguishing between the mechanisms of high-T_c superconductivity.

6.3.1 $^{63}(1/T_1)$

As mentioned in Sec.6.1.1, for $c\|H$, it was not possible to measure T_1 for each Cu site separately because the spectrum for one Cu site overlaps with another upon lowering temperature below 60 K due to nearly the same value of the Knight shift. Accordingly, the T-dependence of $^{63}(1/T_1)$ below T_c is presented only in case of $H \perp c$.

Figures II-18(a) and (b) display $m(t)$ for the square Cu site plotted against t at $T =$ 40 K and 10 K, respectively. Solid line in Fig.II-18(a) indicates a best fit with a single $^{63}T_1$ component in eq.(31). On the other hand, short $^{63}T_1$ components become appreciable in $T \leq 30$ K as seen in Fig.II-18(b), associated with the presence of vortex cores. A prominent finding is, however, that all the $^{63}T_1$ components follow the $T_1T =$ const. law below 7 K as proved from the results that $m(t)$ plotted against the time (t) multiplied by the temperature, $t \cdot T$, is on a single curve as indicated in Fig.II-19. To display an overall T-dependence of $^{63}(1/T_1)_{ab}$ below T_c, a long component of $^{63}(1/T_1)_{ab}$ below 30 K is tentatively extracted from a fit of eq.(31) to the data of $m(t)$ smaller than 0.5 as indicated by solid line in Fig.II-18(b).

Figures II-20(a) and (b) show the T-dependence of $^{63}(1/T_1)_{ab}$ (o) below T_c for 4– and $5-fold$ site, respectively, under a magnetic field of $\sim$ 11 T. The magnitude of uncertainty of the data is comparable to the size of symbol. For both sites, $^{63}(1/T_1)_{ab}$ reveals a similar relaxation behavior to most of high-T_c cuprates, i.e. a power-law like behavior without any coherence peak followed by $T_1T =$ const. behavior well below T_c.

The relaxation behavior in the superconducting mixed state is affected by normal fluxoid cores. An array of fluxoids gives rise to two different relaxation processes: (a) the thermal

fluctuation of fluxoids which generates the transverse fluctuating field,[59] and (b) the spin diffusion to vortex cores.[60] In the former, $1/T_1$ should be suppressed with increasing field, whereas in the latter, $1/T_1$ is enhanced with increasing the number of fluxoids. The nuclear relaxation measurements in the superconducting mixed state were reported in $YBCO_7$[61, 62] and Y124[63] thus far. From the result that $1/T_1$ is linearly enhanced by the magnetic field, the nuclear relaxation for these compounds was shown to be dominated by the spin diffusion process to vortex cores. By contrast, $^{63}(1/T_1)$ for Bi2212[36] and Tl2223,[64] which followed the T_1T=const. law, did not reveal any appreciable field dependence down to low temperatures. As a result, the relaxation behavior in these compounds was concluded to be dominated by the presence of residual DOS at the Fermi level, as seen in Fig.II-22(a). As discussed extensively in the literatures,[4, 36, 44, 64, 65] the gapless superconductivity caused by some imperfections presenting in the crystals provided an important clue to address the pairing state for high-T_c cuprates to be of a d-wave type where the nonmagnetic potential scattering acts as pair-breaker.

The magnetic field dependences of $^{63}(1/T_1)_{ab}$ at low-T in Hg1223 for both Cu sites were measured in a field range of $6 - 11$ T. Below 7 K, where all the $^{63}T_1$ components follow the T_1T = const. law, $^{63}(1/T_1)_{ab}$ is well fitted by

$$^{63}(1/T_1)_{ab} = a + bH \tag{47}$$

for both Cu sites as displayed in Figs.II-21(a) and (b). In a rapid spin diffusion limit, which is valid in low-T and high-field, $1/T_1$ can be expressed as follows:[66]

$$(1/T_1)_{obs,i} = (1/T_{1n} - 1/T_{1s})_i \frac{H}{\Phi}\xi_j\xi_k + (1/T_{1s})_i \qquad (i,j,k = a,b,c) \tag{48}$$

where $1/T_{1n}$ and $1/T_{1s}$ are the relaxation rates in and out of vortex cores, Φ is the flux quantum and ξ_i is the coherence length along the i-direction, respectively. A good correspondence between the experiment and the theory is obtained with such relations as

$$a = (1/T_{1s}) \tag{49}$$

$$b = (1/T_{1n} - 1/T_{1s})\frac{\xi_{ab}\xi_c}{\Phi} \tag{50}$$

Here, $1/T_{1s}$ inherent to the superconducting state is determined from the extrapolation to zero field. Below 7 K, it is remarkable that $^{63}(1/T_{1s})$ follows the $T_{1s}T$ = const. law which is

indicative of the gapless nature of superconductivity. Furthermore, since $^{63}(1/T_1)_{obs}$ above 7 K was also confirmed to follow the eq.(48), the T-dependence of $^{63}(1/T_{1s})$ is plotted by closed circles (•) in the Figs.II-20(a) and (b) together with the results below 7 K. It is substantial that $^{63}(1/T_{1s})$ decreases over four orders of magnitude below T_c and behaves as T_1T = const. below 7K. In contrast to the case for Bi2212[36] and Tl2223,[64] the relaxation behavior in the mixed state at low-T for Hg1223 is significantly affected by the spin diffusion process to vortex cores. On the other hand, the superconductivity has been found to be in the gapless state as well. In order to compare the fraction of the residual DOS presenting in Hg1223 with that in Tl2223,[64] $(1/T_{1s}T)$ normalized by the value at T_c is related to a residual fraction of DOS from a formula

$$\frac{(1/T_{1s}T)}{(1/T_1T)_{T_c}} = (\frac{N_{res}}{N_0})^2 \tag{51}$$

where N_0 is defined as an effective DOS at T_c. A fraction of N_{res}/N_0 is a measure to address to what extent the effective DOS is lost due to the onset of superconductivity. N_{res}/N_0 for Hg1223 is estimated to be ~ 0.05, which is very smaller than $N_{res}/N_0 \sim 0.3$ for Tl2223.[64]

Next, we analyze the T-dependence of $^{63}(1/T_{1s})$ below T_c for both sites in terms of the 2D gapless d-wave model with line nodes at the cylindrical Fermi surface as $\Delta(\phi) = \Delta(T)\cos 2\phi$ with $d_{x^2-y^2}$ symmetry where the residual DOS, N_{res}, at the Fermi level is taken into account. The gapless d-wave model explained consistently the NMR results in Zn-doped $YBCO_7$,[4] LSCO (x≥0.20),[44] Bi2212,[36] Tl2223[64] and Tl2201.[65] As extensively argued in the literatures,[67, 68, 69, 70] such residual DOS is produced at the Fermi level by treating the impurity scattering in terms of the unitarity limit in the d-wave model. It is crucial that not only the magnetic impurity scattering, but also the potential scattering by some imperfections bring about the pair breaking effect. As indicated by solid lines in Figs.II-20(a) and (b), $^{63}(1/T_{1s})$ is well reproduced with parameters of $2\Delta/k_BT_c = 8$ and $N_{res}/N_0 = 0.05$. The reduction rate of T_c by impurity scattering, $\Delta T_c/T_{c0}$, for d-wave superconductor is investigated,[71] shown in Fig.II-22(b), and is estimated to be as small as 0.02 for $N_{res}/N_0 = 0.05$, which is smaller than $\Delta T_c/T_{c0} = 0.13$ for $N_{res}/N_0 = 0.30$ in Tl2223.[64] This result points to the better quality of Hg1223 than Tl2223,[64] as supported also from the narrower NMR line width.

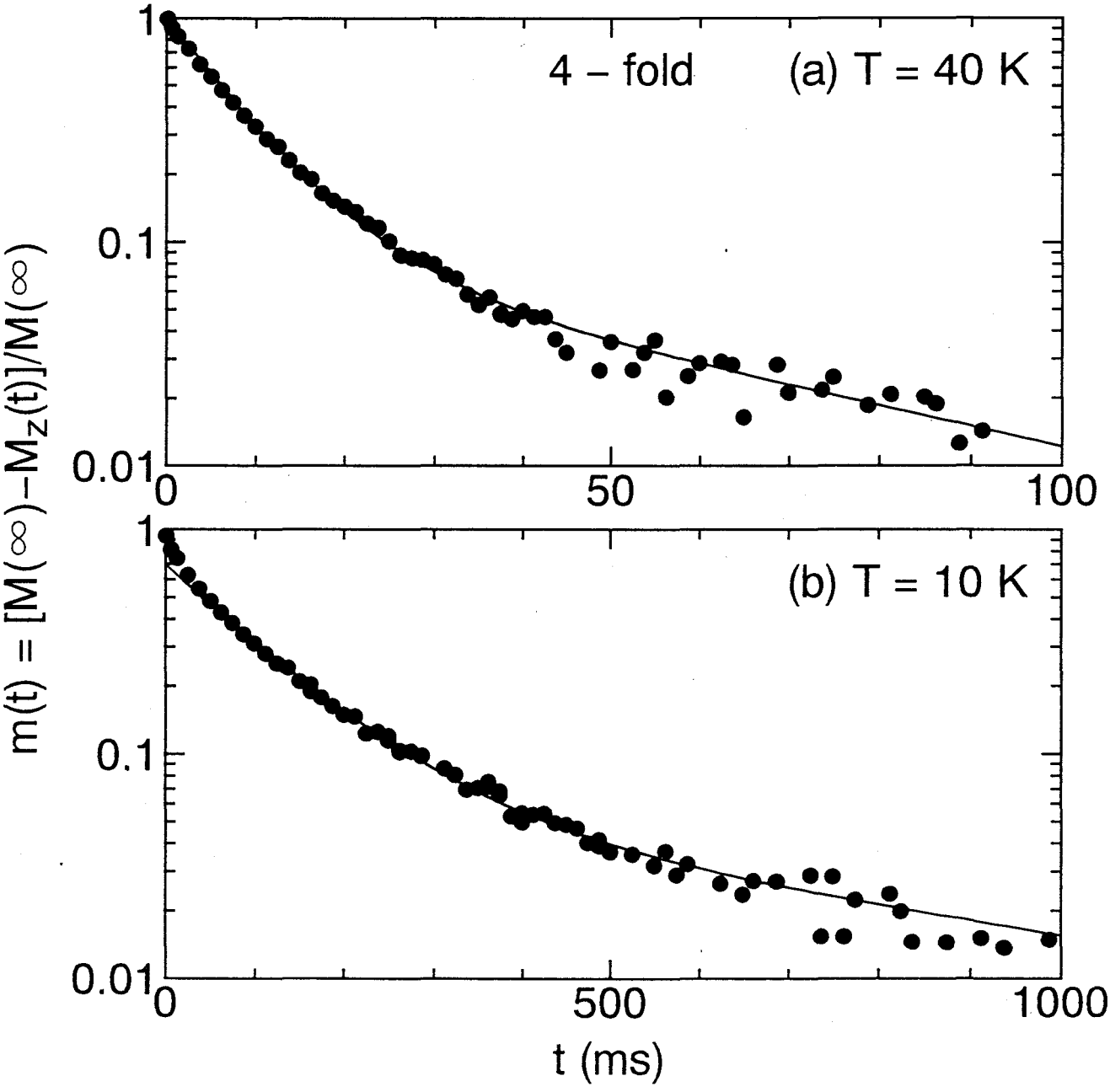

Fig.II-18. Relaxation curves plotted against t after saturation pulse at (a)$T = 40$ K and (b)10 K, respectively, under the magnetic field of ~ 11 T perpendicular to the c-axis. Solid lines are the results fitted by the relaxation function of eq.(31).

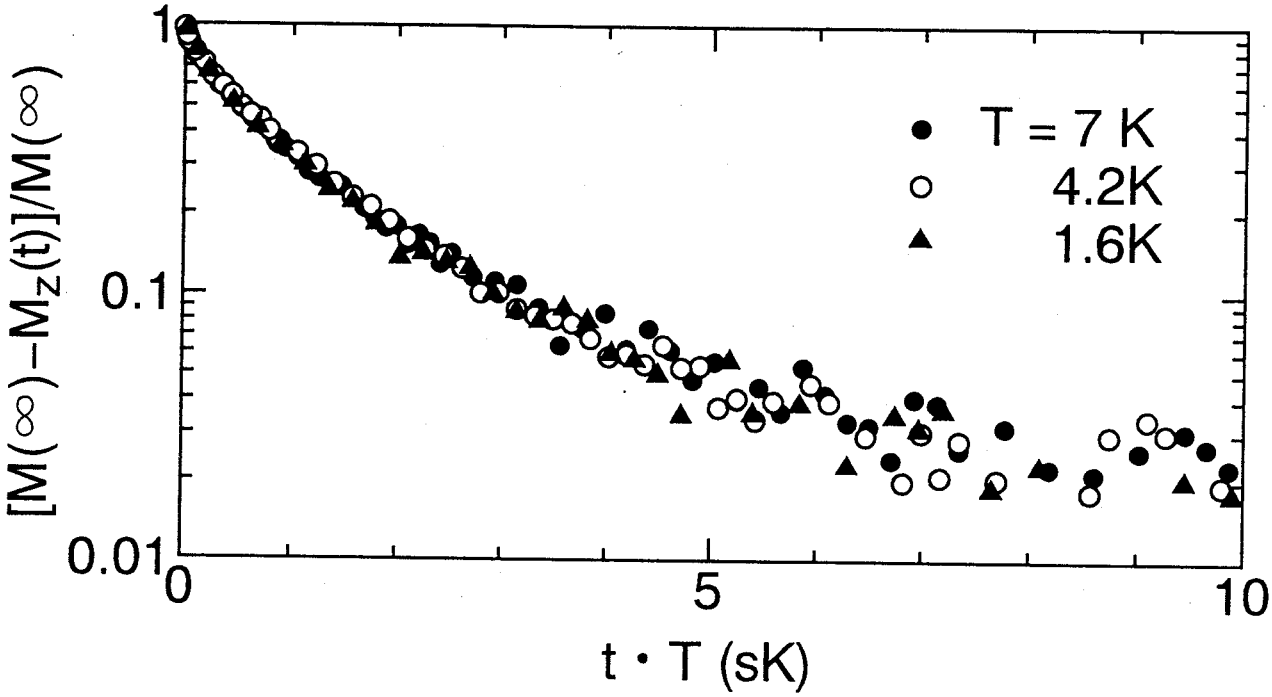

Fig.II-19. Relaxation curves well below T_c plotted against the time multiplied by the temperature, $t \cdot T$, is on a single curve, showing that all the $^{63}T_1$ components follow the T_1T = const. law below 7 K.

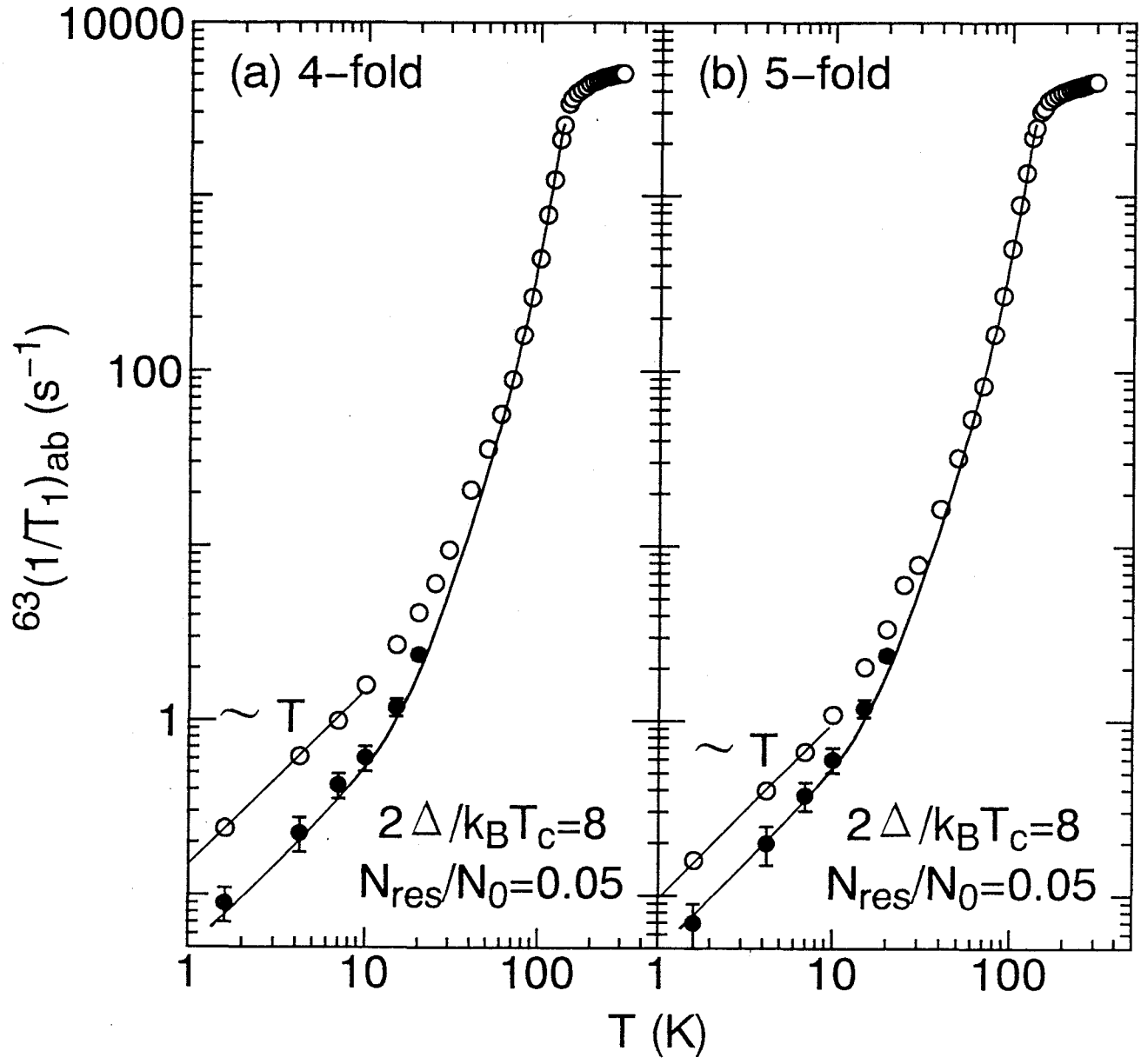

Fig.II-20. T-dependence of $^{63}(1/T_1)_{ab}$ below T_c for (a)4– and (b)5 – *fold* sites, respectively. o and • indicate the value at 11 T and the extrapolated value to the zero magnetic field, respectively. Solid lines are calculated using gapless d-wave model with the parameters of $2\Delta/k_BT_c = 8$ and $N_{res}/N_0 = 0.05$.

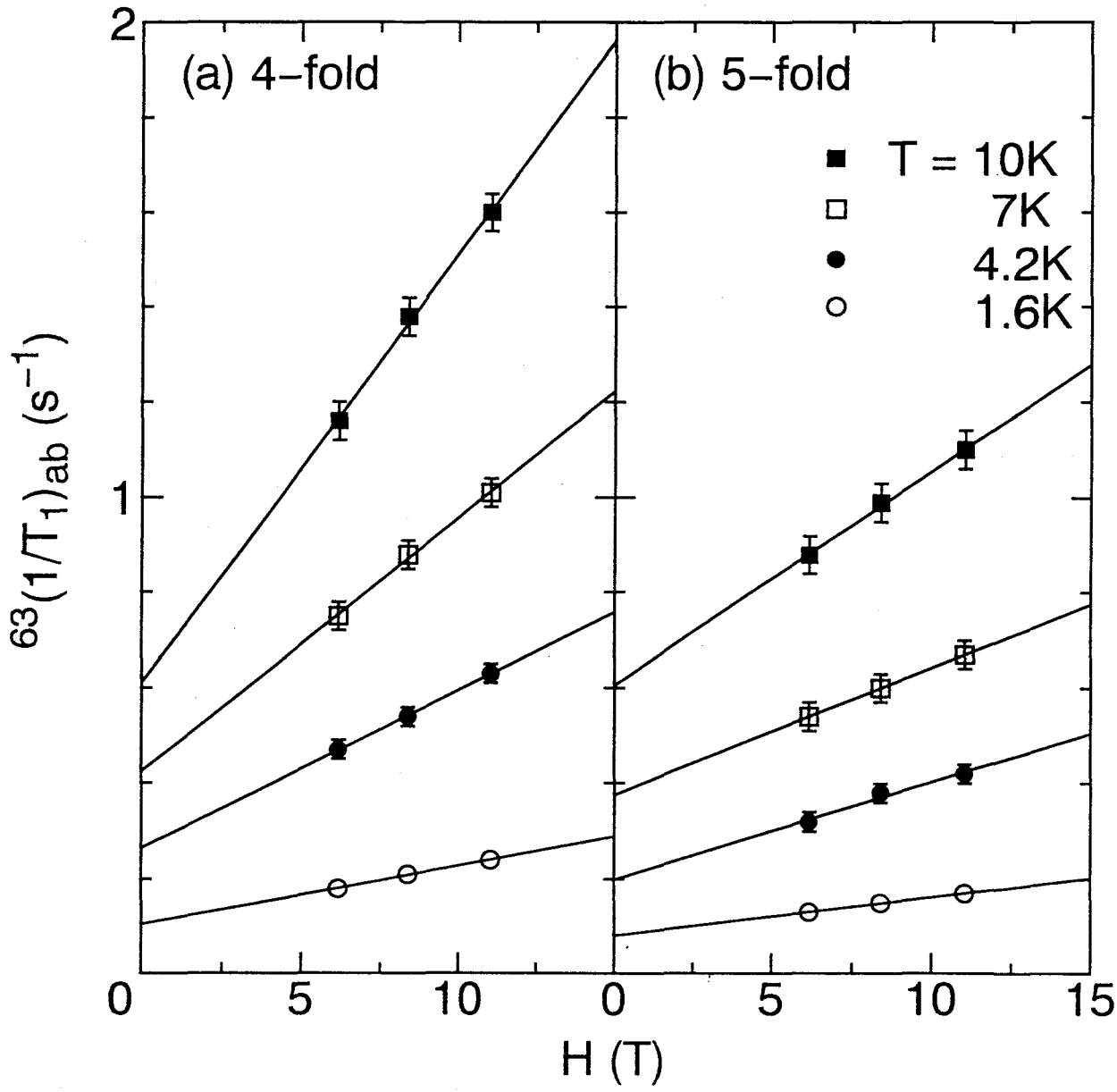

Fig.II-21. Magnetic field dependence of $^{63}(1/T_1)_{ab}$ at several temperatures below 10 K for (a)4− and 5 − *fold* sites, respectively.

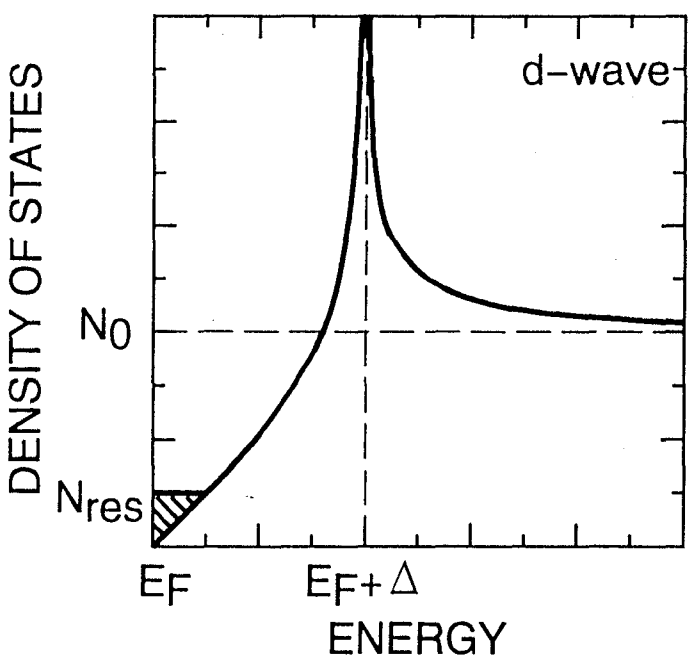

Fig.II-22(a). Density of states based on the gap function of 2D d-wave model with such gap nodes at the cylindrical Fermi surface as $\Delta(\phi) = \Delta(T)\cos(2\phi)$ corresponding to $d_{x^2-y^2}$ symmetry and the finite density of states, N_{res}, is taken into consideration.

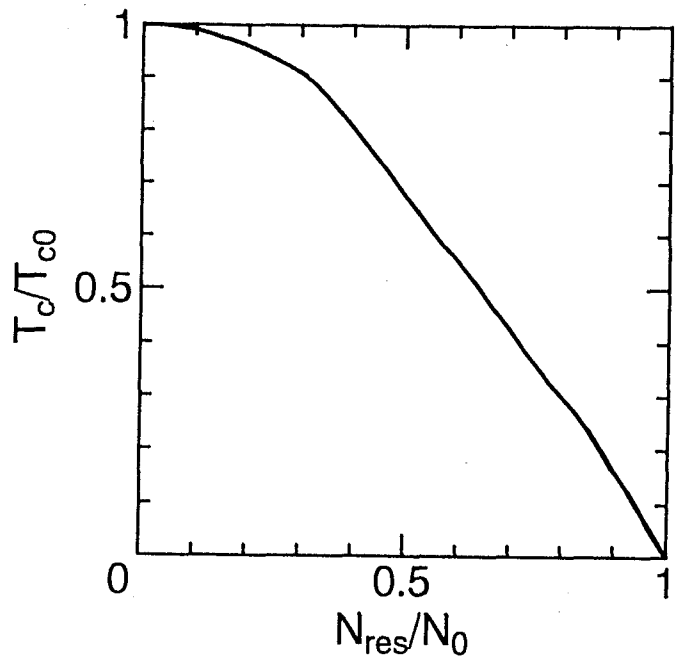

Fig.II-22(b). T_c/T_{c0} is plotted against N_{res}/N_0. The solid line is the calculation based on the non-magnetic impurity scattering in the unitary limit by Schmitt-Rink, Miyake and Varma.[71]

6.3.2 ^{63}K

In the superconducting state, it is suggested that the Copper-pair is spin-singlet from a sudden and large decrease of the Knight shift components below T_c, as seen in Fig.II-7.

For $c\|$H, it is not possible to determine separately the accurate value of $^{63}K_c$ for each Cu site at low temperature because the spectrum for one Cu site overlaps with another upon lowering temperature below 60 K due to nearly the same value of $^{63}K_c$, as mentioned in Sec.6.1.1. Further, the effect of a diamagnetic shielding by supercurrents and a change of the value of the Knight shift component are larger and smaller than those in case of $c \perp$ H, respectively. Accordingly, the T-dependence of $^{63}K_s$ below T_c is presented in case of $c \perp$ H.

Figure II-23 shows the T-dependence of the spin Knight shift, $^{63}K_s$, normalized by the value at T_c, $^{63}K_{T_c}$, under the magnetic field perpendicular to the c-axis. $^{63}K_s$ is extracted by substracting $^{63}K_{orb}$ from the raw Knight shift data. Since $^{63}K_{orb}$ is proportional to $n_{x^2-y^2}$, $^{63}K_{orb}$'s are estimated to be 0.19 and 0.20 % for $4-$ and $5-$*fold* sites, respectively, using the values for $YBCO_7$ [$n_{x^2-y^2} = 0.86$, $^{63}K_{orb} = 0.24$ %].[4] A solid line is calculated by using the 2D gapless d-wave model with the same parameters ($2\Delta/k_BT_c = 8$ and $N_{res}/N_0 = 0.05$) as in the analysis of the results of T_1, which satisfactorily interprets the experimental results as well. Thus, both the results of the Knight shift and $1/T_1$ are consistently understood in term of the 2D gapless d-wave model with very small N_{res}. This result shows that the anisotropic superconductivity is realized in Hg1223. Together with the results in the normal state, it is suggested that the spin fluctuation plays an important role in the pairing mechanism. Also, the small N_{res} indicates that Hg1223 is the best compound among Bi-[36] and Tl-based ones,[15, 37] as supported also from the narrowest NMR line width.

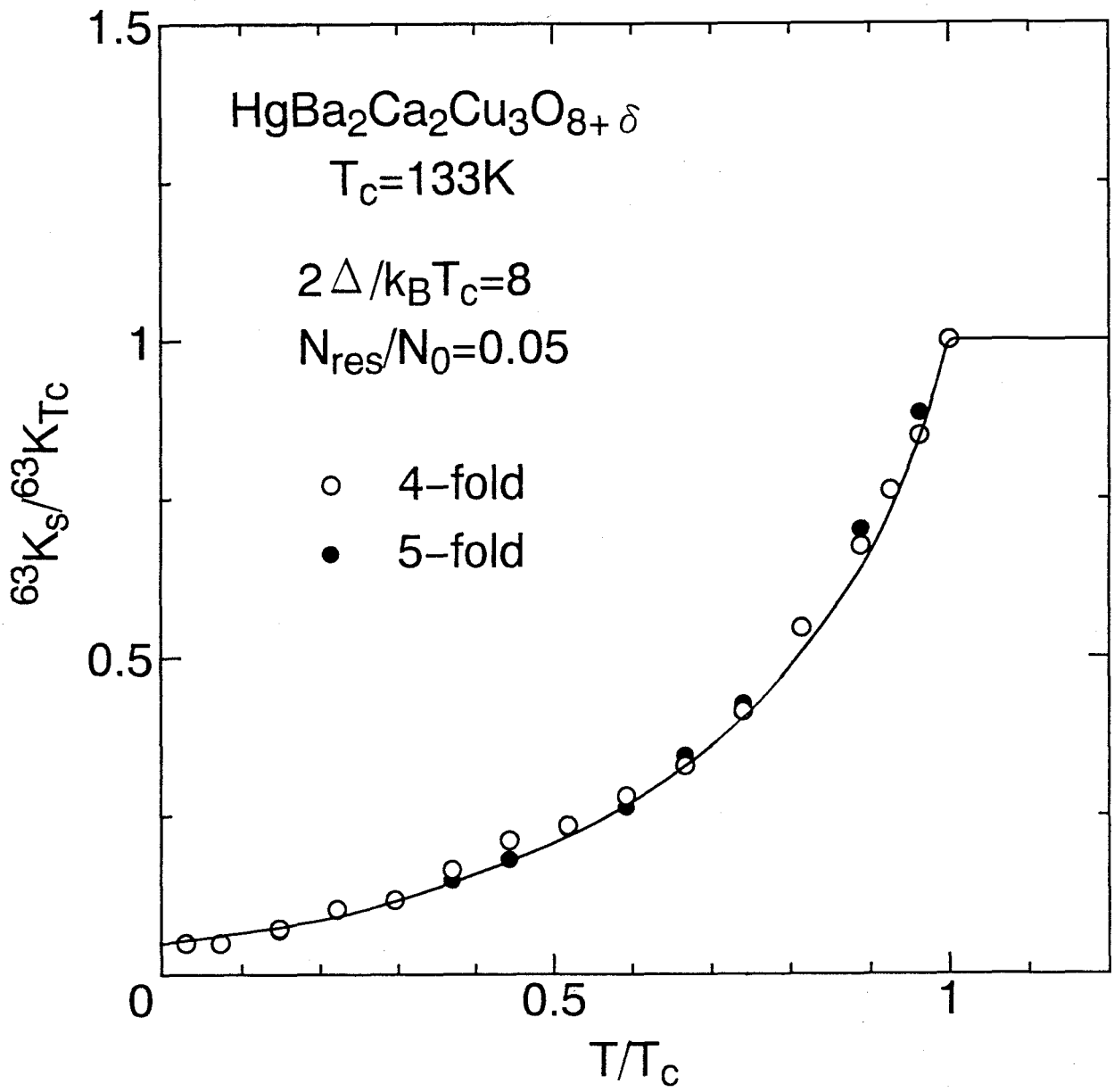

Fig.II-23. T-dependence of ${}^{63}K_s/{}^{63}K_{T_c}$ for $4-$(o) and $5-fold$(•) sites, respectively, plotted against T/T_c. K_{T_c} is the value of K_s at T_c. The solid line is calculated using gapless d-wave model with the parameters of $2\Delta/k_BT_c = 8$ and $N_{res}/N_0 = 0.05$.

7 Summary

The static magnetic property and the spin dynamics in Hg1223 compound were investigated by measuring the nuclear quadupole frequency, ν_Q, the Knight shift, K, the nuclear spin-lattice relaxation rate, $1/T_1$, and the nuclear spin-spin relaxation rate, $1/T_{2G}$, of ^{63}Cu. From the measurements of ν_Q, $K(T)$ and $1/T_1T$ of ^{63}Cu in the normal state, it has been clarified that the local hole carrier density on Cu site, $n_{x^2-y^2}$, the supertransferred hyperfine field from the nearest neighbor Cu site, B, and $^{63}(1/T_1T)_c/(A_{ab}-4B)^2$ ($\propto \chi_Q/\Gamma_Q\xi^2$) are quite smaller, more significantly enhanced and reduced, respectively, than those in $YBCO_7$ and the lightly-doped compounds. Also, from the Curie-Weiss law and the anisotropy of $(1/T_1T)$, it has been shown that the staggered susceptibility, χ_Q should be peaked around $Q=(\pi,\pi)$. Consequently, the appreciable reduction of $^{63}(1/T_1T)_c/(A_{ab}-4B)^2$ as compared with that in $YBCO_7$ has been pointed out to be due to the increase of $\Gamma_Q\xi^2$ in Hg1223, as expected from the relation of $\sum_{q\sim Q}\chi''(q,\omega_n)/\omega_n \sim \chi_Q/\Gamma_Q\xi^2$. This result is supported by the measurement of $1/T_{2G}$ of ^{63}Cu in the normal state. From the analysis of $^{63}(1/T_1T)$ and $1/T_{2G}$, the values of the product of the staggered susceptibility, χ_Q, and the characteristic energy, Γ_Q, of the **AF** spin fluctuation, $\chi_Q\Gamma_Q$, have separately been deduced, and then the value (~ 5.4) of $\chi_Q\Gamma_Q$ for the square CuO_2 plane site has been found to be markedly larger than that for the pyramidal plane in Hg1223 (~ 3.1) and $YBCO_7$ (~ 3.5). A larger value of $\chi_Q\Gamma_Q$ for the square plane seems to make T_c increase from 93 K for $YBCO_7$ to 133 K for Hg1223. Together with the recent result on Tl2223, the large $\chi_Q\Gamma_Q$ is suggested to be the reason for the high T_c for the cuprates with three CuO_2 planes. **This experimental signature is consistent with the spin-fluctuation-induced superconducting mechanism**, which predicts the higher T_c for the larger $\chi_Q\Gamma_Q$, provided that the spin fluctuation is peaked around $Q=(\pi,\pi)$.

On the other hand, in the superconducting mixed state in Hg1223, $^{63}(1/T_1)$ reveals a similar relaxation behavior to most of high-T_c cuprates, i.e. a power-law like behavior without any coherence peak followed by T_1T = const. behavior well below T_c. It suggested that the anisotropic superconductivity is realized in this system. Also, $^{63}(1/T_1)$ has revealed the T_1T=const. law at low temperatures with a linear magnetic field dependence below 7

K, regardless of its distribution. The latter experimental signature was consistent with the relaxation process characteristic for the spin diffusion to vortex cores as well as for $YBCO_7$ and Y124 reported so far. By eliminating the contribution to T_1 associated with fluxoids, the value of T_1T=const. inherent to the superconducting state has been deduced. As a result, the superconducting state of Hg1223 is concluded to be of gapless type with a finite DOS at the Fermi level, which amounts to $\sim 5\%$ of the value at T_c, $N_{res}/N_0 \sim 0.05$.

Based on the 2D d-wave model, it has been shown that this gapless state, which is possibly produced by some imperfections, produces a small T_c-reduction rate of $\Delta T_c/T_{c0} \sim 0.02$ for $N_{res}/N_0 \sim 0.05$, which is smaller than $\Delta T_c/T_{c0} \sim 0.13$ for $N_{res}/N_0 \sim 0.3$ in Tl2223. One of the origins for the higher value of T_c in Hg1223 than in Tl2223 is hence ascribed to the better quality of Hg1223, as supported by the narrow NMR spectra.

Part III
^{63}Cu NMR Study of $TlSr_2CaCu_2O_{7-\delta}$ (Tl1212)

8 Introduction

$TlSr_2CaCu_2O_{7-\delta}$ (Tl1212) compound consists of **two pyramidal CuO_2 layers** in the unit cell where Cu is surrounded by pyramidal oxygens like $YBCO_{6+x}$ compounds but without the CuO chain structure.[72] So, Cu atoms have single site crystallographically. T_c of these compounds shows a gradual reduction from 70 K to 0 K as oxygen content is increased,[72] assuring that Tl1212 is a typical material belonging to so-called **heavily-doped** superconductor as in Tl2201 system.[14] The Hall coefficient, R_H, and the electronic resistivity, ρ, have anomalous T-dependence in the normal state, as seen in other high-T_c compounds. The former for all oxygen content shows a broad peak around 100~140 K, above which Hall number, $n_H = 1/R_H e$, shows T-linear dependence. The latter, on the other hand, shows the power-law T-dependence of $\rho = \rho_0 + T^n$ and the exponent, n, gradually changes from 1 to 2 with decreasing T_c, i.e. with increasing hole.[72]

Thus far, a systematic experiment on the heavily-doped system is the only case for Tl2201 compounds with a single CuO_2 layer.[15] The remarkable finding is that the **AF** spin correlation disappears in non-superconducting Tl2201 compound, suggesting that the **AF** spin correlation is responsible for the occurrence of the superconductivity.[15] Therefore, in order to establish further the magnetic and superconducting properties in heavily-doped superconductors with double CuO_2 layers from the microscopic point of view, extensive ^{63}Cu NMR studies have been carried out in Tl1212 compounds.

Most remarkably, it is reported that the carrier density is so largely changed as to cover from heavily- to lightly-doped system by partially substituting lutetium (Lu^{3+}) into Ca^{2+} sites.[73] So, the systematic studies from lightly- to heavily-doped region can be made on this series of compounds. Lu-doped Tl1212 exhibits a spin-gap behavior in lightly-doped region, which is the common behavior in lightly-doped bi-layered high-T_c compounds. In this compound, the disorder is induced into the Ca(Lu) layers sandwiched by CuO_2 bi-

layers. In order to clarify the origin of the spin-gap, that is, the relation between the spin-gap and the number of CuO_2 layers, the exsistence of the CuO chain and/or the disorder in the lightly-doped high-T_c compounds, ^{63}Cu and ^{205}Tl NMR measurements have been carried out in Lu-doped Tl1212 compounds.

In this part (**III**), from the measurements of the quadrupole frequency, $^{63}\nu_Q$, the Knight shift, ^{63}K, the nuclear-spin lattice relaxation rate, $^{63}(1/T_1)$, and the nuclear spin-spin relaxation rate, $1/T_{2G}$, the magnetic and superconducting properties are investigated on heavily-doped Tl1212 in the **section 10**, and further compared with a part of results on Lu-doped Tl1212 in the **section 11**.

9 Sample

9.1 Preparation, Structure and Phase Diagram

The Tl1212 polycrystalline samples were prepared by the conventional solid-state reaction method.[72] Tl_2O_3, SrO, CaO and CuO powders were mixed, pressed into a pellet, sealed in a gold crucible, and sintered in oxygen at about 900°C for several days with several intermediate grindings. The sample quality is very sensitive to the preparation conditions such as sintering temperature, probably because of the large volatility of Tl.

The crystal structure was examined by X-ray diffraction experiment.[72] X-ray diffraction did not show any impurity phase for all compounds, that is, the samples were confirmed to be almost of single-phase. All peaks of the X-ray diffraction pattern could be assigned to those for the crystal-structure model (**tetragonal** space group $P4/mmm$), presented in Fig.III-1. All cation sites are fully occupied, while some local displacement of Tl in the *a-b* plane are suggested. Since the refined occupancy for the Ca site is considerably larger than unity, about 19 % of the Ca site seems to be substituted by Tl. Also, it is suggested that $3 - 5$ % of Tl site are replaced by Cu atoms from the Rietvelt analysis of X-ray diffraction experiment. According to the neutron-diffraction study,[74] some oxygen deficiency is detected on the Tl-O layer.

The as-sintered samples are metallic and non-superconducting. However, they show the superconductivity after annealing in argon at $350 - 550$°C for 5 hours. T_c depends on the annealing condition, and the higher T_c value is obtained as the annealing temperature is rised. The superconductivity again disappeared by annealing in oxygen at 350°C for 10 hours. These facts strongly suggest the significant role of the oxygen non-stoichiometry.

Figure III-2 shows the relationship between T_c and the relative change in oxygen content, Δy, in the formula of $TlSr_2CaCu_2O_y$ ($y \sim 7$).[72] As shown in Fig.III-2, T_c is increased almost linearly with decreasing the oxygen content, which is quite similar to the result for Tl2201. The maximum T_c value is $\sim$ 70 K.

Figure III-2 also shows subtle but systematical changes in the lattice parameter a and c.[72] The lattice parameter becomes longer for the higher T_c sample. It is found that the distance between Cu and apical oxygen becomes shorter as T_c is higher.

The good sample homogeneity is also suggested by the sharp and single transition in the Meissner signal as shown in Fig.III-3,[72] which is consistent with the results of the X-ray diffraction experiment.

In this study, three samples with T_c = 70, 52 and 10 K were used. T_c was defined at the onset temperaure of the diamagnetic signal appearing in ac-susceptibility. The sample was crushed into powder with size smaller than 20 μm in diameter for the NMR measurements. Also, the sample was magnetically aligned along the c-axis by use of the anisotropy of the susceptibility and fixed with the polymer in a magnetic field of 11 T.

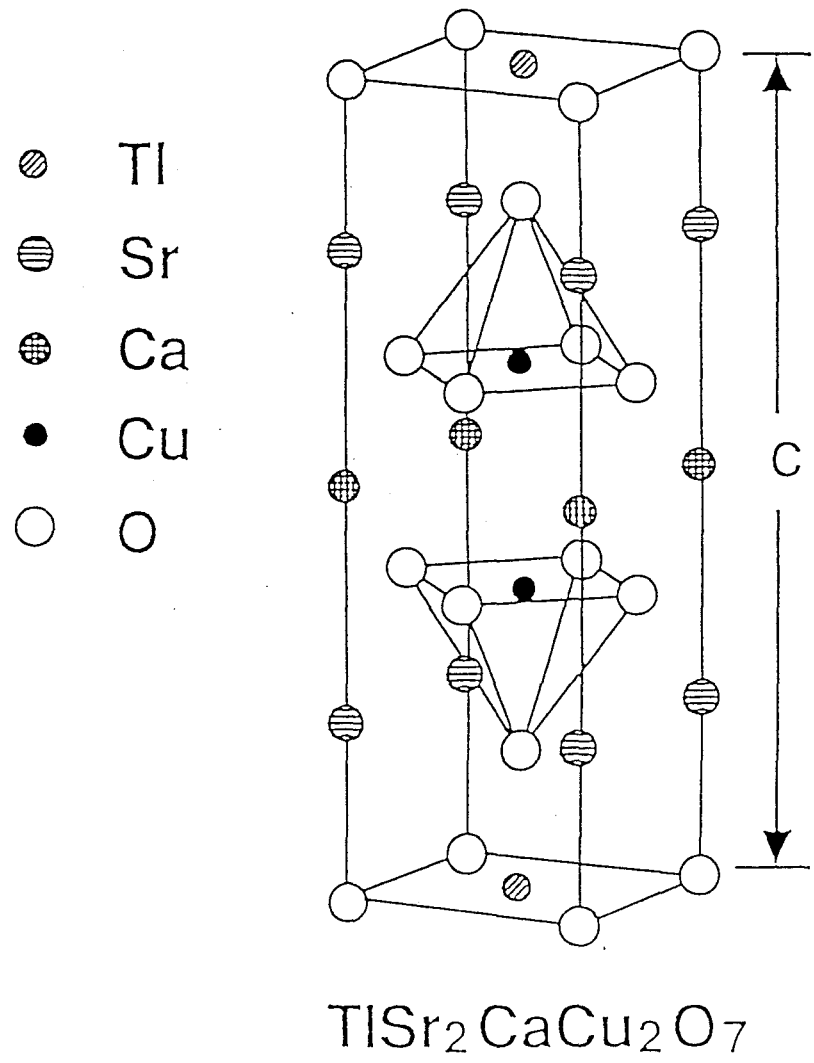

Fig.III-1. Crystal-structure model of $TlSr_2CaCu_2O_{7-\delta}$ (Tl1212).

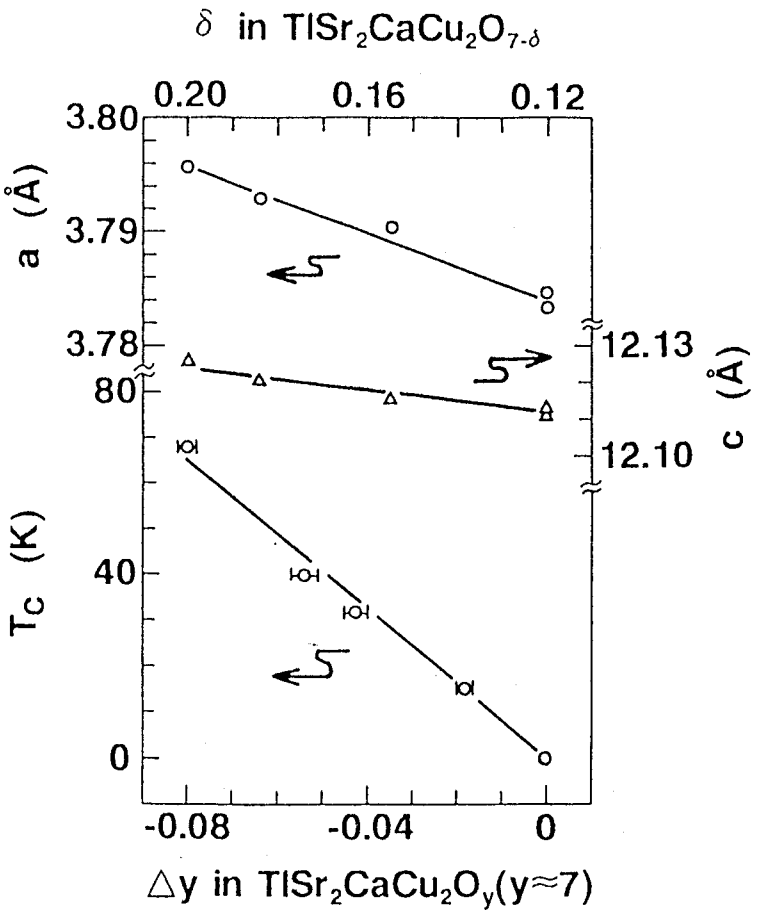

Fig.III-2. T_c and lattice parameters, a and c, plotted against the oxygen content for $TlSr_2CaCu_2O_{7-\delta}$.[72] The lower axis shows the relative change in oxygen content, Δy, measured from the oxygen-annealed state. The upper axis shows the δ values ($\delta = 0.12 - \Delta y$) based on the neutron-diffraction study.[74]

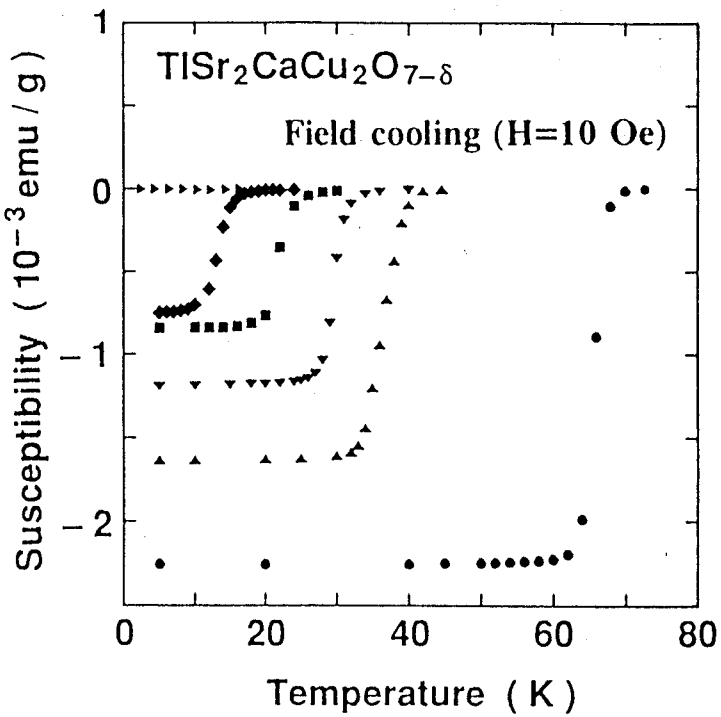

Fig.III-3. Meissner signals measured under the constant field of 10 Oe for $TlSr_2CaCu_2O_{7-\delta}$ with various T_c's.[72]

9.2 Transport Properties

Figures III-4(a) and (b) show the temperature dependences of the resistivity, ρ, and Hall number, $n_H = 1/R_H e$, respectively, for samples with different δ's.[72] Both the resistivity and positive Hall coefficient, R_H, decrease with increasing oxygen content, which demonstrates the hole doping by oxygen clearly.

The temperature dependence of the resistivity is fitted well by a simple power-law dependence, $\rho = \rho_0 + T^n$, for all δ's. The exponent, n, is gradually increased from 1 to 2 with doping. The results strongly suggested that both T-linear and T^2-dependences, as well as the intermediate ones, should be understood within the same framework. These results are difficult to explain in terms of electron-phonon scattering, but are very similar to those for Tl2201.[14] One plausible way to understand the results is to cosider that the T^2-dependece of the resistivity is characteristic of metal and is evidence of the electron-electron scattering in the usual Fermi-liquid. In that case, the T-linear anomaly emerging with decreasing carrier density is explained in term of some usual deviation from the canonical Fermi-liquid, such as magnetic fluctuation, localization or Fermi surface nesting.[20]

On the other hand, the Hall coefficient, R_H, shows a broad maximum at 100 – 140 K for all δ's, above which it is slowly decreased so that the Hall number, n_H, shows a linear temperature dependence. It is interesting that even the metallic sample (A) still shows a linear temperature dependence of n_H, which is a common behavior in high-T_c superconductors, but incompatible with a simple Fermi-liquid description. These features are also vey similar to those for Tl2201.[14] It should be noted that R_H is always positive and only gradually and continuously decreased upon doping without showing any anomalies at the superconductor-metal phase boundary. This is quite similar to the results for Tl2201,[14] but is in sharp contrast to that for overdoped LSCO,[75] where R_H decreases rapidly with doping and finally changes sign to negative. It seems that no singularity exists at the superconductor-metal phase boundary, which suggests that the electronic structures for the superconducting and the metallic states are quite similar.

It is believed that the present results of transport properties on polycrystalline samples mainly reflect the a-b plane properties because of the large electrical anisotropy. This situation was found to be appropriate for other high-T_c cuprates.

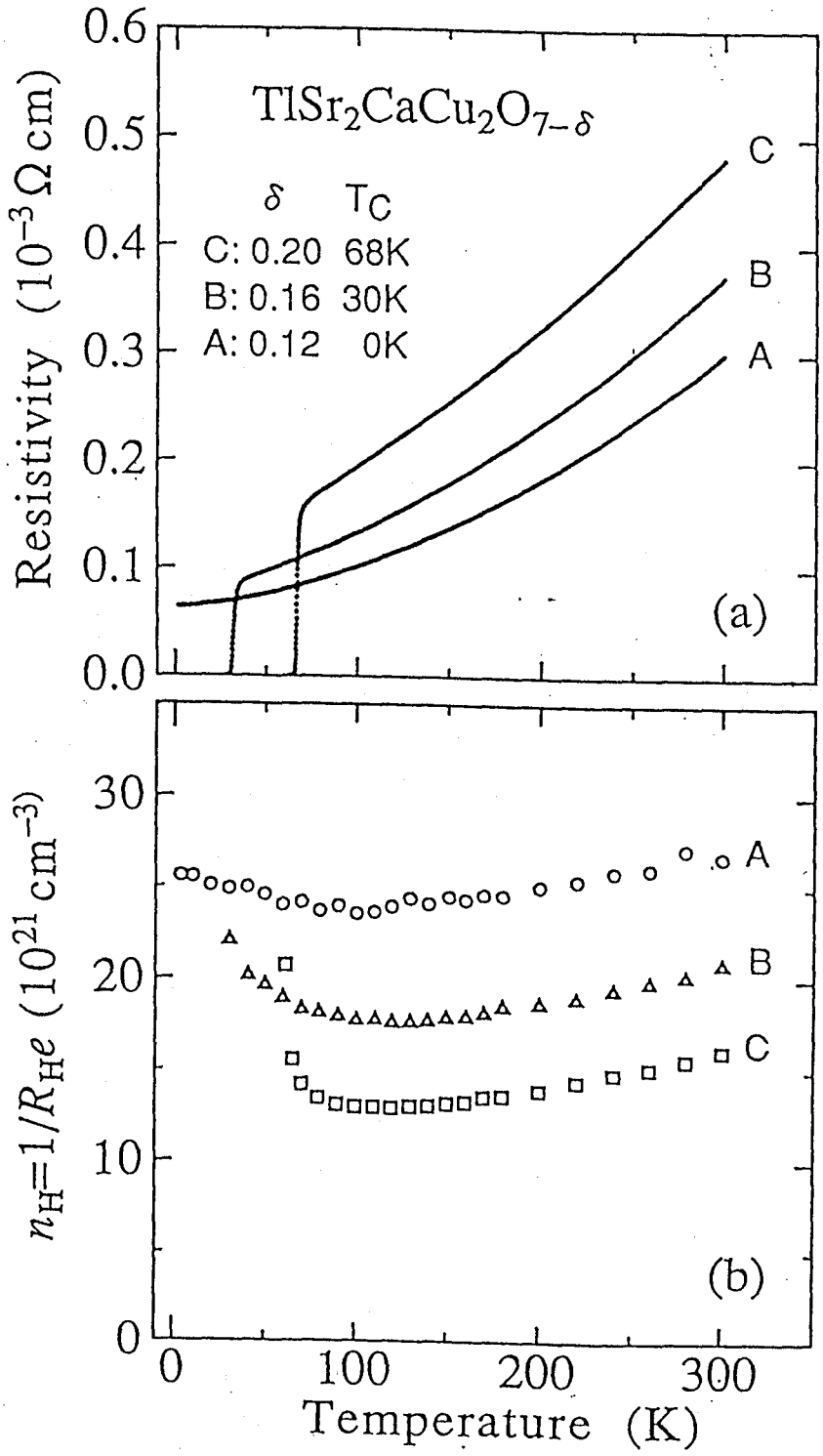

Fig.III-4. T-dependences of (a)resistivity and (b)Hall number for $TlSr_2CaCu_2O_{7-\delta}$ with various δ's.[72]

9.3 Magnetic Susceptibility

Figure III-5 shows the temperature dependence of the normal-state magnetic susceptibility, χ,[72] which was measured at 1 T, after correcting the core diamagnetic susceptibility, χ_{core}. The χ_{core} value is about -8.75×10^{-5} emu/mol-Cu, which is calculated using tablated values.[76] The non-superconducting sample shows a small Curie-like upturn below $\sim$ 50 K. As will be described in Sec.10.1.2, the Knight shift is T-independent, that is, the T-invariant spin susceptibility, χ_s, is an intrinsic behavior in heavily-doped Tl1212. Therefore, this small upturn of the bulk susceptibility is suggested to be not intrinsic but due to the Cu^{2+} ions substituted for Tl site and/or the small impurities which are undetectable by X-ray diffraction experiment.

It is noted that the susceptibility is increased with hole doping, and no significant changes are observed between the superconducting and metallic samples. This feature is also similar to the results for Tl2201.[14] It seems to be no singularity at the superconductor-metal phase boundary, together with the results for the transport properties as described in Sec.9.2, and suggests that the electronic structures for the superconducting and metallic states are quite similar.

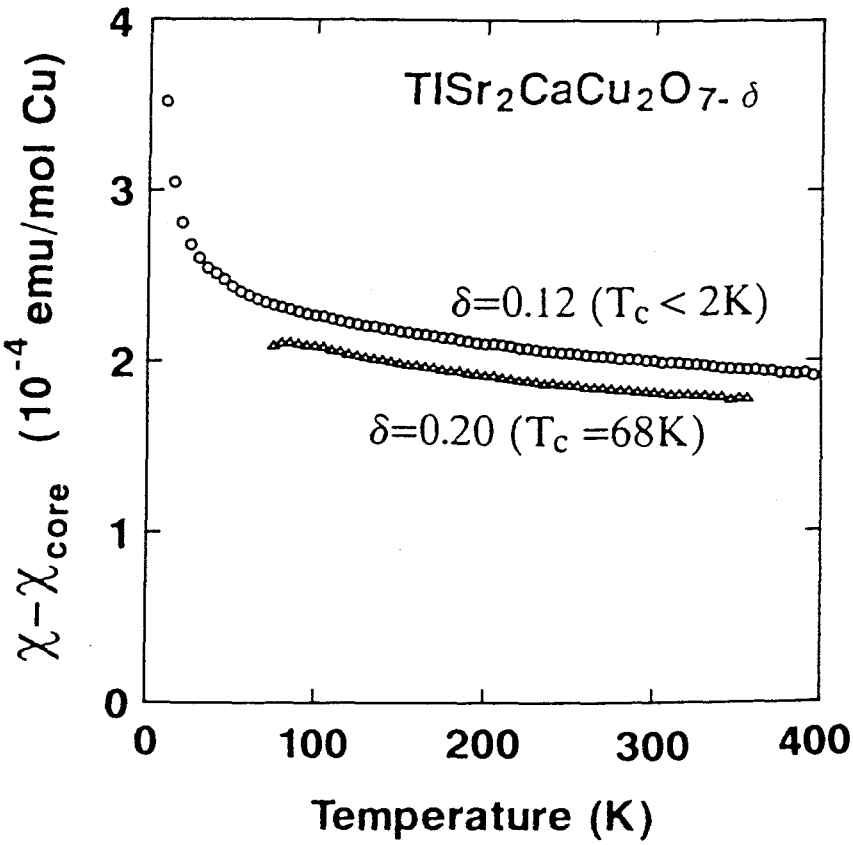

Fig.III-5. T-dependence of the magnetic susceptibility after correcting the core diamagnetism, χ_{core}, for $TlSr_2CaCu_2O_{7-\delta}$.[72)]

10 Experimental Results and Discussions in Heavily-Doped $TlSr_2CaCu_2O_{7-\delta}$

10.1 Static Properties in the Normal State

10.1.1 ^{63}Cu NMR Spectra and $^{63}\nu_Q$

Figures III-6(a) and (b) show the ^{63}Cu NMR spectra at $T = 4.2$ K and $f = 125.1$ MHz for the compound with $T_c = 52$ K for the central transition ($m = 1/2 \leftrightarrow -1/2$) in the partially oriented powder with the c-axis parallel and perpendicular to the external magnetic field, H, respectively. As seen in each figure, there is a broad spectrum in higher field region associated with the unoriented powders, as in the case of Hg1223 as shown in Fig.II-1. The solid and dash arrows correspond to the peaks arising from grains with $\theta = 90°$ and 41.8° to the c-axis, respectively. From the integrated intensity ratio of the spectra with the peaks in lower field region to the broad spectrum, the fraction of the oriented powder with the c-axis parallel to the field is anticipated to be $\sim$ 60 % of the whole powder. As will be described in Sec.10.2.1, since $^{63}T_1$ has been determined with a single component in the normal state, some contribution to the spectrum from the unoriented powder is considered to be negligible, if any. Although the orientation is not perfect, it is enough to determine the shift precisely. The shift was determined from the gravity of the spectra.

The full-width at the half-maximum (FWHM) of the NMR spectra for $c\|H$ is about 300 Oe in the normal state, which is similar to those in other Bi-[36] and Tl-based compounds,[15, 37, 38] but is broader than the case of Y- and Hg-based compounds ($\leq$ 100 Oe), suggesting that the homogeneity in the CuO_2 plane is not so good as that in case of Y- and Hg-based systems.

As mentioned in Sec.6.1.2, $^{63}\nu_Q$ is estimated from the analysis of the series of the NMR spectra.[72, 39] In order to determine the Knight shift and the quadrupolar shift separately, the spectra have been measured at several different frequencies in a range of 80.1$\sim$125.1 MHz as seen in Fig.III-7. The result of the Knight shift will be described in Sec.10.1.2.

$^{63}\nu_Q$ was estimated from eq.(33) as $\sim$ 20.7, 22.5 and 25.8 MHz for the samples with T_c = 70 K, 52 K and 10 K, respectively. Apparently, $^{63}\nu_Q$ increases with decreasing T_c, i.e. by doping holes. As mentioned in Sec.6.1.2, the observed $^{63}\nu_Q$ is related to the local hole

density at Cu site, $n_{x^2-y^2}$, from eq.(34). $n_{x^2-y^2}$ is estimated as $\sim$ 0.77, 0.78 and 0.81 for the sample with T_c = 70 K, 52 K and 10 K, respectively, showing that the hole number at the Cu site increases with increasing oxygen content. Such an analysis of $^{63}\nu_Q$ has been made in various cuprates, showing that $n_{x^2-y^2}$ is in the range of 0.7 $\sim$ 0.9.[43] $n_{x^2-y^2}$'s in Tl1212 are similar to those in heavily-doped Tl2201compounds, but are smaller than those in lightly-doped compounds such as La- and Y-systems.

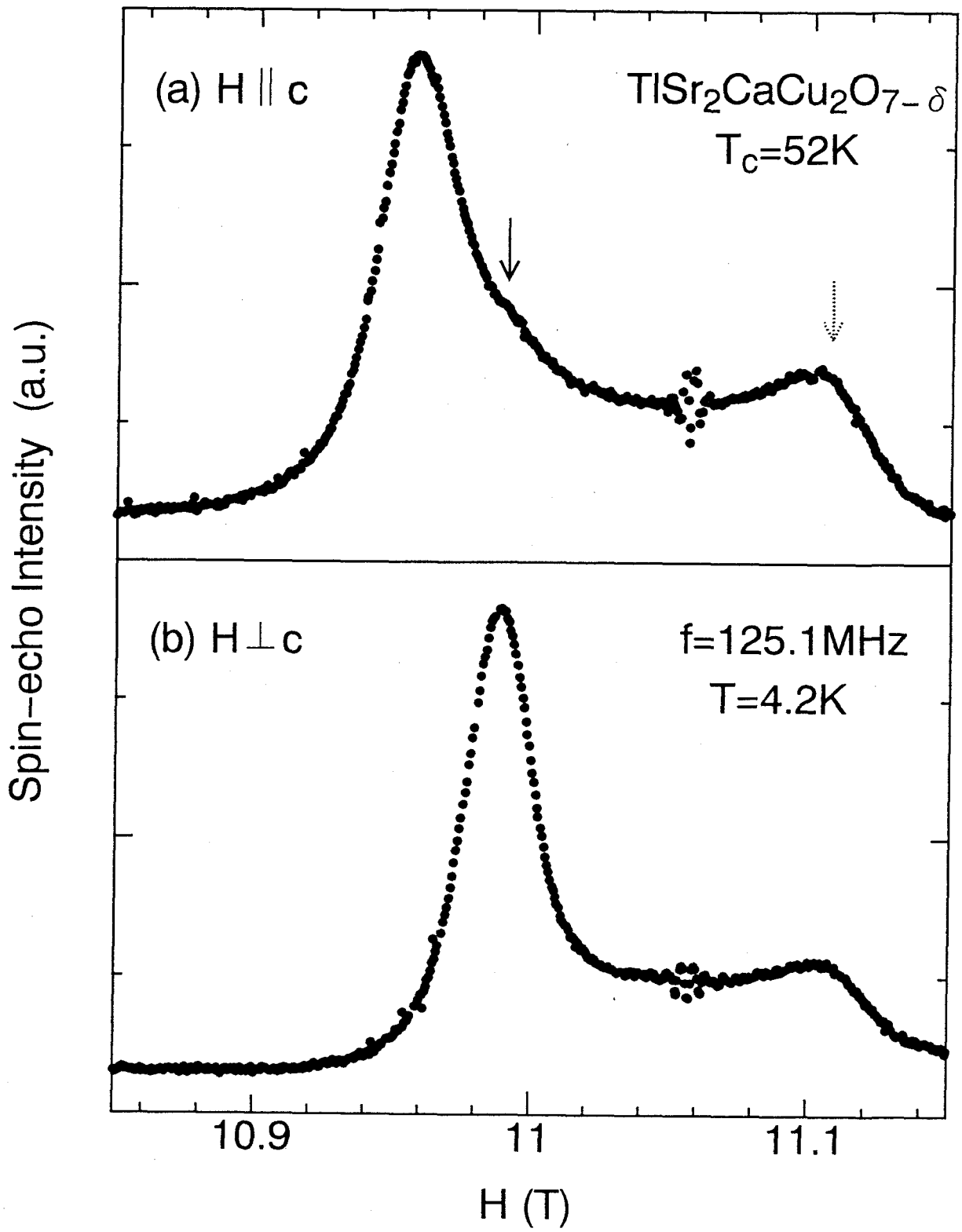

Fig.III-6. ^{63}Cu NMR spectra of Tl1212 for the compound with T_c = 52 K at T = 4.2 K and f = 125.1 MHz for (a)$H \| c$ and (b)$H \perp c$, respectively. Solid and dash arrows correspond to the peaks arising from grains associated with the unoriented powder with θ = 90° and 41.8° to the c-axis, respectively.

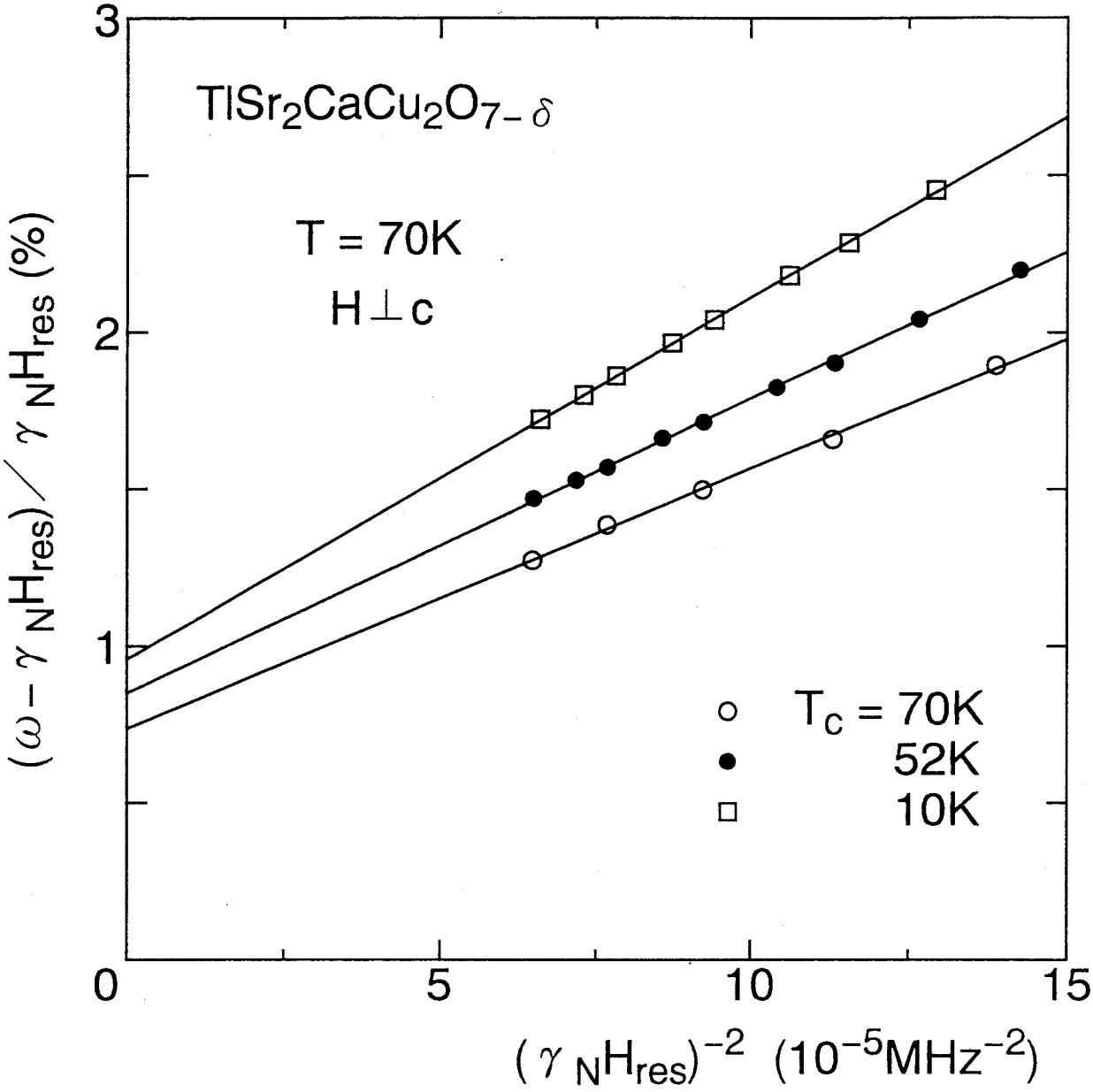

Fig.III-7. The value of $(\omega - \gamma_N H_{res})/(\gamma_N H_{res})$ is plotted against $(\gamma_N H_{res})^{-2}$ in the field perpendicular to the c-axis for different NMR frequencies. H_{res} is the field for resonance corresponding to the compounds with T_c = 70 K (○), 52 K (●) and 10 K (□), respectively.

10.1.2 ^{63}K and Hyperfine Coupling Constants

As for the magnetic properties in Tl1212, the magnetic susceptibility, $\chi(T)$, shows a small Curie-like upturn at low temperature as seen in Fig.III-5, which is probably associated with the presence of Cu^{2+} spins substituted into Tl-sites. So, it is difficult to extract the intrinsic magnetic behavior from $\chi(T)$. However, the local susceptibility at each atomic site can be extracted from the Knight shift measurement without any appreciable influence of impurity spins. In order to extract an intrinsic magnetic property inherent to the CuO_2 plane, the Knight shift measurements were carried out.

Figures III-8(a) and (b) show the T-dependence of the Knight shift components perpendicular, $^{63}K_{ab}$, and parallel, $^{63}K_c$, to the c-axis for the compounds with T_c = 70 K, 52 K and 10 K, respectively. Both $^{63}K_{ab}$ and $^{63}K_c$ decrease rapidly below T_c. This large reduction of ^{63}K below T_c demonstrates that the Cooper-pair in the superconducting state is spin-singlet (s- or d-wave pairing). Also, this behavior is in contrast to that in lightly-doped compouds, where $^{63}K_c$ is dominated by the T-independent orbital contribution. When $H \| c$, T_c drops to $\sim$ 63 K and $\sim$ 42 K for the samples with T_c = 70 K and 52 K, respectively, indicating that the superconductivity is more easily destroyed by the field parallel than perpendicular to the c-axis, similar to the case in Tl2201.[65] On the other hand, in the normal state, a remarkable feature is that both shifts are T-independent, that is, the spin susceptibility, χ_s, is T-independent, as in the cases of $YBCO_7$[77] and Tl2201,[15, 65] It suggests that the T-invariant χ_s is a common behavior in optimum- and heavily-doped region. This is in contrast to the T-dependent behavior of $^{63}K_{ab}$ in lightly-doped LSCO,[44] Y124[45, 78] and oxygen-deficient $YBCO_{6+x}$.[24] Actually, it is reported that $^{63}K_{ab}$ decreased gradually upon lowering temperature in lightly-doped $TlSr_2(Lu_{0.7}Ca_{0.3})Cu_2O_y$ (T_c = 40K) as will be shown in Fig.III-29, suggesting that a decrease of $^{63}K_{ab}$ is a common behavior in lightly-doped systems. Also, from the quantitative point of view, the absolute value of the T-independent ^{63}K increases with decreasing T_c.

In order to estimate the hyperfine fields, A_α and B, that is, in order to estimate the spin Knight shift, $^{63}K_{s,\alpha}$, the orbital Knight shift, $^{63}K_{orb,\alpha}$, must be substracted from the raw data above T_c, because the both Knight shifts components in Tl1212 are, unfortunately, T-invariant. Since $^{63}K_{orb}$ is proportional to $n_{x^2-y^2}$ from eq.(14), it is estimated to be $\sim$

0.21, 0.22 and 0.23 % from the value of $^{63}\nu_Q$, in the same manner as the case of Hg1223 in Sec.6.3.2. From eq.(13), the anisotropy of $^{63}K_s$ is expressed as follows:

$$\frac{^{63}K_{s,c}}{^{63}K_{s,ab}} = \frac{A_c + 4B}{A_{ab} + 4B} \tag{52}$$

where $\chi_s(T)$ is assumed to be isotropic. The anisotropy of $^{63}K_s$ in Tl1212 is evaluated as $\sim$ 0.42, 0.48 and 0.57 for the compounds with T_c=70 K, 52 K and 10 K, respectively. If the on-site hyperfine fields are assumed to be independent of the hole content with the values of $A_{ab} \sim$ 37 kOe/μ_B and $A_c \sim -170$kOe/μ_B,[24, 44, 45, 46, 47, 48] the super-transferred hyperfine fields, B's, are estimated to $\sim$ 80, 90 and 110 kOe/μ_B from eq.(52), respectively. As in the case for heavily-doped Tl2201,[15, 65] B in Tl1212 compounds increases with increasing oxygen content, being larger than a typical value ($B \sim$40kOe/μ_B) in lightly-doped LSCO,[44] Y124[45] and $YBCO_{6+x}$.[24] Thus, **it is a common feature that the Cu($3d_{x^2-y^2}$)-O($2p\sigma$)-Cu(4s) hybridization in heavily-doped region is larger than that in lightly-doped region and further enhanced by an increase of holes.**

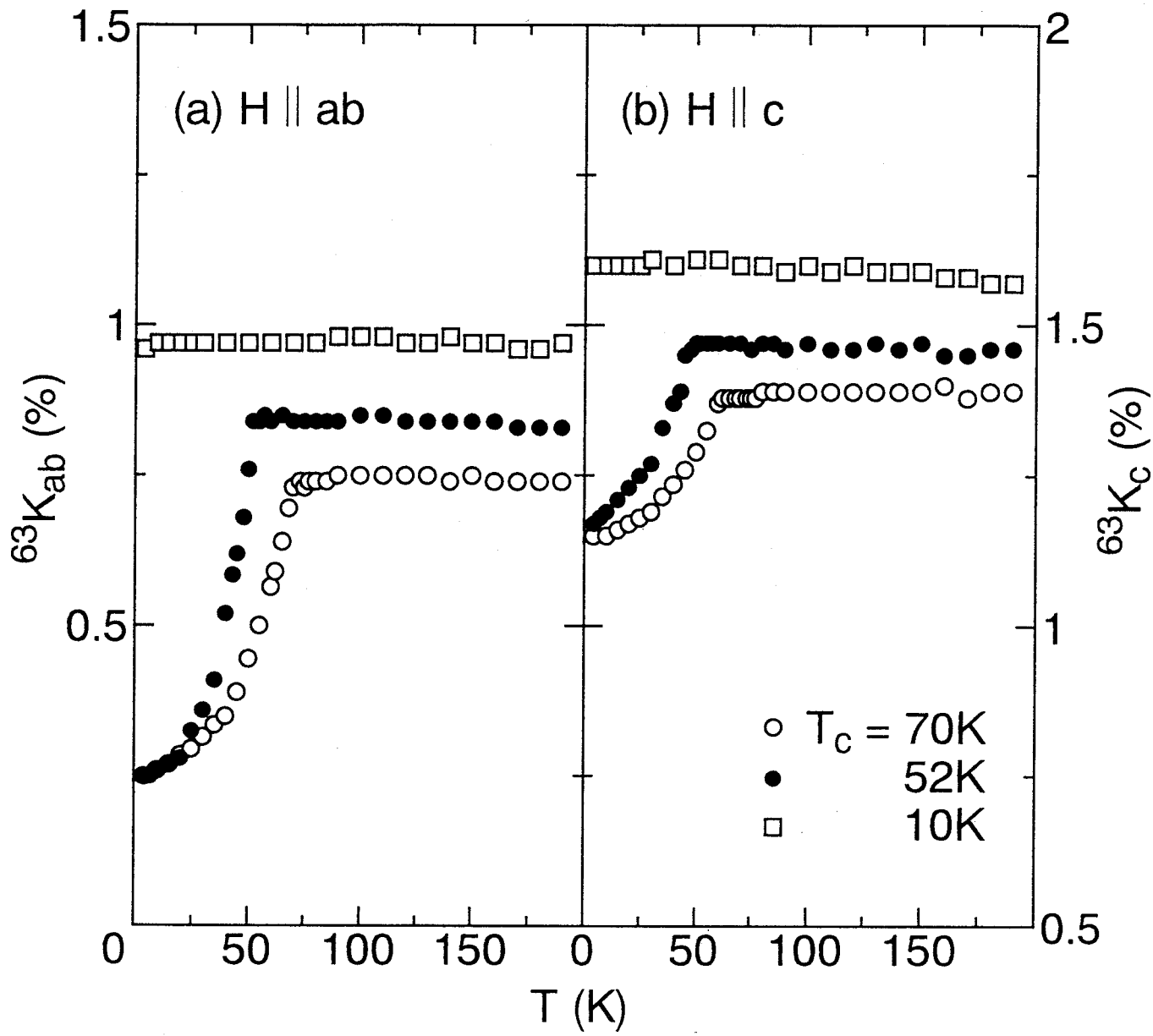

Fig.III-8. T-dependence of the Knight shift components (a)perpendicular, $^{63}K_{ab}$, and (b)parallel, $^{63}K_c$, to the c-axis for the compounds with T_c = 70 K (○), 52 K (●) and 10 K (□), respectively.

10.2 Character of Spin Fluctuation in the Normal State

10.2.1 $^{63}(1/T_1)$

Figures III-9(a) and (b) show the relaxation curve of $m(t)$ plotted against the time, t, after saturation pulse at 70 K (above T_c) and 1.4 K (below T_c), respectively, for the compound with T_c=70 K under the magnetic field of $\sim$ 11 T perpendicular to the c-axis. Solid curves in the figures are the best fit to eq.(31). As described in Sec.10.1.1, the orientation of the sample is not perfect. But, it is shown that the data above T_c was well fitted by eq.(31) with a single $^{63}T_1$ component as seen in Fig.III-9(a), suggesting that some contributions from the unoriented powder is considered to be negligible if any. On the other hand, short components, which are affected by the vortex cores, appear below T_c, as seen in Fig.III-9(b).

Figure III-10 shows the T-dependence of $^{63}(1/T_1T)_{ab}$ for the compounds with T_c = 70 K(o), 52 K(•) and 10 K(□). As seen in figure, $^{63}(1/T_1T)_{ab}$ has a broad peak around T^* ($\sim$ 90 K, 70 K and 30 K for the compounds with T_c = 70 K, 52 K and 10 K, respectively,) just above T_c without any coherence peak just below T_c. Also, the behavior of $^{63}(1/T_1T)_c$ component parallel to the c-axis is quite similar to that of $^{63}(1/T_1T)_{ab}$. In the inset of Fig.III-10, $^{63}(T_1T)_{ab}$ plotted against T reveals a T-linear dependence down to T^*, indicating that $^{63}(1/T_1T)_{ab}$ follows a Curie-Weiss behavior down to T^* as in the case of LSCO[8, 44] and $YBCO_7$,[2, 79] which are indicated in the figure as well, in contrast to the T-invariant Knight shift. This behavior is observed in most of high-T_c cuprates. As mentioned in Sec.6.2.1, it is considered that this behavior reflects the Curie-Weiss law of $\chi_Q(T)$ ($\chi_Q = C/(T+\theta)$), and is probing the presence of the **AF** spin correlation. As seen in the inset of Fig.III-10, the Weiss temperature, θ, increases with increasing hole content, as in the case of LSCO.[44] The increase of θ seems to be the result in a decrease of χ_Q, meaning that the **AF** spin correlation is weakened by doping holes.

It was shown that T^2-term of electric resistivity was enhanced by the staggered susceptibility as $\rho(T) \sim \chi_Q(T)T^2$ in the 2D case on a Fermi-liquid picture.[80] When $\chi_Q(T)$ follows a Curie-Weiss law, there is a crossover from $\rho \propto T$ above θ to $\rho \propto T^2$ below θ for the T-dependence of the resistivity. Thus, the NMR results and the anomalous T-dependence of

resistivity (as seen in Fig.III-4(a)) can be understood within the framework of the Fermi-liquid picture in which the short-range **AF** spin correlation is taken into consideration.

Also, from the quantitative point of view, the absolute value of $^{63}(1/T_1T)_{ab}$ is reduced with decreasing T_c, i.e. with doping holes. From eq.(43), $^{63}(1/T_1T)$ is related to the value of α/Γ_Q, where Γ_Q is the characteristic energy of the **AF** spin fluctuation, and α is a scale factor between the staggered susceptibility, χ_Q, and the **AF** correlation length, ξ, respectively. In order to extract the doping dependence of the value of α/Γ_Q, the observed $^{63}(1/T_1T)_{ab}$ should be corrected by the hyperfine form factor $[(A_{ab}-4B)^2+(A_c-4B)^2]$, since B increases with increasing holes from the analysis of the Knight shift. The result is shown in Fig.III-11 where the short-range **AF** spin correlation at the zone boundary is assumed to be significantly dominated even in the heavily-doped Tl1212 system, supported by the Curie-Weiss behavior of $^{63}(1/T_1T)_{ab}$. As seen in the figure, the decrease of the $^{63}(1/T_1T)_{ab}$ divided by the form factor suggests that Γ_Q in the Tl1212 compounds are progressively enhanced with increasing holes, if α is invariable for all samples.

Also, in order to know how the relative magnitude of α/Γ_Q changes from lightly- to heavily-doped system, the T-dependence of $^{63}(1/T_1T)_c$ divided by the hyperfine form factor, $(A_{ab}-4B)^2$, is shown in Fig.III-12, together with the results of lightly-doped LSCO[44] and $YBCO_7$.[4] In the sample with T_c=70 K, Γ_Q is larger than those in the lightly-doped LSCO[44] and $YBCO_7$,[4] similar to the case in Hg1223.

On the other hand, in order to estimate the magnitude of the **AF** spin correlation, the anisotropy of the relaxation rate of ^{63}Cu, $^{63}R = (1/T_1T)_{ab}/(1/T_1T)_c$, were measured. As mentioned in Sec.6.2.1, ^{63}R reflects indirectly the q-dependence of the spin fluctuation, that is, the magnitude of the **AF** spin correlation.[15, 48] ^{63}R is nearly T-independent, and decreases from $\sim$ 1.7, 1.6 to 1.3 for the compounds with T_c = 70 K, 52 K and 10 K, respectively.

Figure III-13 shows ^{63}R plotted against B, together with the results of Hg1223, $YBCO_7$[50] and Tl2201.[15] $^{63}R_{AF}$ and $^{63}R_r$ are calculated by eqs.(38) and (39) using the values of A_{ab}, A_c and B obtained from the analysis of the Knight shift mentioned. As seen in figure, ^{63}R is smaller than $^{63}R_{AF}$ as in the case of Tl2201, in contrast to the results of $YBCO_7$ and Hg1223 where $^{63}R \sim ^{63}R_{AF}$, suggesting that the **AF** correlation in Tl1212 is smaller

than those in $YBCO_7$ and Hg1223, as in the case of Tl2201. Moreover, ^{63}R decreases progressively down to $^{63}R_r$ with increasing B, i.e. with increasing holes, indicating that the **AF** spin correlation is suppressed with increasing holes. As a result, T_c is suppressed. Thus, it seems that **the AF spin fluctuation is closely related to the occurrence of the superconductivity.**

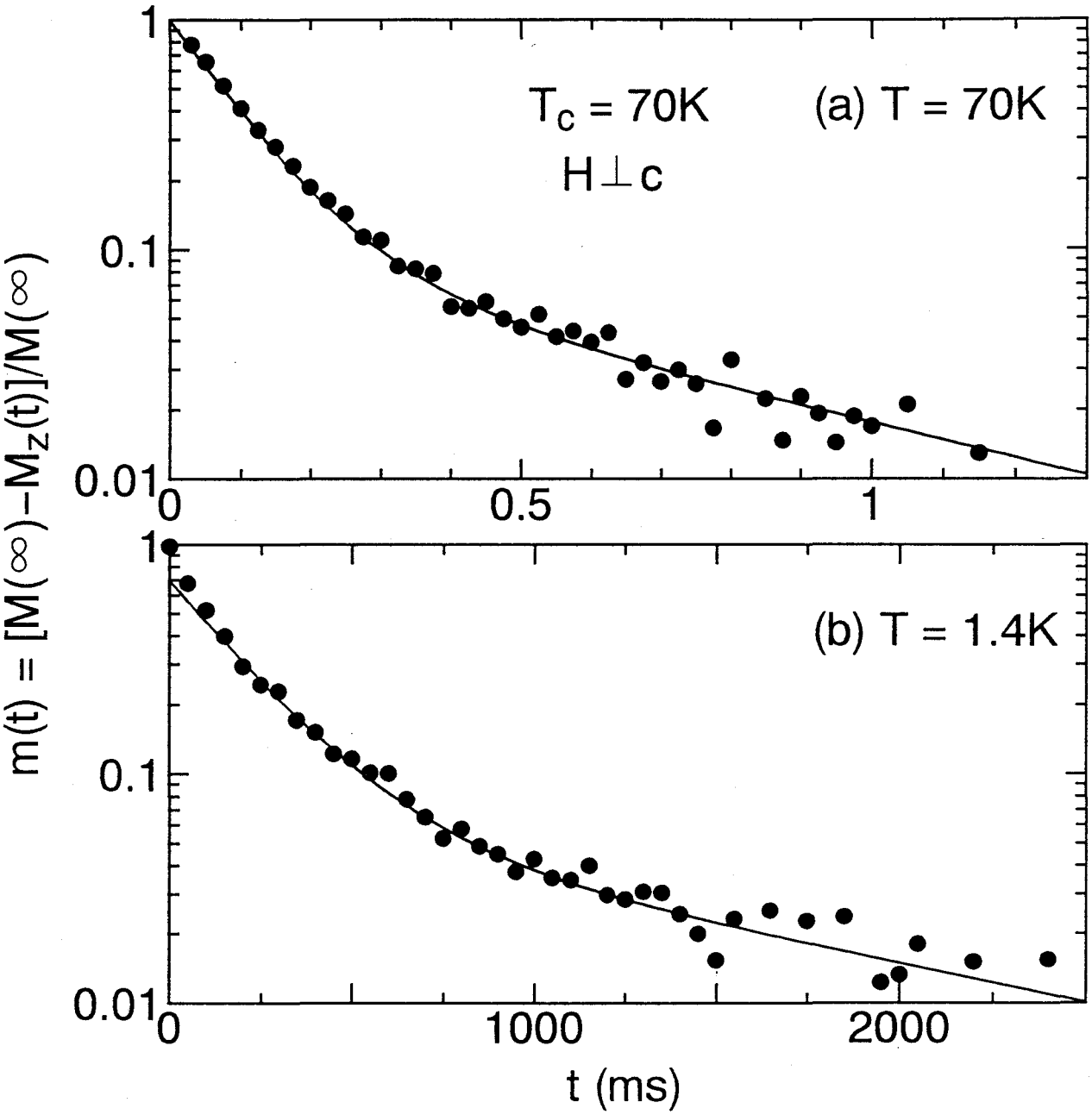

Fig.III-9. Relaxaion curves plotted against t after saturation pulse at (a)T = 70 K and (b)1.4 K, respectively, for the compound with $T_c = 70$ K under the magnetic field of $\sim$ 11 T perpendicular to the c-axis. Solid lines are the results fitted by the relaxation function of eq.(31).

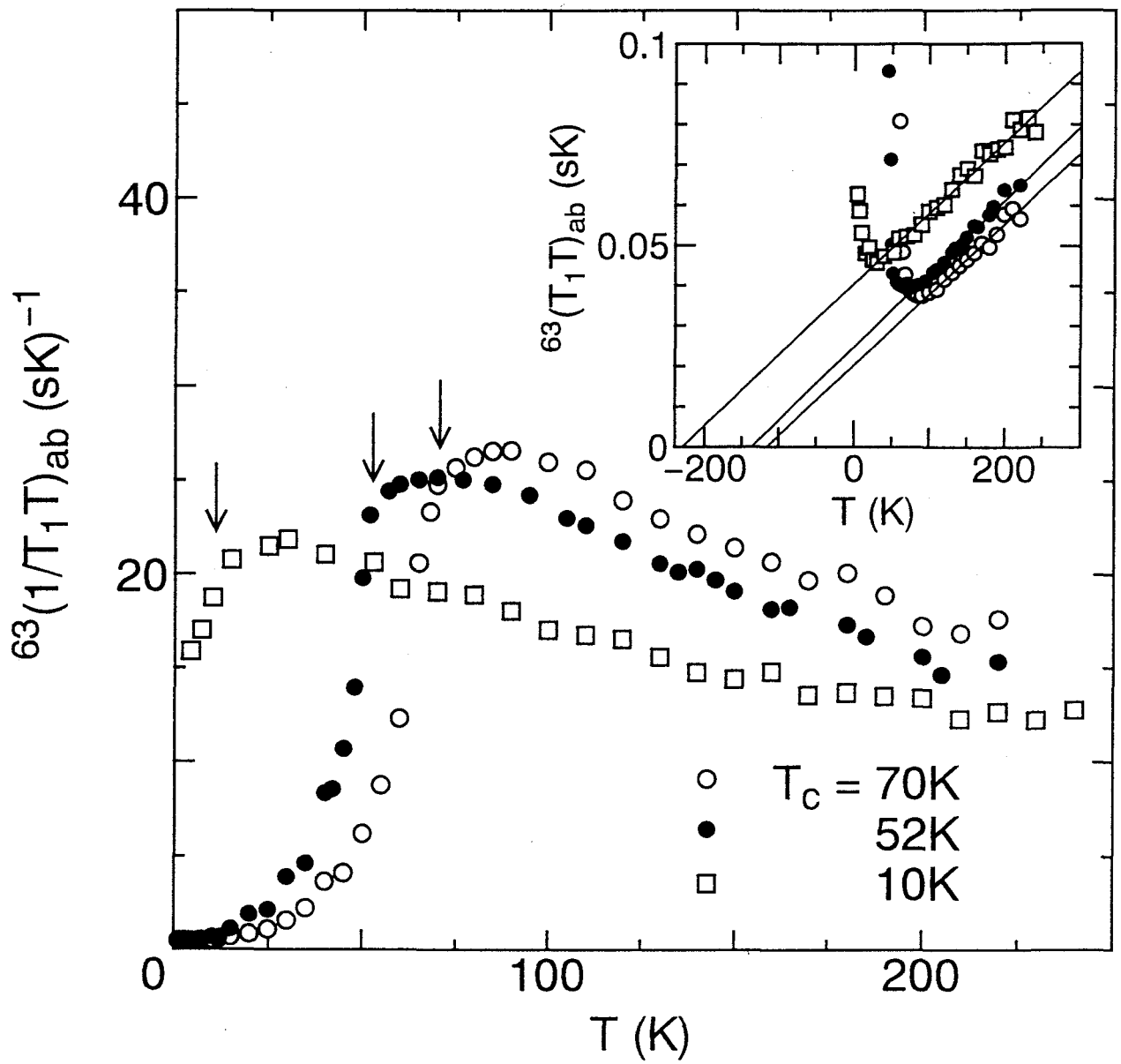

Fig.III-10. T-dependence of $^{63}(1/T_1T)_{ab}$ for the compounds with T_c = 70 K (○), 52 K (●) and 10 K (□), respectively. Inset indicates T-dependence of $^{63}(T_1T)_{ab}$, which shows that $^{63}(1/T_1T)_{ab}$ follows the Curie-Weiss behavior.

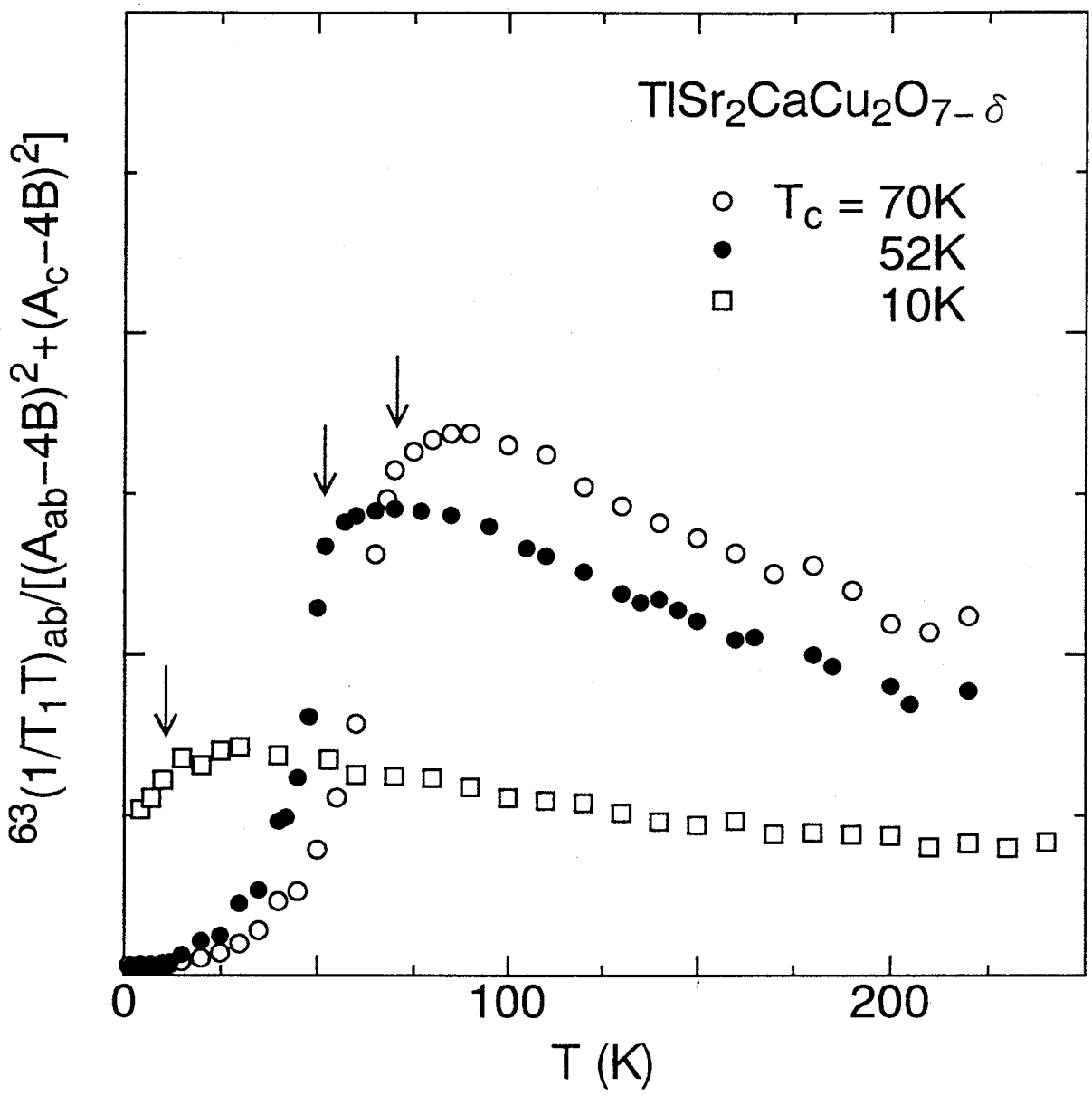

Fig.III-11. Comparison of the value of $^{63}(1/T_1T)_{ab}/[(A_{ab}-4B)^2+(A_c-4B)^2]$ in Tl1212, scaled approximately to $\sim \alpha/\Gamma_Q$.

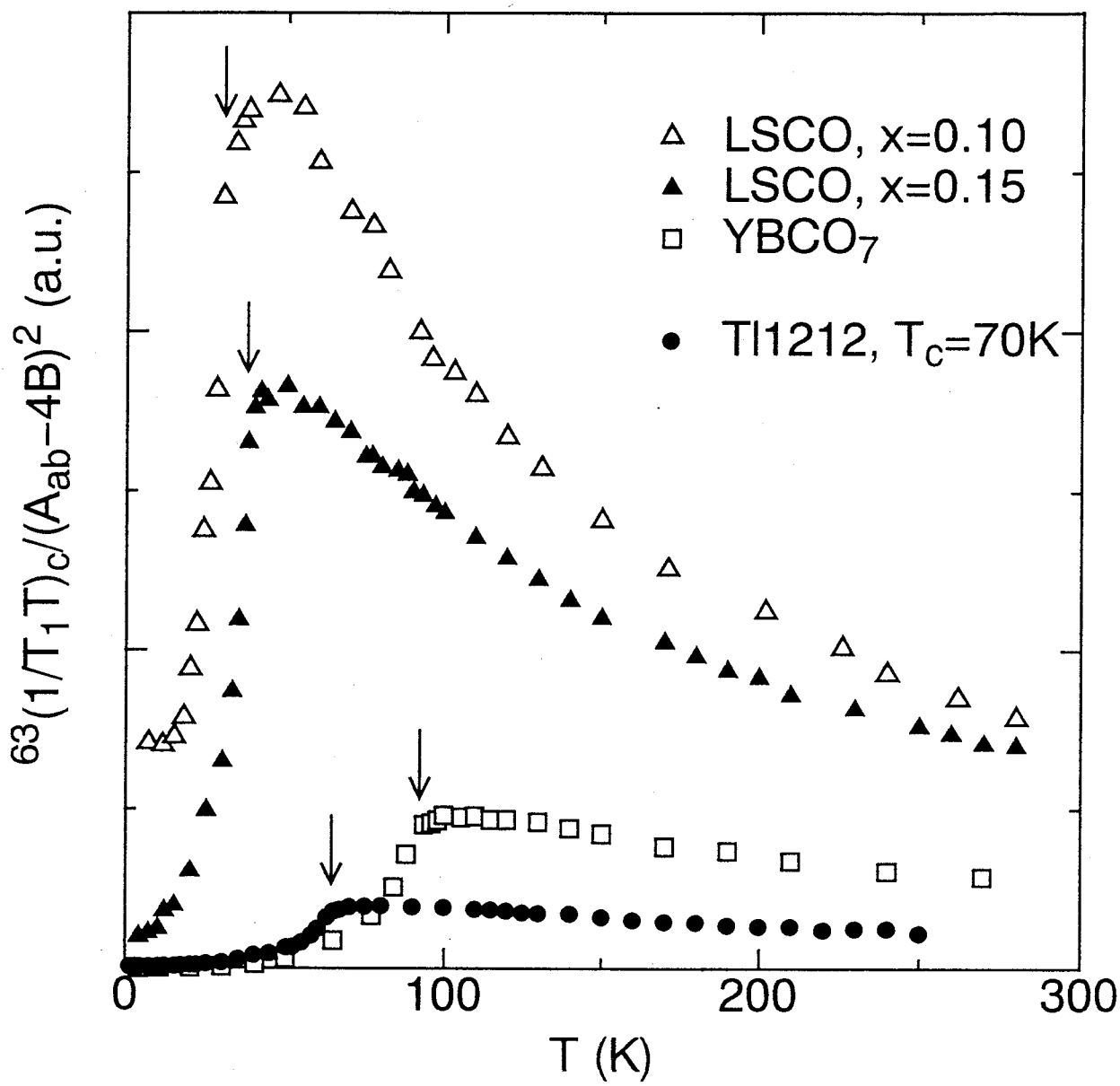

Fig.III-12. Comparison of the value of $^{63}(1/T_1T)_c/(A_{ab}-4B)^2$, scaled approximately to $\sim \alpha/\Gamma_Q$, with the results of lightly-doped LSCO[44] and $YBCO_7$.[4]

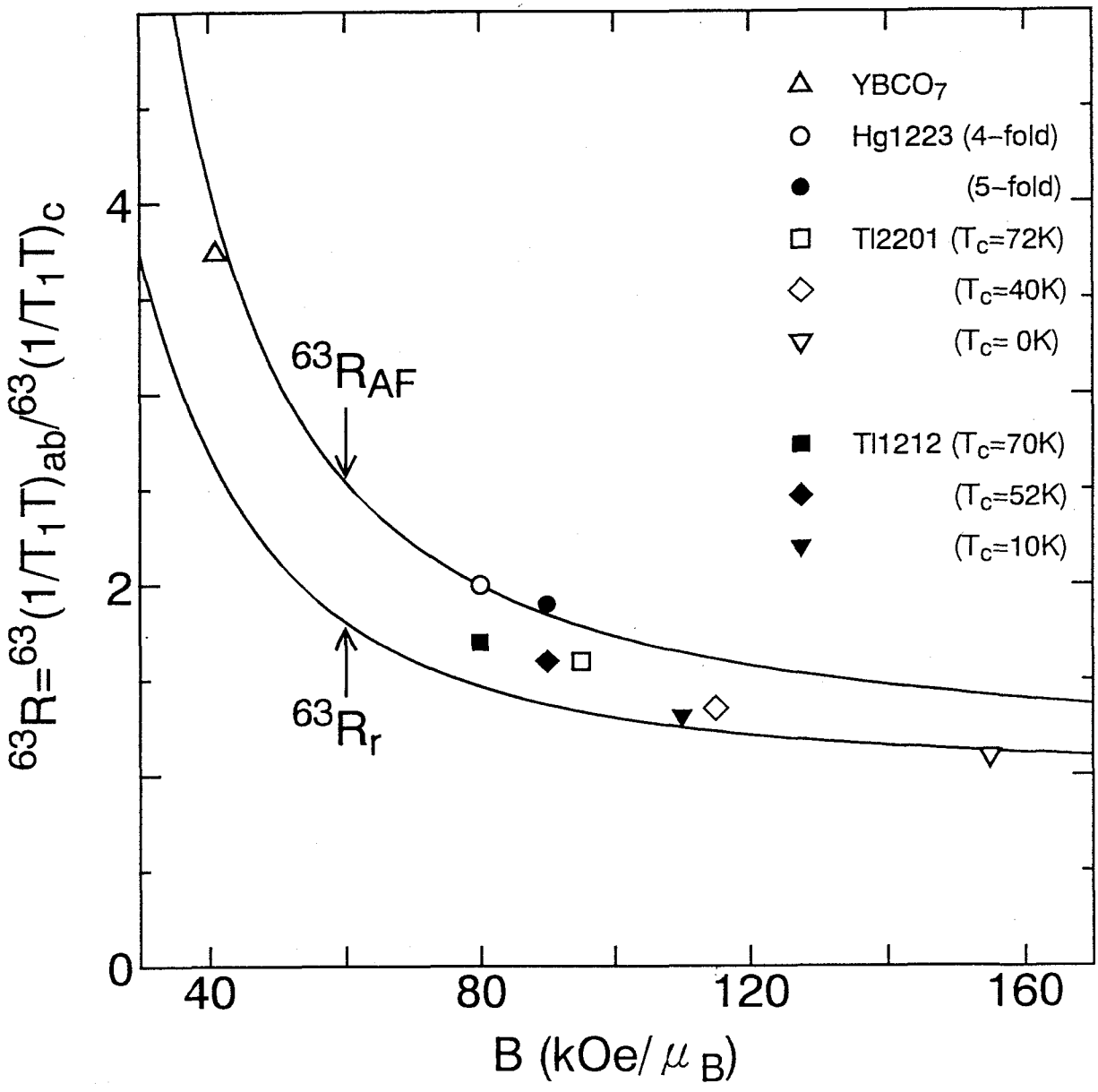

Fig.III-13. Anisotropy of $^{63}(1/T_1T)$, ^{63}R, plotted against the super-transferred hyperfine coupling constant, B, together with the results for several materials.[15, 50)]

10.2.2 $1/T_{2G}$

Figure III-14 shows the ^{63}Cu nuclear spin-echo decay at $T = 100$ K under the magnetic field of ~ 11 T parallel to the c-axis for the compounds with $T_c = 70$ K(o), 52 K(•) and 10 K(□), respectively, plotted against t, where t is the time interval between the $\pi/2$ pulese and spin-echo. The spin-echo decay curves (the solid lines) are well fitted to eq.(32). So, most of spins may be flipped.

Figure III-15 shows the T-dependence of the Gaussian component of the spin-spin relaxation rate, $1/T_{2G}$, in Tl1212 for the compounds with $T_c = 70$ K(o), 52 K(•) and 10 K(□), respectively, together with the results of $YBCO_7$.[53] A remarkable feature is that $1/T_{2G}$'s for all samples in Tl1212 increase with decreasing temperature followed by a peak just above T_c, which is almost the same temperature where $^{63}(1/T_1T)$ shows a broad peak, similar to the cases in Hg1223 and heavily-doped Tl2201,[81] in contrast to that in lightly-doped compounds such as $YBCO_{6+x}$[51] and Y124.[54]

Also, from the quantitative point of view, the absolute values of $1/T_{2G}$ is reduced with decreasing T_c, i.e. with doping holes. In order to extract the doping dependence of the **AF** spin correlation, the observed $1/T_{2G}$ should be corrected by the hyperfine form factor, $(A_c-4B)^2$, expected from eq.(45), since B increases with increasing holes from the analysis of the Knight shift as mentioned in Sec.10.1.2. The result is shown in Fig.III-16, together with the results of $YBCO_7$[53] and Hg1223, where the short-range **AF** spin correlation at the zone boundary is assumed to be significantly dominated even in the heavily-doped Tl1212 system, supported by the Curie-Weiss behavior of $^{63}(1/T_1T)$. As seen in figure, the decrease of the value of $1/T_{2G}$ divided by the form factor suggested that **the AF spin correlation in the Tl1212 compounds is smaller than those in $YBCO_7$ and Hg1223 and is progressively weakened with increasing holes**, if the scale factor, α, is invariable for all compounds. The results are supported by the analysis of the anisotropy of $^{63}(1/T_1)$, mentioned in Sec.10.2.1.

As mentioned in Sec.6.2.2, $^{63}(T_1T)/(T_{2G})^2$ is related to $\chi_Q\Gamma_Q$ from eq.(46), which is proportional to the value of T_c in MP's expression.[55] The magnitude is shown in the inset of Fig.III-17, together with the results of $YBCO_7$[53] and Tl2201.[81] A remarkable feature is that the value of $\chi_Q\Gamma_Q$ is smaller as T_c is lower, which is consistent with the MP's expression

of T_c.[55] It suggests that the reduction of T_c in heavily-doped region can be explained by the spin-fluctuation-induced superconducting mechanism, and that the spin fluctuation is related intimately to high-T_c superconductivity.

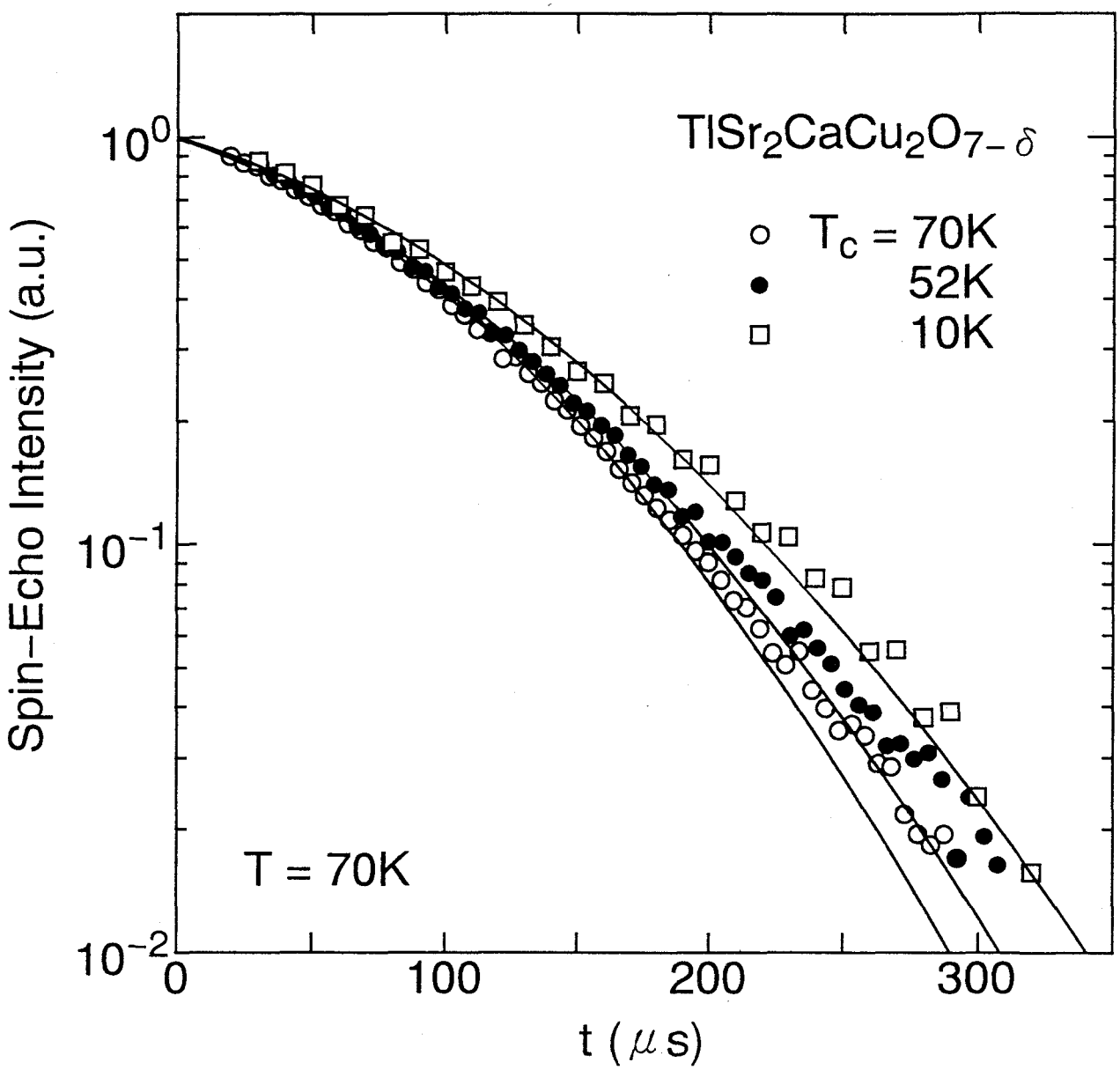

Fig.III-14. Spin-echo decay curves at $T = 70$ K for the compounds with $T_c =$ 70 K (○), 52 K (●) and 10 K (□), respectively, plotted against t, where t is the time interval between the 1st pulse and the spin-echo. Solid lines are the results fitted by eq.(32).

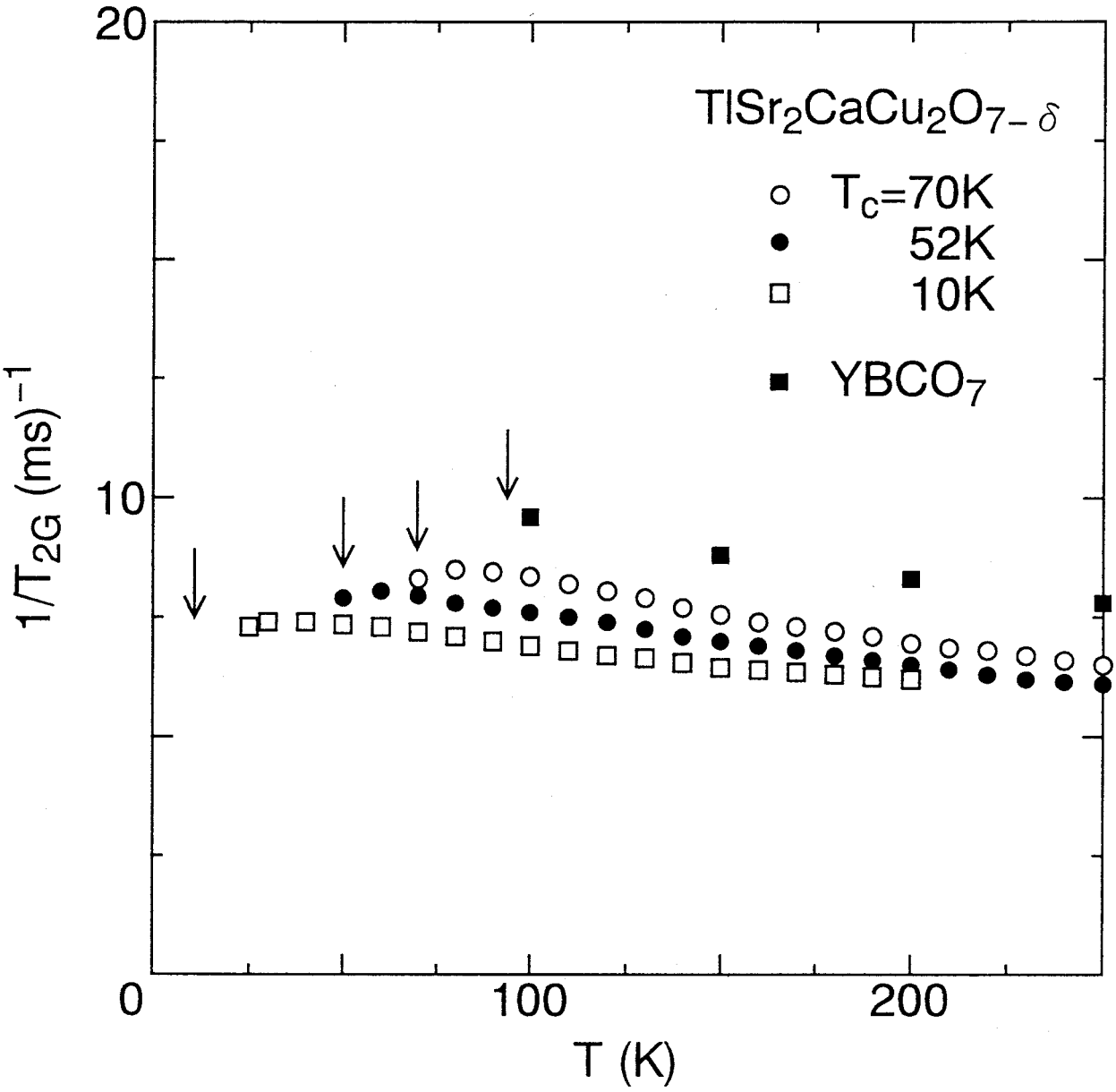

Fig.III-15. T-dependence of $1/T_{2G}$ for the compounds with T_c = 70 K (○), 52 K (●) and 10 K (□), respectively, together with the results for $YBCO_7$.[53]

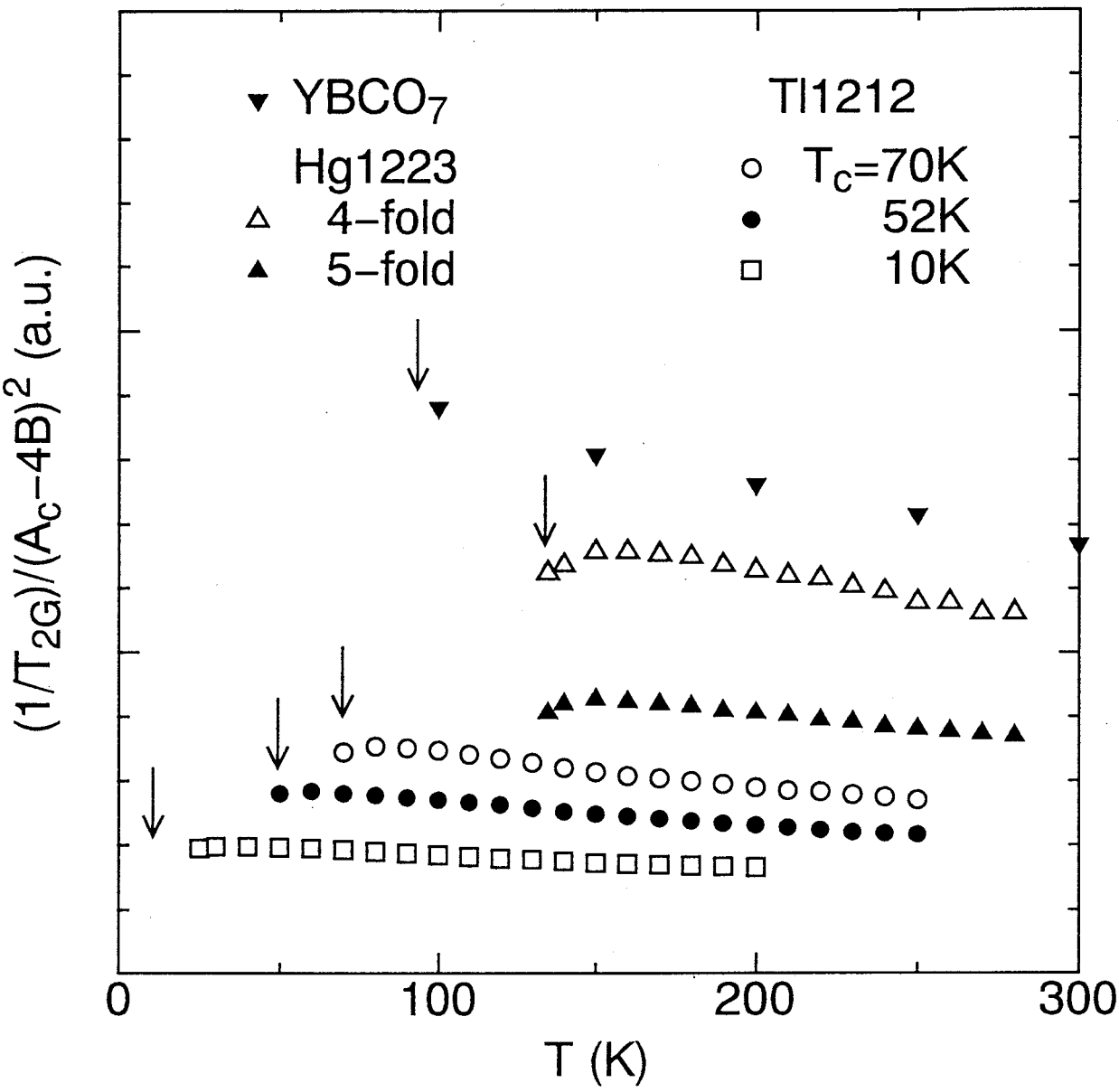

Fig.III-16. Comparison of the value of $(1/T_{2G})/(A_c - 4B)^2$ in Tl1212, scaled approximately to $\sim \chi_Q/\xi(= \alpha\xi)$, with the results for $YBCO_7$[53] and Hg1223.

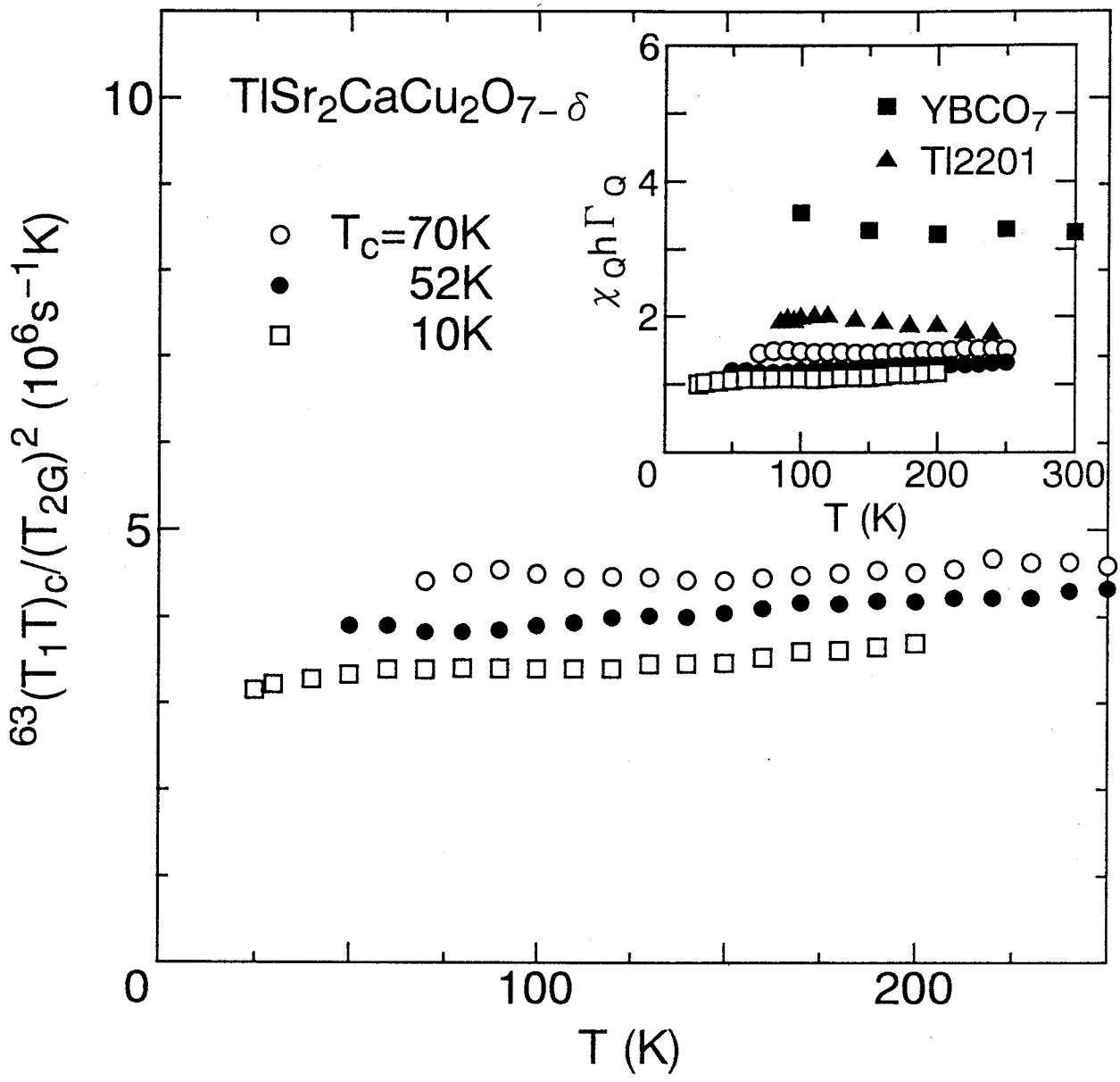

Fig.III-17. T-dependence of the ratio, $^{63}(T_1T)_c/(T_{2G})^2$, for the compounds with $T_c = 70$ K (o), 52 K (•) and 10 K (□), respectively. Inset indicates the comparison of the value of $\chi_Q \hbar \Gamma_Q$ with the results for $YBCO_7$[53] and Tl2201.[81]

10.3 Symmetry of Pairing State

10.3.1 $^{63}(1/T_1)$

As stated in Sec.10.2.1, the relaxation curve below T_c is not fitted by eq.(31) due to the presence of the vortex cores. The short component arises from the nuclei close to the vortex cores, while the long component from those far away from the vortex cores. To display the overall T-dependence of $^{63}(1/T_1)$ below T_c, the long component of $^{63}(1/T_1)$ is tentatively extracted in the same manner as the case in Hg1223, that is, from a fit of eq.(31) to the data of $m(t)$ smaller than 0.5 as indicated by solid line in Fig.III-9(b).

Figures III-18(a) and (b) show the T-dependence of the long component of $^{63}(1/T_1)_{ab}$ (o) and $^{63}(1/T_1)_c$ (•) below T_c for the compounds with T_c = 70 K and 52 K, respectively, in a logarithmic scale. As observed universally in high-T_c cuprates, $^{63}(1/T_1)$ for both samples in Tl1212 decreases rapidly following a power-law like T-dependence below T_c without any enhancement just below T_c. At low temperature well below T_c, $^{63}(1/T_1)$ is proportional to the temperature, that is, obeys T_1T = const. law.

Figure III-19 shows a relaxation function, $m(t)$, well below T_c plotted against the product of time, t, and T for the compound with T_c = 70K under the external magnetic field of $\sim$ 11 T parallel to the c-axis. $m(t)$ falls on a unique curve over a T-range of 1.4 $\sim$ 10 K, suggesting that all the $^{63}T_1$ components follow the T_1T = const. law at low temperature, regardless of the distribution of $^{63}T_1$.

As mentioned in Sec.6.3.1, the relaxation behavior below T_c under the magnetic field is affected by the normal fluxoid cores. In order to investigate the relaxation process below T_c in Tl1212, the H-dependence of $^{63}(1/T_1)$ was measured.

Figures III-20(a) and (b) show the H-dependence of $^{63}(1/T_1)$ components parallel (•) and perpendicular (o) to the c-axis at T = 4.2 K for the compounds with T_c=70 K and 52 K, respectively. As seen in the figure, $^{63}(1/T_1)$ at low temperature well below T_c is enhanced by the magnetic field for both materials, and exhibits nearly H-linear dependence as eq.(47). Furthermore, the H-dependence is more pronounced in $H \| c$ than in $H \perp c$. As seen in eq.(48), in a rapid spin diffusion limit, $1/T_1$ is enhanced by the external magnetic field, and depends on the direction of the applied magnetic field due to the anisotropy of the coherence

length, ξ_i (in general, $\xi_{ab} \geq \xi_c$). Therefore, this experimental results indicates that the relaxation process in Tl1212 at low temperature under the magnetic field is dominated by the spin-diffusion process to the vortex cores, as in the case of $YBCO_7$,[61, 62] Y124[63] and Hg1223. The fact that T_1T = const. law holds at low temperature under the magnetic field suggests that the electronic state in the vortex cores is described by the Fermi-liquid picture. As mentioned in Sec.10.2.1, T_c drops for both samples in case of $H \| c$, that is, the value of T_c under the magnetic field is ambiguous. Thus, the T-dependence of $^{63}(1/T_1T)$ below T_c is presented only in case of $H \perp c$.

Figures III-21(a) and (b) show the H-dependence of $^{63}(1/T_1)_{ab}$ for the compounds with T_c = 70 K and 52 K, respectively, at several temperatures in a range of 1.4 $\sim$ 10 K. The intrinsic value, $^{63}(1/T_{1s})$, in the superconducting state is determined from the extrapolation to zero field ($H \rightarrow 0$), as seen in eq.(48).

Figures III-22(a) and (b) show the T-dependence of $^{63}(1/T_1)_{ab}$ for the compounds with T_c = 70 K and 52 K, respectively. o and • show the value under the magnetic field of $\sim$ 11 T and the extrapolated value to zero field, respectively. Below 7K, it is remarkable that $^{63}(1/T_{1s})$ inherent to the superconducting state follows the $^{63}T_{1s}T$ = const. law, which is indicative of the gapless nature of superconductivity, such as Zn-doped $YBCO_7$,[4] LSCO (x $\geq$ 0.20),[44] Bi2212,[36] Tl2223[64] and Tl2201[65]. The fractions of the residual DOS, N_{res}/N_0, are estimated to be about $\sim$ 0.10 for both samples with T_c = 70 K and 52 K, from eq.(51). An important result is that N_{res}/N_0 is nearly the same for the two samples with the different T_c values. This suggests that the difference of T_c in these samples is not due to the difference in N_{res}/N_0 but actually the increase of holes.

Next, the T-dependence of $^{63}(1/T_{1s})_{ab}$ in Tl1212 compounds is estimated by the gapless 2D d-wave model with line nodes at the cylindrical Fermi surface as $\Delta(\phi) = \Delta(T)\cos(2\phi)$ corresponding to $d_{x^2-y^2}$ symmetry where the additional finite density of states, N_{res}, at the Fermi level is taken into account, as shown in Fig.II-22(a). In this model, it is assumed that the T-dependence of the superconducting order parameter, $\Delta(T)/\Delta$, is the same as that in the case of BCS superconductor. This **gapless d-wave pairing model** has consistently explained the NMR results in Zn-doped $YBCO_7$,[4] LSCO (x$\geq$0.20),[44] Bi2212,[36] Tl2223[64] and Tl2201.[65] As indicated by solid lines in Figs.III-22(a) and (b), the best fit to $^{63}(1/T_{1s})_{ab}$

(•) in Tl1212 are roughly reproduced by this model with the parameters $N_{res}/N_0 = 0.10$ and $2\Delta/k_BT_c = 8$ for both samples with $T_c = 70$ K and 52 K, suggesting that the d-wave pairing in the superconducting state is realized in Tl1212 compounds. The validity of the gapless d-wave model was also confirmed from the Knight shift measurements, as will be described in Sec.10.3.2.

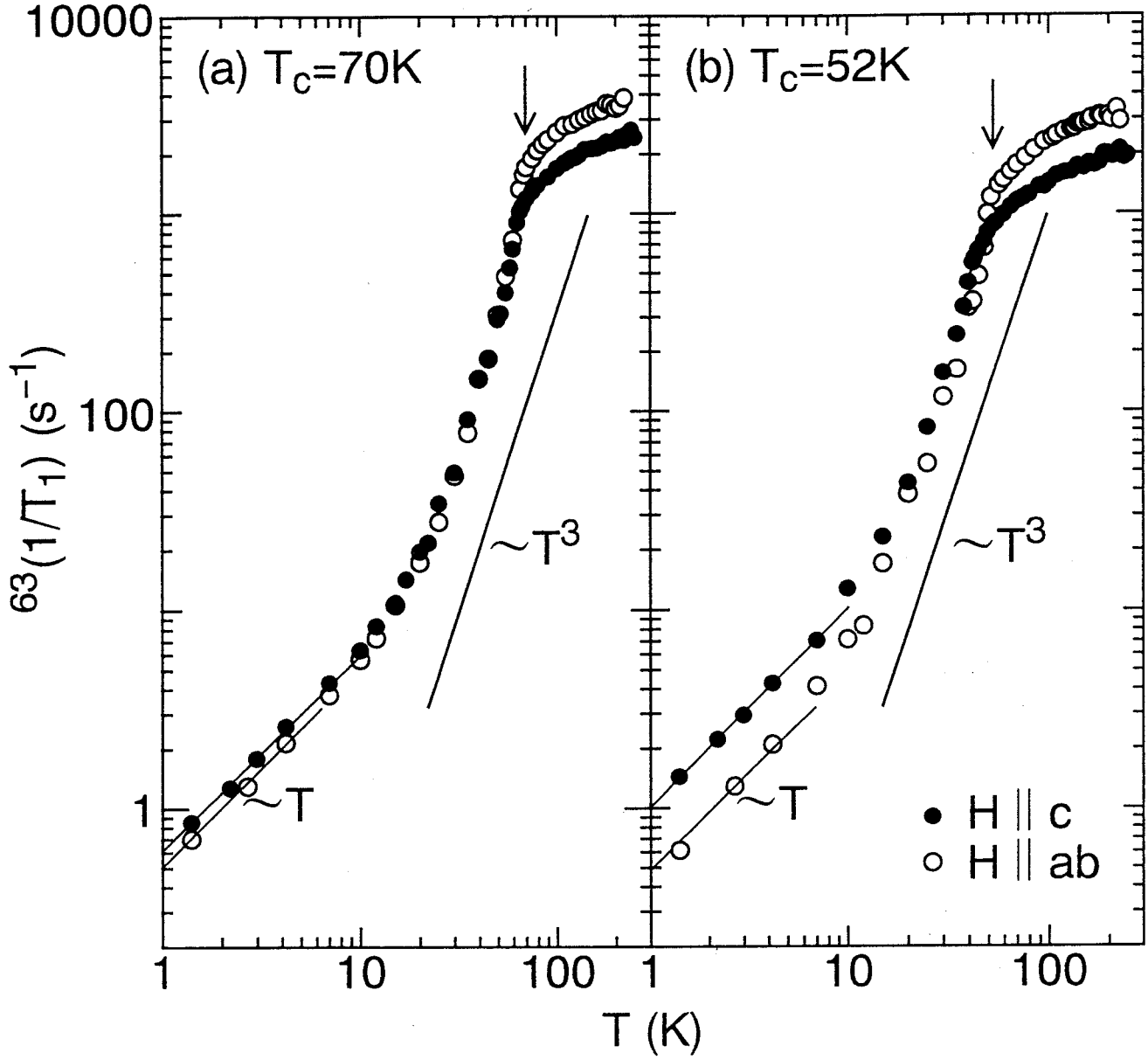

Fig.III-18. T-dependence of $^{63}(1/T_1)_{ab}$(○) and $^{63}(1/T_1)_c$(●) below T_c for the compounds with (a)T_c = 70 K and (b)52 K, respectively, under the magnetic field of ~ 11 T.

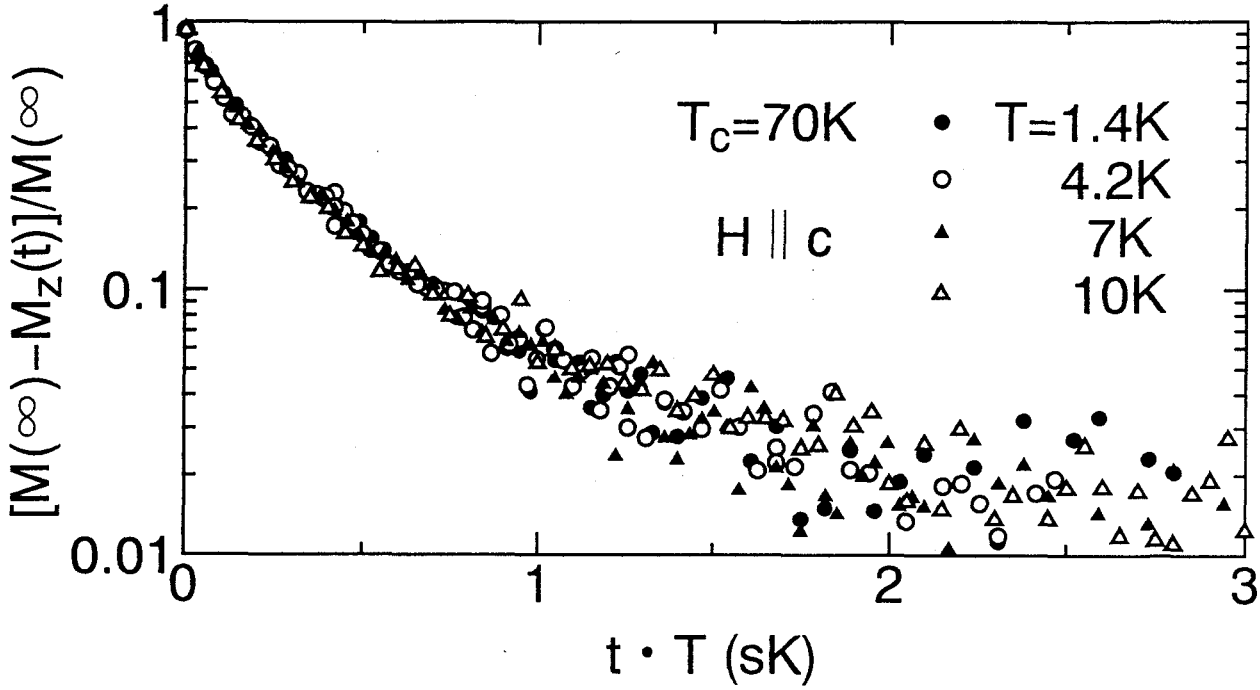

Fig.III-19. Relaxation curves plotted against $t \cdot T$ is on a single curve, showing that all the $^{63}T_1$ components follow the T_1T = const. law below 10 K.

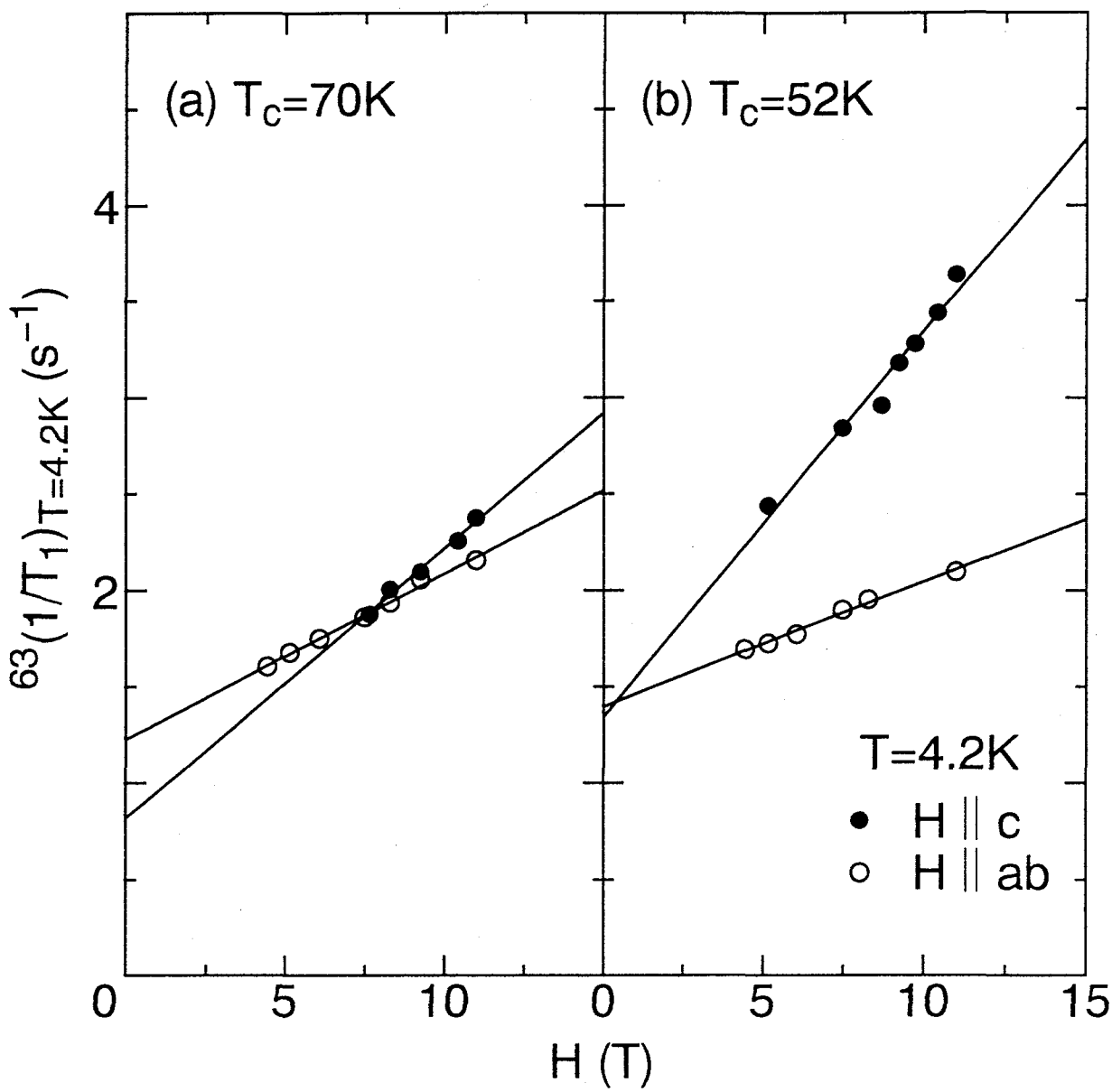

Fig.III-20. Magnetic field dependence of $^{63}(1/T_1)$ components parallel (•) and perpendicular (○) to the c-axis at $T = 4.2$ K for the compound with (a)$T_c = 70$ K and (b)52 K, respectively.

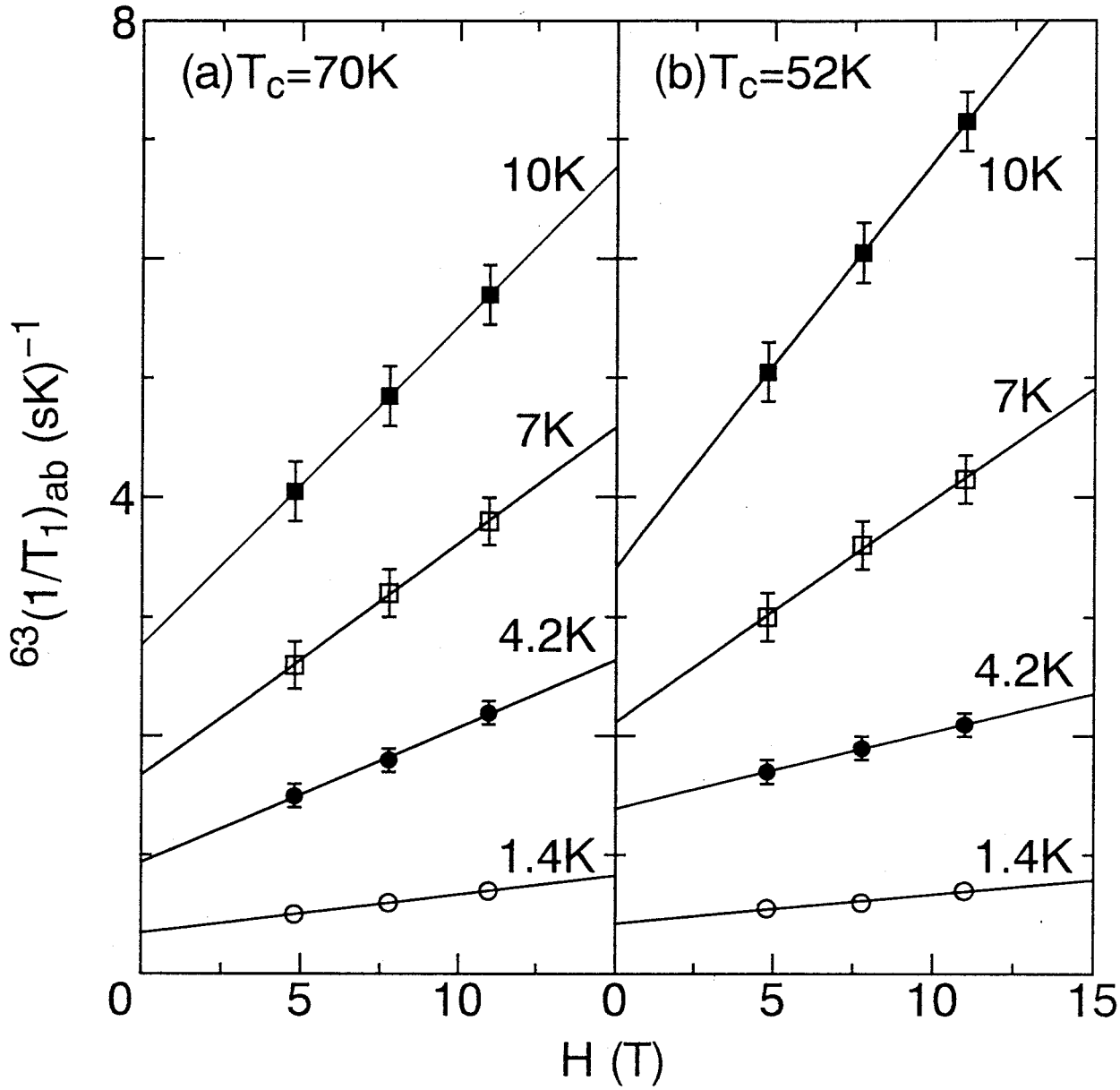

Fig.III-21. Magnetic field dependence of $^{63}(1/T_1)_{ab}$ at several temperatures below 10 K for the compounds with (a)T = 70 K and (b)52 K, respectively.

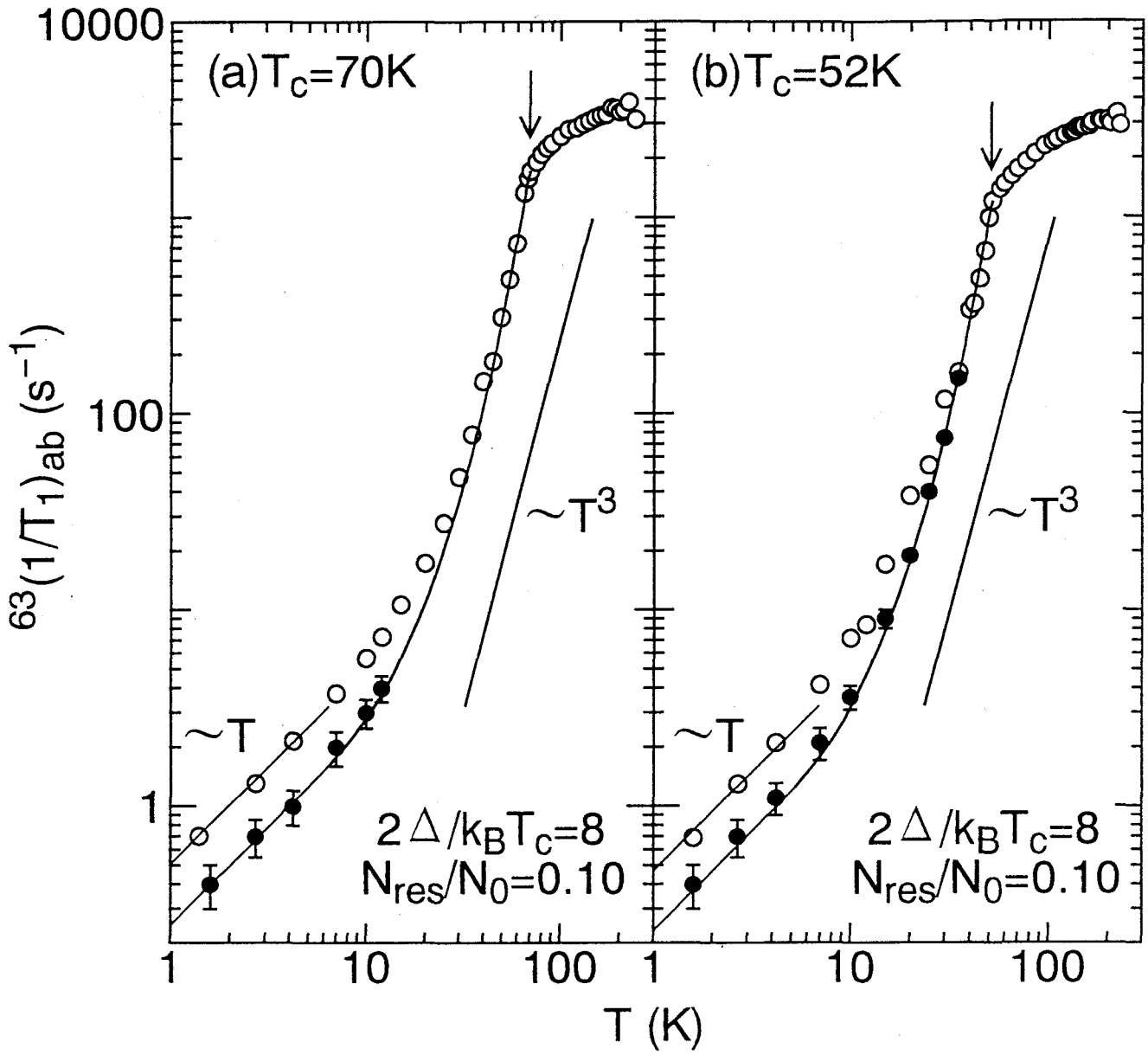

Fig.III-22. T-dependence of $^{63}(1/T_1)_{ab}$ below T_c for the compounds with (a)T_c = 70 K and (b)52 K, respectively, o and • indicate the value at $\sim$ 11 T and the extrapolated value to the zero magnetic field, respectively. Solid lines are calculated using the gapless d-wave model with the parameters of $2\Delta/k_BT_c = 8$ and $N_{res}/N_0 = 0.10$.

10.3.2 ^{63}K

As described in Sec.10.1.2, both components of the Knight shift decrease rapidly below T_c as seen in Figs.III-8(a) and (b), indicating that the Cooper-pair is spin-singlet. Also, in case of $H\|c$, T_c drops to $\sim$ 63 K and $\sim$ 42 K for the samples with T_c = 70 K and 52 K, respectively, indicating that the superconductivity is more easily destroyed by the field parallel than perpendicular to the c-axis. The residual density of states, N_{res}, is induced by the pair-breaking effects such as not only impurity, imperfection of the crystal but also the magnetic field. Thus, the pair-breaking effect due to the external magnetic field in case of $H\|c$ is more effective than that in case of $H \perp c$. In order to extract the pair breaking due to the quality of the sample, the T-dependence of ^{63}K below T_c is presented only in case of $H \perp c$.

The residual shift at low temperature is not always ascribed to the T-independent orbital shift, but includes the residual spin shift originating from the finite density of states at the Fermi level due to imperfection of the crystal and impurity. Therefore, the spin Knight shift, $^{63}K_s$, must be obtained by substracting the orbital Knight shift, $^{63}K_{orb}$, from the raw data, as described in Sec.10.1.2.

Figure III-23 shows the T-dependence of the spin Knight shift, K_s, normalized by the value at T_c, K_{T_c}, under the magnetic field perpendicular to the c-axis. Solid line is calculated using the gapless d-wave model with the same parameters ($2\Delta/k_BT_c$ = 8 and N_{res}/N_0 = 0.10) as in the analysis of $^{63}(1/T_{1s})$, mentioned in Sec.10.3.1, which satisfactorily interprets the experimental results as well. Thus, both the results of ^{63}K and $^{63}(1/T_1)$ are consistently understood in terms of **the gapless d-wave model** in which the finite density of states is induced at the Fermi level. This feature is similar to the case in Tl2201,[65] suggesting that the d-wave superconductivity is a common property in heavily-doped region, as in the cases of lightly-doped compounds. The spin-fluctuation-induced superconductivity mechanism, which is consistent with the results in the normal state, gives rise to a d-wave pairing state, suggesting that the spin fluctuation is responsible for the high-T_c superconductivity.

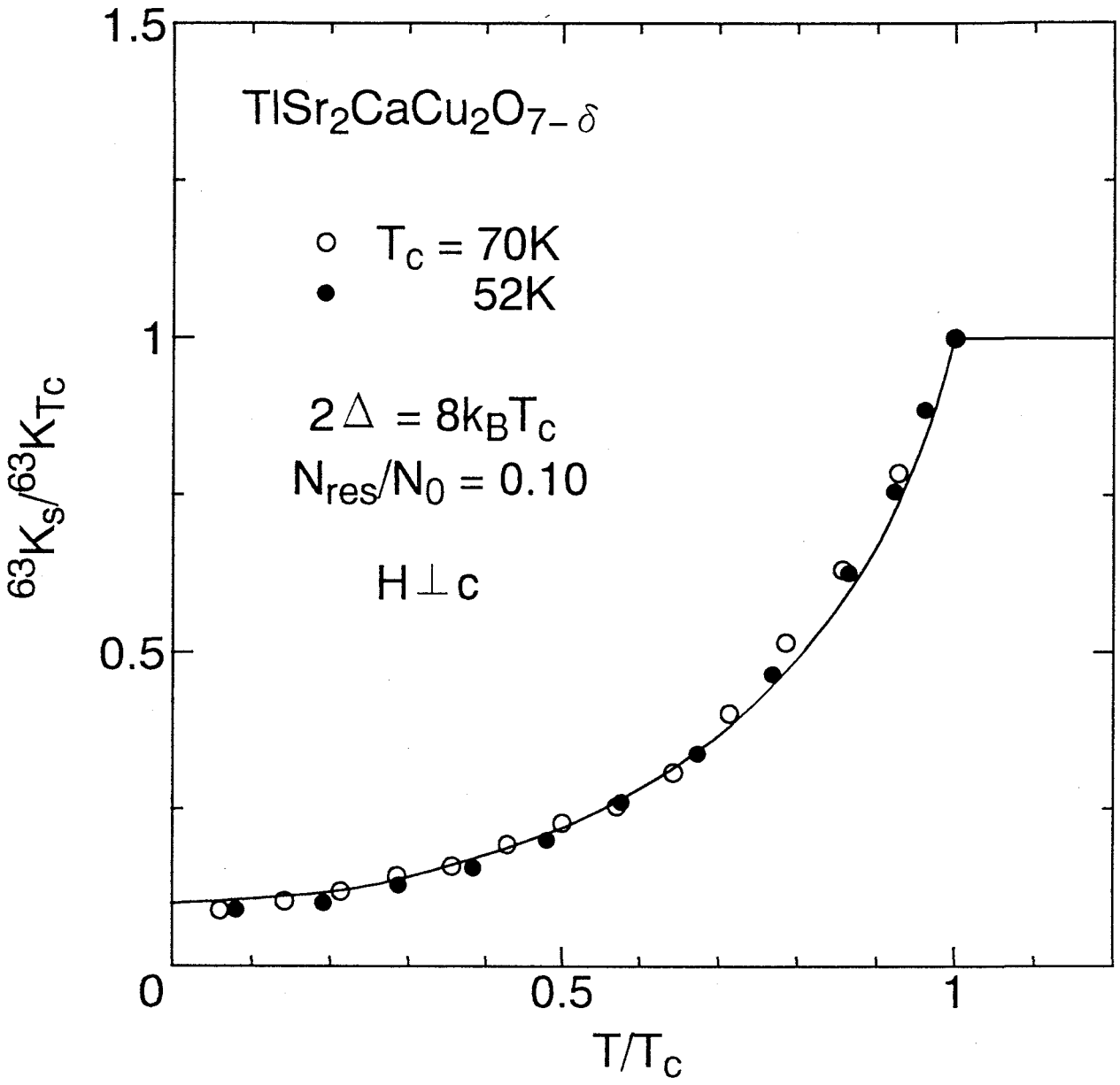

Fig.III-23. T-dependence of $^{63}K_s/^{63}K_{T_c}$ plotted against T/T_c for the compounds with T_c = 70 K (○) amd 52 K (●), respectively. $^{63}K_{T_c}$ is the value of $^{63}K_s$ at T_c. Solid line is calculated using the gapless d-wave model with the parameters of $2\Delta/k_BT_c = 8$ and $N_{res}/N_0 = 0.10$.

11 Spin Gap like Behavior in Lightly-Doped Region of $TlSr_2(Lu_{0.7}Ca_{0.3})Cu_2O_y$ (T_c = 40 K)

11.1 Introduction

In the lightly-doped high-T_c compounds, the uniform susceptibility, $\chi_s(T)$, decreases commonly with lowering temperature. $^{63}(1/T_1T)$ exhibits a broad peak well above T_c in oxygen-deficient $YBCO_{6+x}$[9, 10] and Y124[11] with double CuO_2 layers. This spin-gap behavior attracts a great interest, suggesting a possible formation of the spin-singlet well above T_c. Initiated by the RVB picture,[13] this anomalous property in the normal state is argued to reflect that the superconductivity would occur in the non-Fermi liquid state. The physical origin of the spin gap is still under debate. Within the Hubbard model[18] and t-J model,[13] the spin gap is caused by the nesting property of the Fermi surface.

In contrast to the above two compounds, it was shown from the Cu nuclear relaxation[8] and the inelastic neutron scattering measurements[12] that LSCO with smaller hole content does not exhibit any signature of the spin-gap behavior around zone boundary, (π, π). In the above two compounds, the CuO chain controlling the hole content forms an ordered structure, while the La(Sr)O layer in LSCO experiences significant randomness, which may give a hint for the contrast of the magnetic excitation. A difference of the number of layers may be one of the reasons to yield the contrast for the magnetic excitation.

In this section (11), in order to clarify the origin of the spin-gap in the lightly-doped high-T_c compounds, it has been carried out the ^{63}Cu and ^{205}Tl NMR measurements of $TlSr_2(Lu_{1-x}Ca_x)Cu_2O_y$ (Lu-doped Tl1212) systems (T_c = 90 $\sim$ 0 K) with two pyramidal layers like YBCO but without the CuO chain. Replacing Lu atoms into Ca sites and increasing oxygen content make this system lightly- and heavily-doped, respectively, as seen in Fig.III-24.[73] The bulk susceptibility, $\chi(T)$, in lightly-doped $TlSr_2(Lu_{0.7}Ca_{0.3})Cu_2O_y$ (T_c = 40 K) decreases with decreasing temperature, similar to other lightly-doped compounds such as LSCO,[44] $YBCO_{6+x}$[24] and Y124,[45] as shown in Fig.III-25.[73] A spin-gap behavior has been found in the lightly-doped region regardless of the presence of disorder in the Ca(Lu) layers sandwiched by CuO_2 bi-layers, as will be described in Sec.11.3.

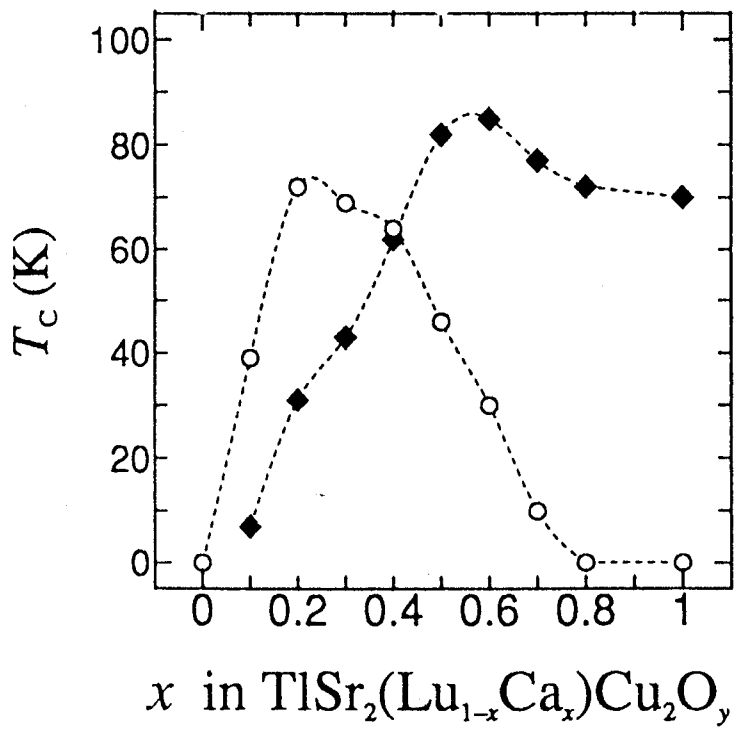

Fig.III-24. T_c values plotted against the Ca concentration, x, for $TlSr_2(Lu_{1-x}Ca_x)Cu_2O_y$.[73] Open circles and closed diamonds represent samples oxygenated at 350°C and argon reduced at 550°C, respectively.

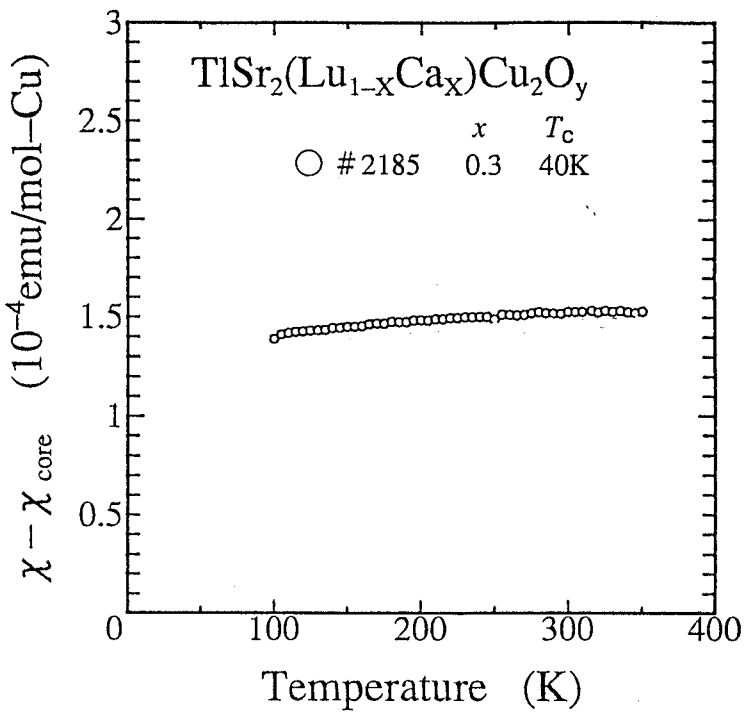

Fig.III-25. T-dependence of the magnetic susceptibility after correction for the core diamagnetism, χ_{core}.[73]

11.2 $^{63}\nu_Q$ and ^{63}K

Unfortunately, the powder sample of Lu-doped Tl1212 is not aligned. So, the Knight shift component perpendicular to the c-axis, $^{63}K_{ab}$, was determained from the peak of $\theta = 90°$ to the c-axis of the powder pattern, as shown in Fig.III-26. On the other hand, the component parallel to the c-axis, $^{63}K_c$, is not determined.

In order to estimate the value of $^{63}\nu_Q$,[39, 72] the specrta has been measured at several different frequencies in a range of 75.1 $\sim$ 130.1 MHz at 4.2 K, as seen in Fig.III-27. $^{63}\nu_Q$ is estimated to be $\sim$ 19.0 MHz from eq.(33). The value is smaller than those in heavily-doped Tl1212 and other lightly-doped compounds,[43] indicating that the hole density at Cu site seems to be smaller than these compounds.

Figure III-28 shows the T-dependence of $^{63}K_{ab}$ for Lu-doped Tl1212 compound with $T_c = 40$ K in lightly-doped region, together with the data for heavily-doped Tl1212 with $T_c = 70$ K and oxygen-deficient $YBCO_{6+x}$.[24] For the heavily-doped Tl1212, $^{63}K_{ab}$ is T-invariant in the normal state, while $^{63}K_{ab}$ for the Lu-doped Tl1212 decreases upon lowering temperature as in the case of oxygen-deficient lightly-doped $YBCO_{6+x}$ compound with single CuO chain,[24] assuring that the decrease of $^{63}K_{ab}$ is one of the universal magnetic behavior in the lightly-doped systems regardless of the presence of CuO chain structure, although the origin of this T-dependence is still unknown.

In the inset of Fig.III-28, $^{63}K_{ab}$ is plotted against the bulk susceptibility, as shown in Fig.III-25. Since ^{63}K is expressed by eq.(13), the super-transferred hyperfine field at Cu site, B, is estimated to be $\sim$ 40 kOe/μ_B from the linear coefficient in the inset of Fig.III-28, if the on-site hyperfine field is assumed to be the same as that of other lightly-doped compounds ($A_{ab} \sim$ 37 kOe/μ_B).[24, 44, 45, 46, 47, 48] This value is similar to that of lightly-doped LSCO with no chain,[44] oxygen-deficient $YBCO_{6+x}$ with single chain[24] and Y124 with double chains,[45] suggesting that the value ($B \sim$ 40 kOe/μ_B) is a typical value regardless of the structure, and is characteristic in the lightly-doped systems.

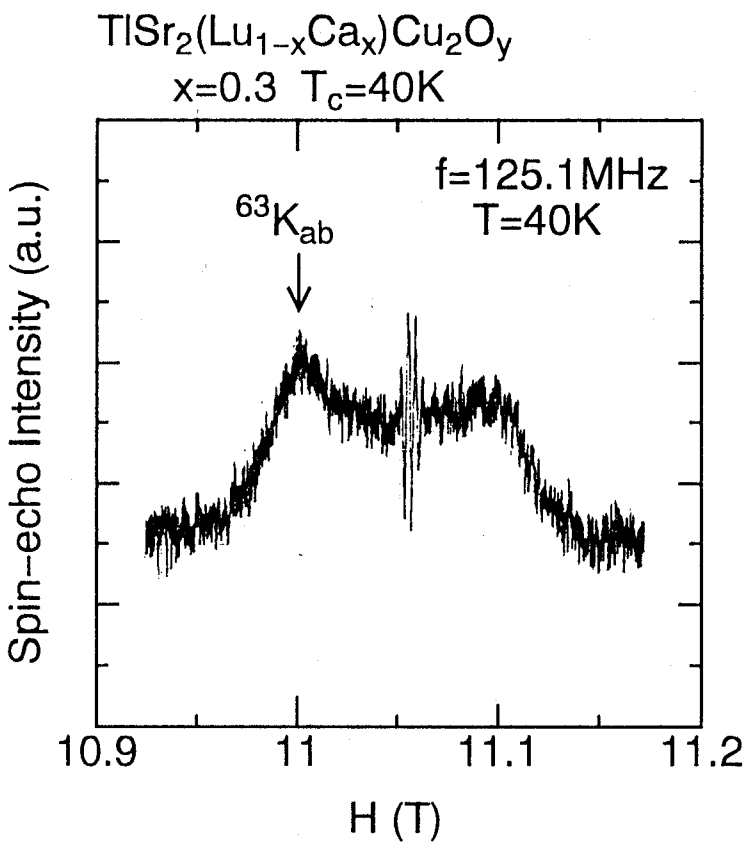

Fig.III-26. ^{63}Cu NMR spectrum for unoriented powder of lightly-doped $TlSr_2(Lu_{0.7}Ca_{0.3})Cu_2O_y$ with T_c = 40 K, which shows the powder-pattern.

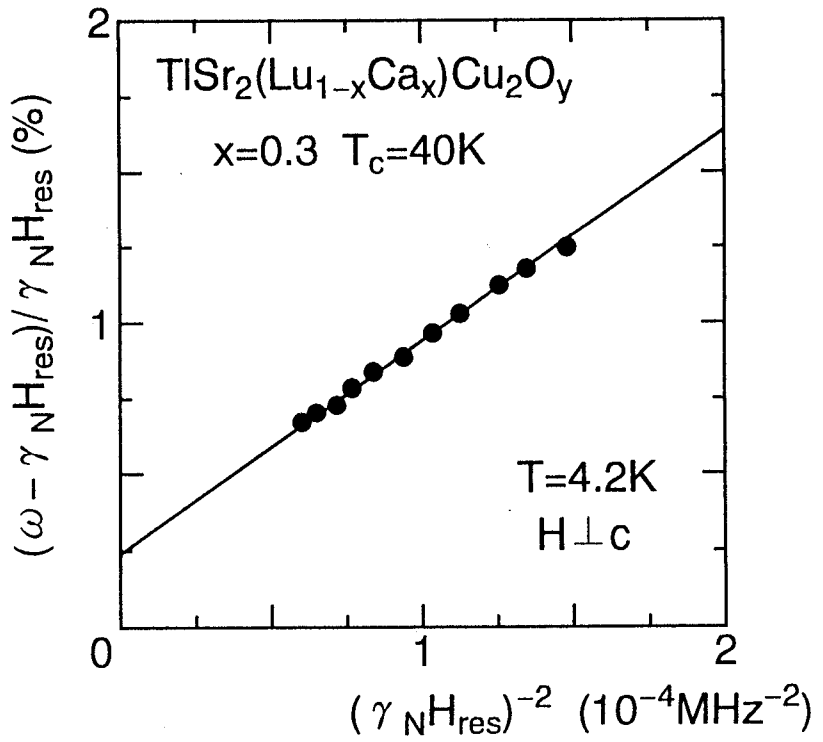

Fig.III-27. The value of $(\omega - \gamma_N H_{res})/(\gamma_N H_{res})$ plotted against $(\gamma_N H_{res})^{-2}$ in the field perpendicular to the c-axis for different NMR frequencies. H_{res} is the field for resonance.

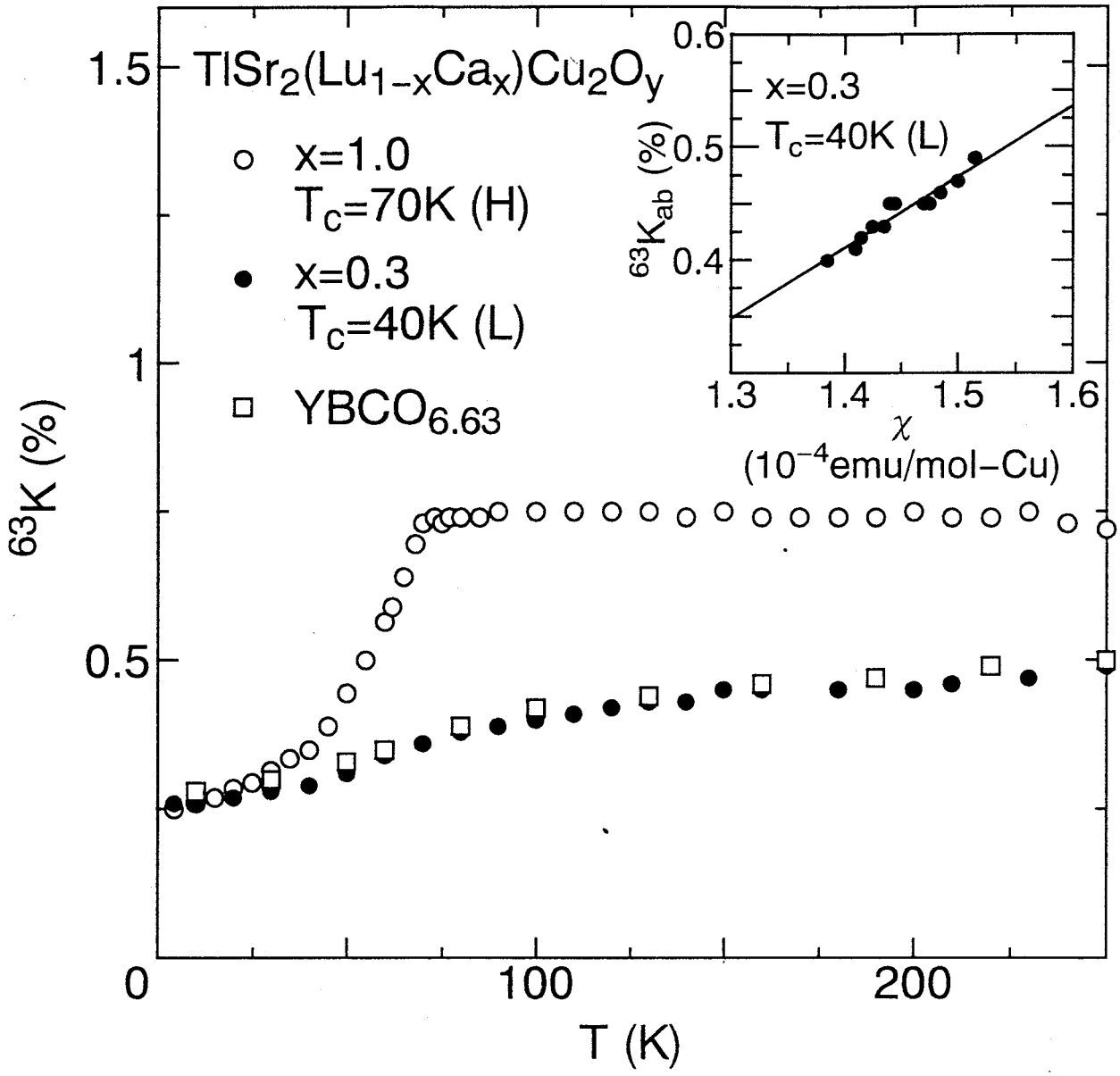

Fig.III-28. T-dependence of $^{63}K_{ab}$ for lightly-doped $TlSr_2(Lu_{0.7}Ca_{0.3})Cu_2O_y$ with T_c = 40 K (•), together with the results for heavily-doped Tl1212 with T_c = 70 K (○) and oxygen-deficient $YBCO_{6.63}$ (□).[24] Inset indicates the linear relation between $^{63}K_{ab}$ and the magnetic susceptibility shown in Fig.III-25.

11.3 Spin Gap Behavior in $^{205}(1/T_1)$

In the lightly-doped Tl1212 compounds, it was difficult to measure the $^{63}(1/T_1)$ accurately, since the powder is not oriented. Instead, T-dependence of $1/T_1$ of ^{205}Tl ($^{205}\gamma_N$ = 2.4567 MHz/kOe) was measured. The Tl atom is located just above Cu and is considered to feel the Cu spin fluctuation being expected to have the same temperature dependence of T_1 as Cu.[15, 65, 82)]

Figure III-29 shows the T-dependences of $(1/T_1T)_{ab}$ for ^{63}Cu and ^{205}Tl in heavily-doped Tl1212 with T_c = 70 K. It is noted that the both behaviors of $^{63}(1/T_1T)_{ab}$ and $^{205}(1/T_1T)_{ab}$ are quite similar to each other. Actually, $^{205}(1/T_1T)$ is confirmed to be well scaled to $^{63}(1/T_1T)$ with temperature as an implicit parameter above T_c for the heavily-doped compound with T_c = 70 K, as shown in the inset of Fig.III-29. The ratio, $^{205}T_1/^{63}T_1$, is constant above T_c, suggesting that the origin of the relaxation is the same in both Tl and Cu sites. Therefore, the relaxation behavior of Cu site seems to be obtained indirectly from that of Tl site.

Figure III-30 shows the relaxation curve of ^{205}Tl, $m(t)$, plotted against the time, t, after saturation pulse in $TlSr_2(Lu_{0.7}Ca_{0.3})Cu_2O_y$ with T_c = 40 K at T = 60 K and f = 211.1 MHz. Since ^{205}Tl has no quadrupole moment (I = 1/2), the relaxation curve should be single exponent type. As seen in the figure, the data was not fitted with a single T_1 component, that is, T_1 component is distributed. It suggested that the disorder is induced in the CuO_2 plane by substituting Lu^{3+} into the Ca^{2+} layer to controlling hole content, as in the case of LSCO system where the disorder is induced by substituting Sr^{2+} into the La^{3+} layer.

Figure III-31 shows the T-dependence of $^{205}(1/T_1T)$ in $TlSr_2(Lu_{0.7}Ca_{0.3})Cu_2O_y$ (T_c = 40 K) under the magnetic field of $\sim$ 11 T. • and ○ indicate the short- and the long-component of $^{205}(1/T_1T)$, which are tentatively extracted from a fit to the data of $m(t)$ larger than 0.5 and smaller than 0.1, respectively, as indicated by solid lines in Fig.III-30. A remarkable feature is that $^{205}(1/T_1T)$ in each component has a broad peak around $T^* \sim$ 120 K well above T_c, that is, shows a spin-gap behavior.

If it is assumed that the nuclear relaxation at Tl site is driven only by the classical dipole-dipole interaction between Tl nuclei and Cu-d spin, the expected value of $^{205}(1/T_1T)$

is much smaller than the observed value. Therefore, the relaxation mechanism at Tl site in Lu-doped Tl1212 is suggested to be dominated by the super-transferred hyperfine interaction with Cu-d spin via the apical-oxygen, as in the cases of hevily-doped Tl1212 and Tl2201.[15, 65, 82] Thus, this behavior of $^{205}(1/T_1T)$ is considered to reflect that of $^{63}(1/T_1T)$, and that its behavior is spin-gap like.

It has proposed that the spin-gap like behavior can be understood by a phase diagram deduced from the mean field theory for the t-J model.[13] Another possible origin is attributed to a precursor of the superconductivity.[83, 84] But the origin of this behavior is still not unclear.

Figure III-32 shows the T-dependence of $^{205}(1/T_1T)$ in some Tl1212 compounds covering from lightly- to heavily-doped region. As seen in the figure, $^{205}(1/T_1T)$ for the lightly-doped one exhibits an appreciable decrease well above T_c, i.e. the spin-gap behavior. It is noteworthy that the CuO_2 bilayer system reveals the spin-gap behavior in the lightly-doped region, even though the disorder is induced into the Ca(Lu) layers controlling hole content and the CuO chain is absent. This result suggests that the lack of the spin-gap behavior in LSCO is not due to the disorder but to the single layer and hence the spin-gap behavior may be associated with the bilayer coupling along the c-axis, as argued by several authors.[85, 86]

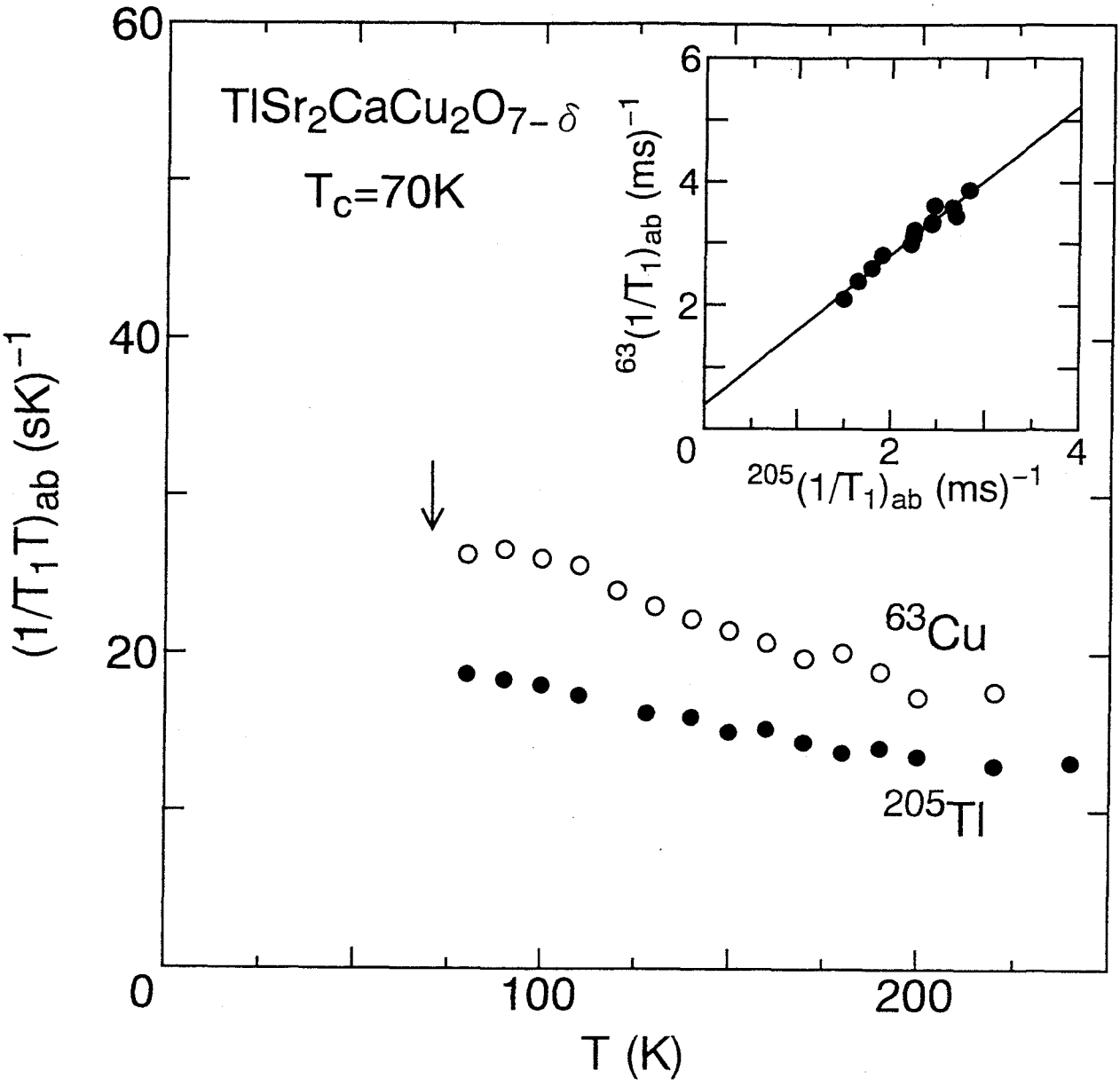

Fig.III-29. T-dependence of $(1/T_1T)_{ab}$ for ^{63}Cu (○) and ^{205}Tl (●) in heavily-doped Tl1212 with $T_c = 70$ K. Inset indicates the linear relation between $^{205}(1/T_1T)_{ab}$ and $^{63}(1/T_1T)_{ab}$.

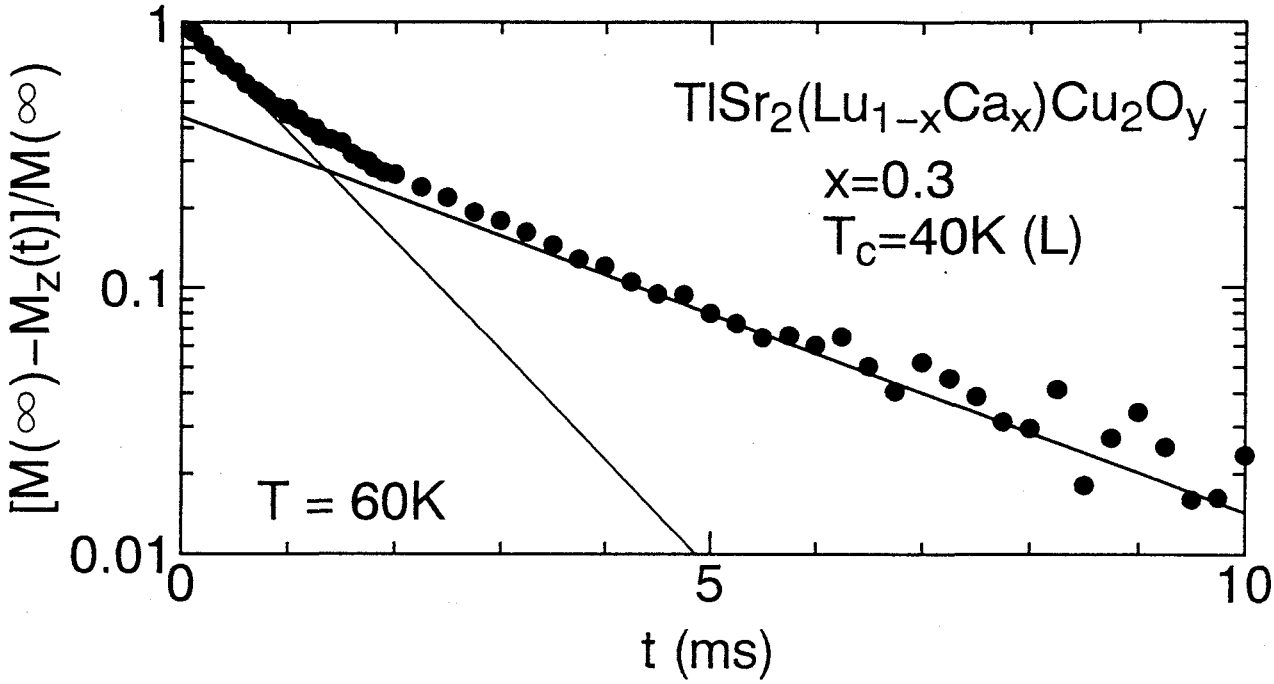

Fig.III-30. NMR relaxation curve of ^{205}Tl plotted against t after saturation pulse in $TlSr_2(Lu_{0.7}Ca_{0.3})Cu_2O_y$ with T_c = 40 K at T = 60 K and f = 211.1 MHz.

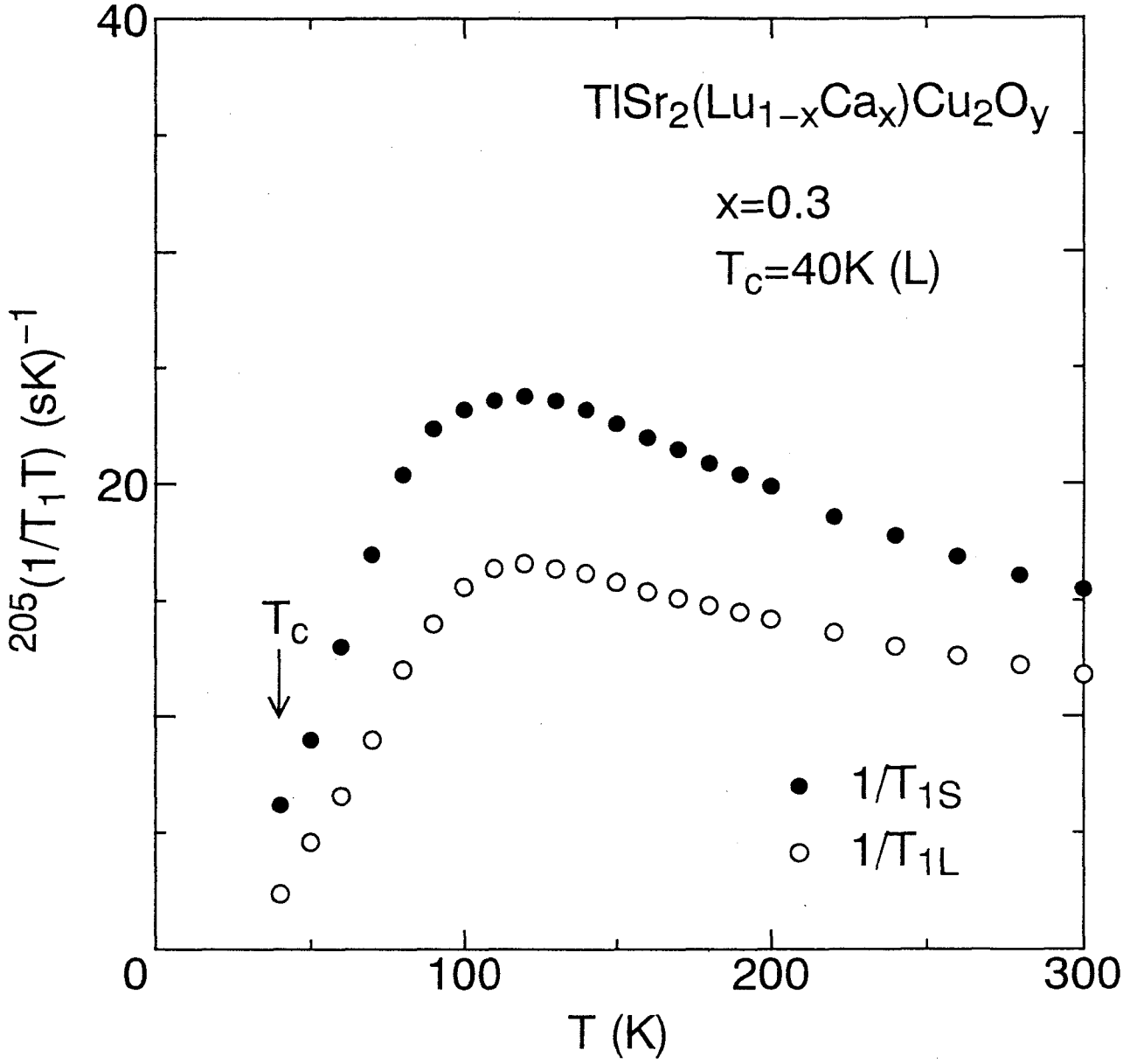

Fig.III-31. T-dependence of $^{205}(1/T_1T)$ in $TlSr_2(Lu_{0.7}Ca_{0.3})Cu_2O_y$ with T_c = 40 K under the magnetic field of $\sim$ 11 T. • and ○ indicate the short- and the long-component of $^{205}(1/T_1T)$, respectively.

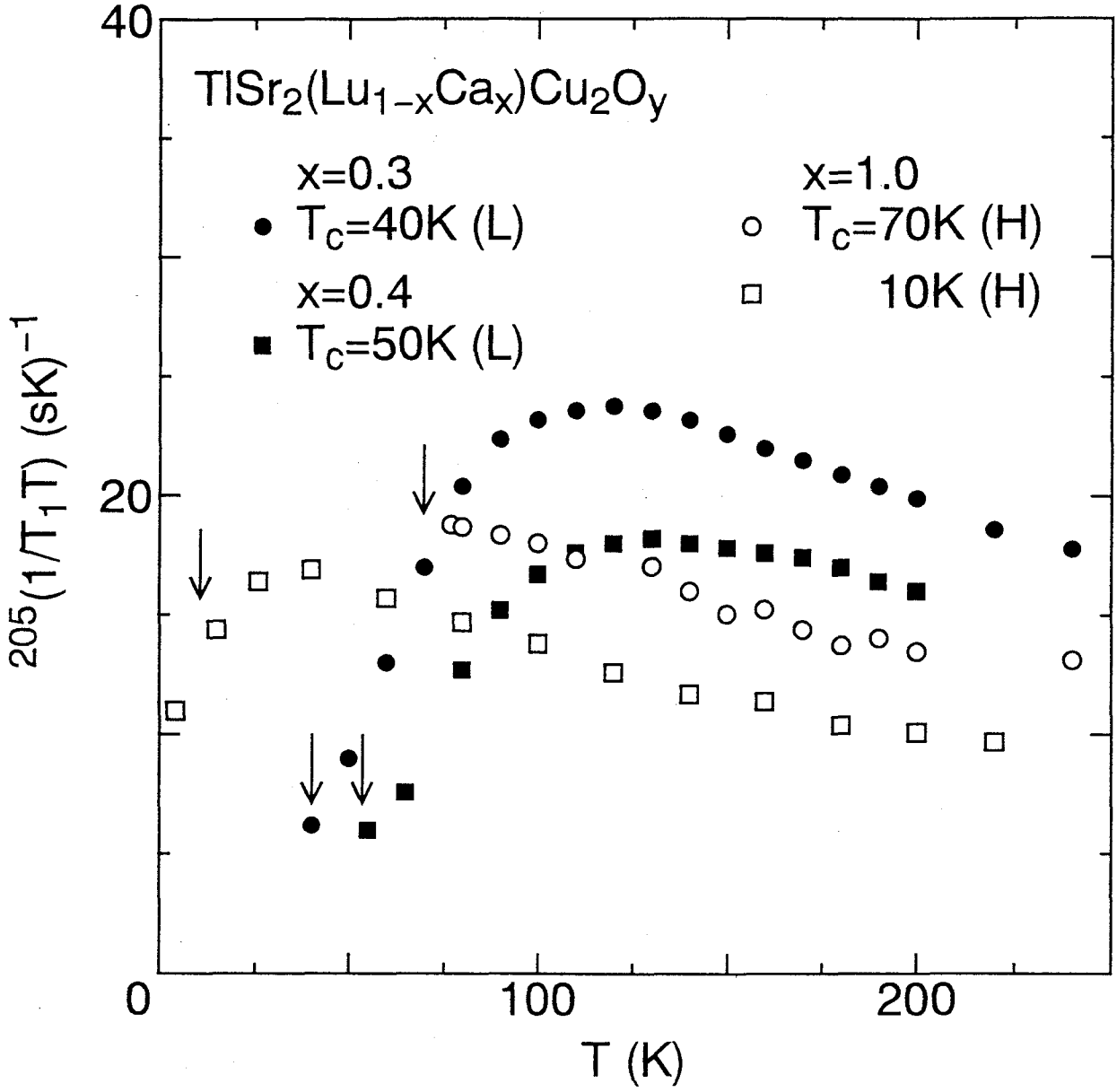

Fig.III-32. T-dependence of $^{205}(1/T_1T)$ in several Tl1212 compounds covering from lightly- to heavily-doped region.

12 Summary

The magnetic property and the spin dynamics in heavily-doped $TlSr_2CaCu_2O_{7-\delta}$ (Tl1212) were investigated by measuring the nuclear quadrupole frequency, ν_Q, the Knight shift, K, the nuclear-spin lattice relaxation rate, $1/T_1$, and the nuclear spin-spin relaxation rate, $1/T_{2G}$, for ^{63}Cu for the compounds with T_c = 70 K, 52 K and 10 K. In the normal state, $^{63}(1/T_1T)$ obeys a Curie-Weiss law, indicating the presence of the **AF** spin correlations, although it is weaker than that in lightly-doped LSCO, $YBCO_7$ and Hg1223. From the analyses of $^{63}(1/T_1)$ and $1/T_{2G}$, it is found that the weaker the **AF** spin correlation with increasing holes, the lower T_c. Hence, the **AF** spin correlation seems to be responsible for the occurrence of the high-T_c superconductivity.

On the other hand, in the superconducting state, the behaviors of ^{63}K and $^{63}(1/T_1)$ resemble that in other high-T_c materials and are explained by **the gapless d-wave model** with a finite density of states at the Fermi level, which was applied to Zn-doped $YBCO_7$, LSCO (x$\geq$0.20), Bi2212, Tl2223 and Tl2201. The pair-breaking effect is almost the same for both compounds with T_c = 70 K and 52 K in Tl1212, showing that the T_c is actually decreased by increasing holes.

To be concluded from extensive NMR studies covering from lightly- to heavily-doped systems is that the superconductivity, which is of d-wave pairing type, is relevant to the presence of the **AF** spin correlation, presumably mediated by spin fluctuations.

On the other hand, in lightly-doped $TlSr_2(Lu_{0.7}Ca_{0.3})Cu_2O_y$ (T_c = 40 K), $^{205}(1/T_1T)$, which reflects the behavior of $^{63}(1/T_1T)$, has a broad peak around $T^* \sim$ 120 K well above T_c, that is, shows a spin-gap behavior, even though the disorder is induced into the Ca(Lu) layers controlling hole content and the CuO chain is absent. It is suggested that the absence of the spin-gap behavior in LSCO system is due to the single layer structure, and that the spin-gap behavior is related to the bi-layered structure.

Part IV
Conclusion

^{63}Cu NMR measurements of the $HgBa_2Ca_2Cu_3O_{8+\delta}$ (Hg1223) system, which currently has the highest value of the transition temperature (T_c = 133 K) to date, has been carried out, in order to elucidate why T_c in this system is so high. In the normal state, from the quantitative analyses of $^{63}(1/T_1)$ and $1/T_{2G}$, it should be noted that the product of the staggered susceptibility and the characteristic energy of the spin fluctuations around the zone boundary, $\chi_Q\Gamma_Q$, for the $4-fold$ CuO_2 plane site is larger than that for $YBa_2Cu_3O_7$ ($YBCO_7$), although that for the $5-fold$ CuO_2 plane site is almost the same. This enhancement of $\chi_Q\Gamma_Q$ is considered to be responsible for the higher T_c in Hg1223 than in $YBCO_7$. In the superconducting state, the behaviors of ^{63}K and $^{63}(1/T_1)$ can consistently be interpreted in terms of the d-wave pairing model with a small additional density of states (DOS), N_{res}, at the Fermi level. The small value of N_{res} indicates that the Hg1223 possesses good quality, as supported by the narrow NMR spectra. It is suggested that one of the origins for the high value of T_c in Hg1223 is due to the better quality than other high-T_c cuprates.

On the other hand, in order to establish the magnetic and superconducting properties in heavily-doped region, ^{63}Cu NMR measurements of $TlSr_2CaCu_2O_{7-\delta}$ (Tl1212) compounds with two pyramidal CuO_2 planes in the unit cell as in $YBCO_7$ have been carried out. In the normal state, from the systematic measurements of $^{63}(1/T_1)$ and $1/T_{2G}$, the **AF** spin correlation is found to be weaker than that in $YBCO_7$, and to be suppressed with decreasing T_c, i.e. with increasing hole content. In the superconducting state, the T-dependences of ^{63}K and $^{63}(1/T_1)$ are almost consistent with a gapless d-wave pairing model with a finite DOS at the Fermi surface, as in the cases for other high-T_c superconductors.

These characters can be explained in terms of the spin-fluctuation-induced superconductivity model as well, and thus it is concluded that the high-T_c superconductivity is due to the spin fluctuations.

Acknowledgements

The author would like to express his sincere thanks to Professor Kunisuke Asayama for guiding him into this field, and for the continuous advice, enlighting discussions and warmheated encouragement throughout this work. He would like to thank Associated Professor Yoshio Kitaoka for continuous guidance, valuable discussions and encouragement. He also thanks Dr.'s Kazuyasu Tokiwa, Akira Iyo, Hideo Ihara in Electrotechnical Laboratory for provision of mercury-based compounds with good quality, and Dr.'s Takashi Kondo, Yu-ichi Shimakawa, Takashi Manako and Yoshimi Kubo in Fundamental Research Laboratories, NEC Corporation for thier material syntheses with good quality and characterizations of Tl-based compounds, and Dr. Guo-qing Zheng, Dr. Kenji Ishida and other colleagues in Asayama laboratory for their cooperation.

References

1) For a review see for example: Proc. of the Int. Conf. on Materials and Mechanism of Superconductivity IV (Grenoble, France, July 1994), eds. P. Wyder, Physica **C235-240** (1994).

2) Y. Kitaoka, S. Hiramatsu, Y. Kohori, K. Ishida, T. Kondo, H. Shibai, K. Asayama, H. Takagi, S. Uchida, H. Iwabuchi and S. Tanaka, Physica **C153-155** (1988) 83.

3) H. Monien and D. Pines, Phys. Rev. **B41** (1990) 6297.

4) K. Ishida, Y. Kitaoka, N. Ogata, T. Kamino, K. Asayama, J. R. Cooper and N. Athanassopoulou, J. Phys. Soc. Jpn. **62** (1993) 2803.

5) S. N. Putlin, E. V. Antipov, O. Chmaissem and M. Marezio, Nature **362** (1993) 226.

6) A. Schilling, M. Cantoni, J. D. Guo and H. R. Ott, Nature **363** (1993) 56.

7) C. W. Chu, L. Gao, F. Chen, Z. J. Huang, R. L. Meng and Y. Y. Xue, Nature **365** (1993) 323.

8) Y. Kitaoka, S. Ohsugi, K. Ishida and K. Asayama, Physica **C170** (1990) 189; S. Ohsugi, Y. Kitaoka, K. Ishida and K. Asayama, J. Phys. Soc. Jpn. **60** (1991) 2351.

9) W. W. Warren. Jr., R. E. Walstedt, G. F. Brennert, R. J. Cava, R. Tyckjo, R. F. Bell and G. Dabbagh, Phys. Rev. Lett. **62** (1989) 1193.

10) H. Yasuoka, T. Imai and T. Shimizu, Strong Correlation and Superconductivity (Springer-Verlag, Berlin, 1989) 254.

11) H. Zimmerman, M. Mali, D. Brinkmann, J. Karpinsky, E. Kaldis and S.Ruciecki, Physica **C159** (1989) 681; T. Machi, T. Tomeno, T. Miyatake, N. Koshizuka, S. Tanaka, T. Imai and H. Yasuoka : Physica **C173** (1990) 32.

12) J. Rossat-Mignod, L. P. Regnault, C. Vettier, P. Burlet, J.Y.Henry and G. Lapertot, Physica **B169** (1991) 58; J. Rossat-Mignod, L. P. Regnault, C. Vettier, P. Bourges, P. Burlet, J. Bossy, J. Y. Henry and G. Lapertot, Physica **C185-189** (1991) 89; J. Rossat-Mignod, L. P. Regnault, P. Bourges, C. Vettier, P. Burlet and J. Y. Henry, Physica **B186-188** (1993) 1.

13) T. Tanamoto, K. Kohno and H. Fukuyama, J. Phys. Soc. Jpn. **61** (1992) 1886; **62** (1993) 717; **62** (1993) 1455; **63** (1994) 2739.

14) Y. Shimakawa, Y. Kubo, T. Manako and H. Igarashi, Phys. Rev. **B40** (1989) 11400; Y. Kubo, Y. Shimakawa, T. Manako and H. Igarashi, Phys. Rev. **B43** (1991) 7875.

15) Y. Kitaoka, K. Fujiwara, K. Ishida, K. Asayama, Y. Shimakawa, T. Manako and Y. Kubo, Physica **C179** (1991) 107.

16) A. J. Mills, H. Monien and D. Pines, Phys. Rev. **B42** (1990) 167; P. Monthoux, A. Balatsky and D. Pines, Phys. Rev. Lett. **26** (1991) 344;

17) T. Moriya, Y. Takahashi and K. Ueda, J. Phys. Soc. Jpn. **59** (1990) 2905; T. Moriya and K. Ueda, J. Phys. Soc. Jpn. **63** (1994) 1871.

18) N. Bulut and D. J. Scalapino, Phys. Rev. Lett. **67** (1991) 2898; Phys. Rev. **B45** (1992) 2731.

19) D. Thelen, D. Pines and J. P. Lu, Phys. Rev. **B47** (1993) 9151.

20) K. Levin, J. H. Kim, J. P. Lu and Q. Si, Physica **C175** (1991) 449; Y. Zha, Q. Si and K. Levin, Physica **C212** (1993) 413; Q. Si, Y. Zha, K. Levin and J. P. Lu, Phys. Rev. **B47** (1993) 9055.

21) A. Abragam, *The principles of Nuclear magnetism* (Clarendon, Oxford, 1961).

22) F. Mila and T. M. Rice, Physica **C157** (1989) 561; Phys. Rev. **B40** (1989) 11382.

23) H. Alloul, T. Ohno and P. Mendels, Phys. Rev. Lett. **63** (1989) 1700.

24) M. Takigawa, A. D. Reyes, P. C. Hammel, J. D. Thompson, R. H. Heffner, Z. Fisk and K. C. Ott, Phys. Rev. **B43** (1991) 247.

25) T. Moriya, J. Phys. Soc. Jpn. **18** (1963) 516.

26) P. C. Hammel, M. Takigawa, R. H. Heffner, Z. Fisk and K. C. Ott, Phys. Rev. Lett. **63** (1989) 1992.

27) C. H. Pennington, D. J. Durand, C. P. Slichter, J. P. Rice, E. D. Bukowski and D. M. Ginsberg, Phys. Rev. **B39** (1989) 274; C. H. Pennington and C. P. Slichter, Phys. Rev. Lett. (1991) 381.

28) A. Leggett, Rev. Mod. Phys. **47** (1975) 331.

29) K. Yosida, Phys. Rev. **110** (1958) 769.

30) A. Narath, Phys. Rev. **B13** (1976) 3724.

31) C. P. Slichter, *Principles of Magnetic Resonance* (Springer-Verlag, New York, 1990), 3rd ed.

32) D. E. Farrell, B. S. Chandrasekhar, M. R. McGuire, M. M. Fang, V. G. Kogan, J. R. Clem and F. K. Finnemore, Phys. Rev. **B36** (1987) 4025.

33) Z. J. Huang, R. L. Meng, X. D. Qiu, Y. Y. Sun, J. Kulik, Y. Y. Xue and C. W. Chu, Physica **C217** (1993) 1.

34) M. Hirabayashi, K. Tokiwa, M. Tokumoto and H. Ihara, Jpn. J. Appl. Phys. **32** (1993) L1206.

35) H. Ihara, M. Hirabayashi, H. Tanino, K. Tokiwa, H. Ozawa, Y. Akahama and H.Kawamura, Jpn. J. Appl. Phys. **32** (1993) L1732.

36) K. Ishida, Y. Kitaoka, K. Asayama, K. Kadowaki and T. Mochiku, J. Phys. Soc. Jpn. **63** (1994) 1104.

37) G. -q. Zheng, Y. Kitaoka, K. Asayama, K. Hamada, H. Yamauchi and S. Tanaka, J. Phys. Soc. Jpn. **64** (1995) 3184.

38) S. Kambe, H. Yasuoka, A. Hayashi and Y. Ueda, Phys. Rev. **B47** (1993) 2825.

39) M. Takigawa, P. C. Hammel, R. H. Heffner, Z. Fisk, J. L. Smith and R. Schmary, Phys. Rev. **B39** (1989) 300.

40) K. Schwarz, C. Ambrosch-Draxl and P. Blaha, Phys. Rev. **B42** (1990) 2051; C. Ambrosch-Draxl, P. Blaha and K. Schwarz, Phys. Rev. **B44** (1991) 5141.

41) S. Fraga, J. Karwowski and K. M. S. Sexen, Handbook of Atomic Data (Elsevier Amsterdam 1976).

42) Y. Ohta, W. Koshibae and S. Maekawa, J. Phys. Soc. Jpn. **61** (1992) 2198.

43) G. -q. Zheng, T. Kuse, Y. Kitaoka, K. Ishida, S. Ohsugi, K. Asayama and Y. Yamada, Physica **C208** (1993) 339; K. Asayama, Y. Kitaoka, G. -q. Zheng, K. Ishida and S. Ohsugi, Hyperfine Interaction **79** (1993) 835.

44) S. Ohsugi, Y. Kitaoka, K. Ishida, G. -q. Zheng and K. Asayama, J. Phys. Soc. Jpn. **63** (1994) 700.

45) H. Zimmermann, M. Mali, M. Bamky and D. Brinkmann, Physica **C185-189** (1991) 1145.

46) A. J. Millis, H. Monien and D. Pines, Phys. Rev. **B43** (1991) 275.

47) H. Monien, D. Pines and M. Takigawa, Phys. Rev. **B43** (1991) 258.

48) T. Imai, J. Phys. Soc. Jpn. **59** (1990) 2508.

49) Y. Itoh, J. Phys. Soc. Jpn. **63** (1994) 3522.

50) S. E. Barrett, J. A. Martindale, D. J. Durand, C. H. Pennington, C. P. Slichter, T. A. Friedmann, J. P. Rice and D. M. Ginsberg, Phys. Rev. Lett. **66** (1991) 108.

51) M. Takigawa, Phys. Rev. **B49** (1994) 4158.

52) D. Thelen and D. Pines, Phys. Rev. **B49** (1994) 3528.

53) T. Imai, C. P. Slichter, A. P. Paulikas and B. Veal, Phys. Rev. **B47** (1993) 9158.

54) Y. Itoh, H. Yasuoka, Y. Fujiwara, Y. Ueda, T. Machi, I. Tomeno, K. Tai, N. Koshizuka and S. Tanaka, J. Phys. Soc. Jpn. **61** (1992) 1287.

55) P. Monthoux, A. V. Balatsky and D. Pines, Phys. Rev. Lett. **67** (1991) 3448; P. Monthoux and D. Pines, Phys. Rev. **B47** (1993) 6069;

56) P. Monthoux, A. V. Balatsky and D. Pines, Phys. Rev. **B46** (1992) 14083; P. Mouthoux and D. Pines, Phys. Rev. **B49** (1994) 4261.

57) T. Moriya, Y. Takahashi and K. Ueda, Physica **C185-189** (1991) 114; K. Ueda, T. Moriya and Y. Takahashi, J. Phys. Chem. Solids **53** (1992) 1515.

58) H. Won and K. Maki, Phys. Rev. **B49** (1994) 1397; **B49** (1994) 15305.

59) E. Ehrenfreund, I. B. Goldberg and M. Wegar, Solid State Commun. **7** (1969) 1333.

60) C. Caroli and J. Matricon, Phys. Kond. Mat. **3** (1965) 380.

61) J. A. Martindale, S. E. Barrett, D. J. Durand, K. E. O'Hara, C. P. Slichter, W. C. Lee and D. M. Ginsberg, Phys. Rev. **B50** (1994) 13645.

62) K. Ishida, Y. Kitaoka and K.Asayama, Solid State Commun. **90** (1994) 563.

63) G. -q. Zheng, Y. Kitaoka, K. Asayama and Y. Kodama, Physica **C227** (1994) 169.

64) G. -q. Zheng, Y. Kitaoka, K. Asayama, K. Hamada, H. Yamauchi and S. Tanaka, submitted to Physica **C**.

65) K. Fujiwara, Y. Kitaoka, K. Ishida, K. Asayama, Y. Shimakawa, T. Manako and Y. Kubo, Physica **C184** (1991) 207.

66) I. B. Goldberg and M. Weger, J. Phys. Soc. Jpn. **24** (1968) 1279.

67) S. Schmitt-Rink, K. Miyake and C. M. Varma, Phys. Rev. Lett. **57** (1986) 2575.

68) P. J. Hirshfeld, D. Vollhardt and P. Wolfe, Solid State Commun. **59** (1986) 111.

69) T. Hotta, J. Phys. Soc. Jpn. **62** (1993) 7895.

70) P. J. Hirschfeld and N. Goldenfeld, Phy. Rev. **B48** (1993) 4219.

71) S. Schmitt-Rink, K. Miyake and C. M. Varma, unpublished.

72) Y. Kubo, T. Kondo, Y. Shimakawa, T. Manako and H. Igarashi, Phys. Rev. **B45** (1992) 5553.

73) T. Kondo, Y. Kubo, Y. Shimakawa and T. Manako, Phys. Rev. **B50** (1994) 1244.

74) F. Izumi, T. Kondo, Y. Shimakawa, T. Manako, Y. Kubo, H. Igarashi and H. Asana, Physica **C185-189** (1991) 615.

75) H. Takagi, T. Ido, S. Ishibayashi, M. Uota, S. Uchida, and Y. Tokura, Phys. Rev. **B40** (1989) 2254.

76) R. R. Gupta, in *Diamagnetic Susceptibility*, edited by K. -H. Hellwege and A. M. Hellwege, Landolt-Bornstein, New Series, Group II Vol. 16 (Springer-Verlag, Heidelberg, 1986), p. 402.

77) S. E. Barrett, D. J. Durand, C. H. Pennington, C. P. Slichter, T. A. Friedmann, J. P. Rice and D. M. Ginsberg, Phys. Rev. **B41** (1990) 6283.

78) H. Zimmermann, M. Mali, M. Bamky and D. Brinkmann, Physica **C185-189** (1990) 9574.

79) K. Asayama, G. -q. Zheng, Y. Kitaoka, K. Ishida and K. Fuiwara, Physica **C178** (1991) 281.

80) H. Kohno and K. Yamada, Prog. Theor. Phys. **85** (1991) 1.

81) Y. Itoh, H. Yasuoka, A. Hayashi and Y. Ueda, J. Phys. Soc. Jpn. **63** (1994) 22.

82) S. Kambe, H. Yasuoka, A. Hayashi and Y. Ueda, Phys. Rev. **B48** (1993) 6593.

83) W. W. Warren and R. E. Walstedt, Z. Naturforsh **45a** (1990) 385.

84) K. Miyake, private commun.

85) A. J. Millis and H. Monien, Phys. Rev. Lett. **70** (1993) 2810.

86) Menke U. Ubbens and Patrick A. Lee, Phys. Rev. **B50** (1994) 438.